การติดไบโอตินบนพื้นผิวซิลิกอนที่มีพอลิอะคริลิกแอซิดบรัช

นางสาวปิยะพร อรรคฮาต

ATTACHMENT OF BIOTIN ON SILICON SURFACE-TETHERED POLY(ACRYLIC ACID) BRUSHES

Miss Piyaporn Akkahat

A Thesis Submitted in Partial Fulfillment of the Requirements

for the Degree of Master of Science Program in Petrochemistry and Polymer Science

Faculty of Science

Chulalongkorn University

Academic Year 2005

Thesis Title	Attachment of biotin on silicon surface-tethered poly(acrylic acid) brushes
By	Miss Piyaporn Akkahat
Field of Study	Petrochemistry and Polymer Science
Thesis Advisor	Assistant Professor Voravee P. Hoven, Ph.D.

Accepted by the Faculty of Science, Chulalongkorn University in Partial Fulfillment of the Requirements for the Master's Degree
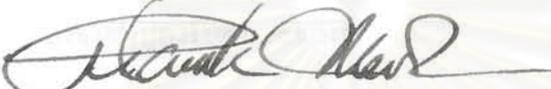
………………………………………………Dean of the Faculty of Science

(Professor Piamsak Menasveta, Ph.D.)

Thesis committee
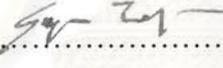
………………………………………………..Chairman

(Associate Professor Supawan Tantayanon, Ph.D.)
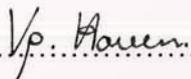
………………………………………………..Thesis Advisor

(Assistant Professor Voravee P. Hoven, Ph.D.)
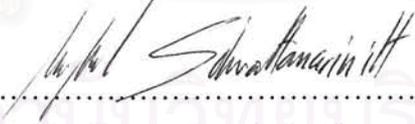
………………………………………………Member

(Associate Professor Mongkol Sukwattanasinitt, Ph.D.)
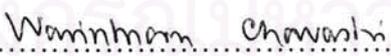
………………………………………………..Member

(Assistant Professor Warinthorn Chavasiri, Ph.D.)

ปิยะพร อรรคฮาต: การติดไบโอตินบนพื้นผิวซิลิกอนที่มีพอลิอะคริลิกแอซิดบรัช (ATTACHMENT OF BIOTIN ON SILICON SURFACE-TETHERED POLY(ACRYLIC ACID) BRUSHES) อาจารย์ที่ปรึกษา: ผศ.ดร.วรวีร์ โฮเว่น; 112 หน้า ISBN: 974-14-1914-7

พอลิอะคริลิกแอซิด (พีเอเอ) บรัชที่ยึดติดบนพื้นผิวมีศักยภาพที่จะสามารถนำไปใช้เป็นฟิล์มฟังก์ชันนัลที่มีความหนาระดับนาโนเมตรสำหรับการประยุกต์ทางด้านเทคโนโลยีหลายประเภท ทั้งนี้เนื่องจากหมู่คาร์บอกซิลของพอลิเมอร์บรัชเป็นหมู่ที่เอื้ออำนวยต่อการดัดแปรทางเคมีได้หลากหลายรวมทั้งการติดด้วยสารชีวโมเลกุล ในงานวิจัยนี้ได้เตรียมพอลิเทอร์เทียรีบิวทิวอะคริเลต (พีทีบียูเอ) บรัชทั้งที่เป็นโซ่ตรงและโซ่กิ่งโดยปฏิกิริยาอะตอมทรานเฟอร์แรดิคัลพอลิเมอไรเซชันที่ริเริ่มจากพื้นผิวของเทอร์เทียรีบิวทิวอะคริเลต และปฏิกิริยาเซลฟ์คอนเดนซิงไวนิลโคพอลิเมอไรเซชันของพีทีบียูเอ และ อะคริลิกแอซิด 2-(2-โบรโมโพรพิโอนิลออกซี)เอทิลเอสเทอร์ (บีพีอีเอ) ตามลำดับ จากนั้นทำปฏิกิริยาไฮโดรไลซิสในสภาวะกรดเพื่อกำจัดหมู่เทอร์เทียรีบิวทิวของพีทีบียูเอ ทำให้ได้พีเอเอ บรัชทั้งที่เป็นโซ่ตรงและโซ่กิ่ง จากการทดลองพบว่าสามารถควบคุมปริมาณของหมู่คาร์บอกซิลของพีเอเอบรัชที่เป็นโซ่ตรงและโซ่กิ่งด้วยการควบคุมความยาวของสายโซ่พอลิเมอร์ (น้ำหนักโมเลกุล) และสัดส่วนโคพอลิเมอร์ ตามลำดับ สามารถพิสูจน์ทราบความสำเร็จของการติดไบโอตินที่หมู่คาร์บอกซิลของพีเอเอบรัชทั้งที่เป็นโซ่ตรงและโซ่กิ่งได้โดยการวิเคราะห์ด้วยเอฟที-ไออาร์และการติดกับสเตรปทาวิดินที่คอนจูเกตกับฟลูออเรสซีนซึ่งตรวจเห็นได้โดยกล้องฟลูออเรสเซนต์ไมโครสโคป

สาขาวิชา ปิโตรเคมีและวิทยาศาสตร์พอลิเมอร์ ลายมือชื่อนิสิต ปิยะพร อรรคฮาต

ปีการศึกษา 2548 ลายมือชื่ออาจารย์ที่ปรึกษา

PIYAPORN AKKAHAT: ATTACHMENT OF BIOTIN ON SILICON SURFACE-TETHERED POLY(ACRYLIC ACID) BRUSHES. THESIS ADVISOR: ASSISTANT PROFESSOR VORAVEE P. HOVEN, Ph.D. 112 pp ISBN: 974-14-1914-7

Surface-tethered poly(acrylic acid) (PAA) brushes can potentially be used as functional nanometer-thick film for many technological applications. Their carboxyl groups serve as versatile moieties for a wide range of chemical modification including an attachment of biomolecules. In this research, linear and branched poly(*tert*-butyl acrylate) (P*t*BuA) brushes were prepared by surface-initiated atom transfer radical polymerization of *tert*-butyl acrylate and self-condensing vinyl copolymerization of P*t*BuA with acrylic acid 2-(2-bromopropionyloxy)ethyl ester (BPEA), respectively. Linear and branched PAA brushes were subsequently obtained after *tert*-butyl groups of P*t*BuA brushes were removed by acid hydrolysis. The carboxyl group density of linear and branched PAA brushes can be varied as a function of chain length (MW) and comonomer ratio (γ), respectively. The success of biotin attachment to the carboxyl groups of both linear and branched PAA brushes was verified by FT-IR analysis and the binding with fluorescein-conjugated streptevidin which was visualized by fluoroscence microscope.

Field of study <u>Petrochemistry and Polymer Science</u> Student's signature <u>Piyaporn Akkahat</u>

Academic year <u>2005</u> Advisor's signature <u>Vp. Hoven.</u>

ACKNOWLEDGEMENTS

CONTENTS

Page

LIST OF FIGURES

Figure   Page

Figure   Page

Figure   Page

LIST OF TABLES

LIST OF SCHEMES

LIST OF ABBREVIATIONS

AFM	: Atomic force microscopy
ATRP	: Atom transfer radical polymerization
Å	: Ångström = 0.1 nm
t-BuA	: $tert$-Butyl acrylate
$CDCl_3$	: Deuterated chloroform
CuBr	: Copper (I) bromide
°C	: Degree Celsius
D_2O	: Deuterium oxide
DB	: Degree of branching
DP	: Degree of polymerization
Eq.	: Equation
GPC	: Gel permeation chromatography
k_{act}	: The activation rate parameter
k_{deact}	: The deactivation rate parameter
MeOH	: Methanol
mg	: miligram
$MgSO_4$	: Magnesium sulfate
min	: minute
mL	: mililiter

mm   : milimeter

mM   : milimolar

mmol   : milimole

$\overline{M}_n$: Number average molecular weight

$\overline{M}_w$: Weight average molecular weight

nm   : nano meter

NMR   : Nuclear magnetic resonance spectroscopy

PAA   : Poly(acrylic acid)

PDI   : Polydispersity Index

PMDETA   : *N, N, N′, N″, N″*-pentamethyldiethylenetriamine

P*t*BuA   : Poly(*tert*-butyl acrylate)

ppm   : part per million

SAM   : Self-assembled monolayer

THF   : Tetrahydrofuran

μL   : microliter

CHAPTER I

INTRODUCTION

1.1 Statement of problem

Development of biosensor largely relies on the immobilization of bioactive species to sensor or measurement platforms. The density of immobilized bioactive species as well as the distance between the surface of sensor and the bioactive species significantly affects sensitivity, detection limit as well as signal-to-noise ratio of the biosensor. A precursor layer for immobilization of bioactive molecules is conventionally based on self-assembled monolayer (SAM) of end-functionalized alkanethiol whose density cannot be broadly varied. The variation of alkyl chain length is also limited due to the fact that long alkyl chains tend to induce non-specific adsorption of the bioactive molecules during the immobilization step. This often causes adverse effect on biosensor efficiency.

Surface-initiated polymerization (SIP) has been introduced as a potential tool to generate surface-tethered polymer brushes which can act as a modifying layer for material's surface that can be useful for biotechnology and nanotechnology applications. SIP or so-called "grafting from" method has attracted much interest holds advantages over the "grafting to" method where the process is suffered entropic barrier due to crowding of initial grafting polymer chains that prevent further insertion of polymer onto the surface leading to relatively low graft density. The "grafting from" method, on the other hand, involves a stepwise growth of polymer chain from the surface by insertion of monomer. This allows a better control over polymer chain length and graft density. SIP coupled with "living radical polymerization" has proven to be the most popular method for creating surface-tethered polymer brushes.

By using the techniques, the molecular weight, molecular weight distribution and architecture of the target polymer can be well controlled. Due to the versatility of the process towards a wide range of readily available monomers, both chemical and

physical properties of surface-tethered polymer brushes can be broadly tailored. In particular, the functional group density of the surface which is a function of the chain length and molecular weight of polymer brush can also be varied.

This research aims to determine the feasibility of using surface-tethered linear and branched poly(acrylic acid) (PAA) brushes generated by surface-initiated polymerization for biotechnology applications. It is anticipated that carboxyl groups along poly(acrylic acid) brushes can function as precursor moieties for immobilization of bioactive species that act as sensing probes of biosensor. Using "living" atom transfer radical polymerization (ATRP), the carboxyl group density which depends on molecular weight of polymer brushes should be conveniently controlled as a function polymerization condition. Reactivity of the carboxyl group is also tested against the immobilization of biotin, a frequently used bioactive molecule in biosensor applications. Subsequent binding with fluorescent-labeled streptavidin is thereby investigated.

The research begins with the formation of linear and branched poly(*tert*-butyl acrylate) (P*t*BuA) brushes by surface-initiated atom transfer radical polymerization of *tert*-butyl acrylate and self-condensing vinyl copolymerization of P*t*BuA with acrylic acid 2-(2-bromopropionyloxy)ethyl ester (BPEA), respectively. Linear and branched PAA brushes were subsequently obtained after *tert*-butyl groups of P*t*BuA brushes were removed by acid hydrolysis. The reactivity of carboxyl groups of PAA brushes was assessed by a reaction with *N*-hydroxysuccinimide (NHS) in the presence of 1-(3-dimethylaminopropyl)-3-ethylcarbodiimide hydrochloride (EDCI). The activated carboxyl groups were then reacted with amino-functionalized biotin.

1.2 Objectives

1. To synthesize linear and branched poly(acrylic acid) brushes by surface-initiated atom transfer radical polymerization from silicon surface.

2. To attach biotin on carboxyl groups of poly(acrylic acid) brushes.

1.3 Scope of investigation

The stepwise investigation was carried out as follows.

1. Literature survey for related research work.

2. To immobilize α-bromoester-containing initiator on silicon oxide surfaces.

3. To synthesize linear and branched PtBuA brushes by surface-initiated polymerization from silicon oxide surfaces containing a monolayer of α-bromoester groups.

4. To prepare linear and branched PAA brushes by hydrolysis of PtBuA brushes.

5. To determine the reactivity of carboxyl groups of PAA brushes.

6. To attach biotin on carboxyl groups of PAA brushes.

7. To test binding ability of biotin attached on PAA brushes with fluorescent-labeled streptavidin

CHAPTER II

THEORY AND LITERATURE REVIEW

2.1 Polymer brush

Polymer brushes refer to an assembly of polymer chains which are tethered by one end to a surface or an interface. Tethering is sufficiently dense that the polymer chains are crowded and forced to stretch away from the surface or interface to avoid overlapping, sometimes much further than the typical unstretched size of a chain. These stretched configurations are found under equilibrium conditions; neither a confining geometry nor an external field is required. This situation, in which polymer chains stretch along the direction normal to the grafting surface, is quite different from the typical behavior of flexible polymer chains in solution where chains adopt a random-walk configuration. A series of discoveries show that the deformation of densely tethered chains affects many aspects of their behavior and results in many novel properties of polymer brushes [1].

Polymer brushes are a central model for many practical polymer systems such as polymer micelles, block copolymers at fluid–fluid interfaces (e.g. microemulsions and vesicles), grafted polymers on a solid surface, adsorbed diblock copolymers and graft copolymers at fluid–fluid interfaces. All of these systems, illustrated in Figure 2.1, have a common feature: the polymer chains exhibit deformed configurations. Solvent can be either present or absent in polymer brushes. In the presence of a good solvent, the polymer chains try to avoid contact with each other to maximize contact with solvent molecules. With solvent absent (melt conditions), polymer chains must stretch away from the interface to avoid overfilling incompressible space.

The interface to which polymer chains are tethered in the polymer brushes may be a solid substrate surface or an interface between two liquids, between a liquid and air, or between melts or solutions of homopolymers. Tethering of polymer chains on the surface or interface can be reversible or irreversible. For solid surfaces, the polymer chains can be chemically bonded to the substrate or may be just adsorbed

onto the surface. Physisorption on a solid surface is usually achieved by block copolymers with one block interacting strongly with the substrate and another block interacting weakly. For interfaces between fluids, the attachment may be achieved by similar adsorption mechanisms in which one part of the chain prefers one medium and the rest of the chain prefers the other.
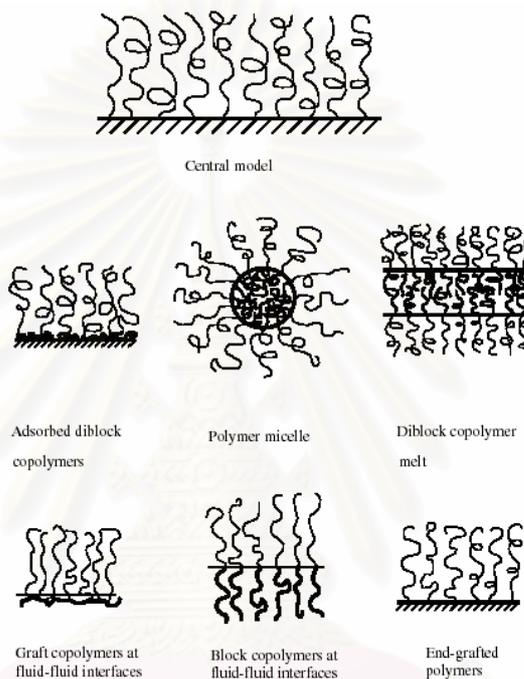
Figure 2.1 Examples of polymer systems comprising polymer brushes.

Polymer brushes (or tethered polymers) attracted attention in 1950s when it was found that grafting polymer molecules to colloidal particles was a very effective way to prevent flocculation [1]. In other words, one can attach polymer chains which prefer the suspension solvent to the colloidal particle surface; the brushes of two approaching particles resist overlapping and colloidal stabilization is achieved. The repulsive force between brushes arises ultimately from the high osmotic pressure inside the brushes. Subsequently it was found that polymer brushes can be useful in other applications such as new adhesive materials [2-3], protein-resistant biosurfaces [4], chromotographic devices [4], lubricants [5], polymer surfactants [1] and polymer compatibilizers [1]. Tethered polymers which possess low critical solution temperature (LCST) properties exhibit different wetting properties above and below

LCST temperature [7]. A very promising field that has been extensively investigated is using polymer brushes as chemical gates. Ito and coworkers [8-10] have reported pH sensitive, photosensitive, oxidoreduction sensitive polymer brushes covalently tethered on porous membranes, which are used to regulate the liquid flowing rate through porous membranes. Suter and coworkers [11-12] have prepared polystyrene brushes on high surface area mica for the fabrication of organic–inorganic hybrids. Cation-bearing peroxide free-radical initiators were attached to mica surfaces via ion exchange and used to polymerize styrene. This process is important in the field of nanocomposites. Patterned thin organic films could be useful in microelectrics [13], cell growth control [14-15], biomimetic material fabrication [16], microreaction vessel and drug delivery [17].

In terms of polymer chemical compositions, polymer brushes tethered on a solid substrate surface can be divided into homopolymer brushes, mixed homopolymer brushes, random copolymer brushes and block copolymer brushes. Homopolymer brushes refer to an assembly of tethered polymer chains consisting of one type of repeat unit. Mixed homopolymer brushes are composed of two or more types of homopolymer chains [18]. Random copolymer brushes refer to an assembly of tethered polymer chains consisting of two different repeat units which are randomly distributed along the polymer chain [19]. Block copolymer brushes refer to an assembly of tethered polymer chains consisting of two or more homopolymer chains covalently connected to each other at one end [20]. Homopolymer brushes can be further divided into neutral polymer brushes and charged polymer brushes. They may also be classified in terms of rigidity of the polymer chain and would include flexible polymer brushes, semiflexible polymer brushes and liquid crystalline polymer brushes. These different polymer brushes are illustrated in Figure 2.2.
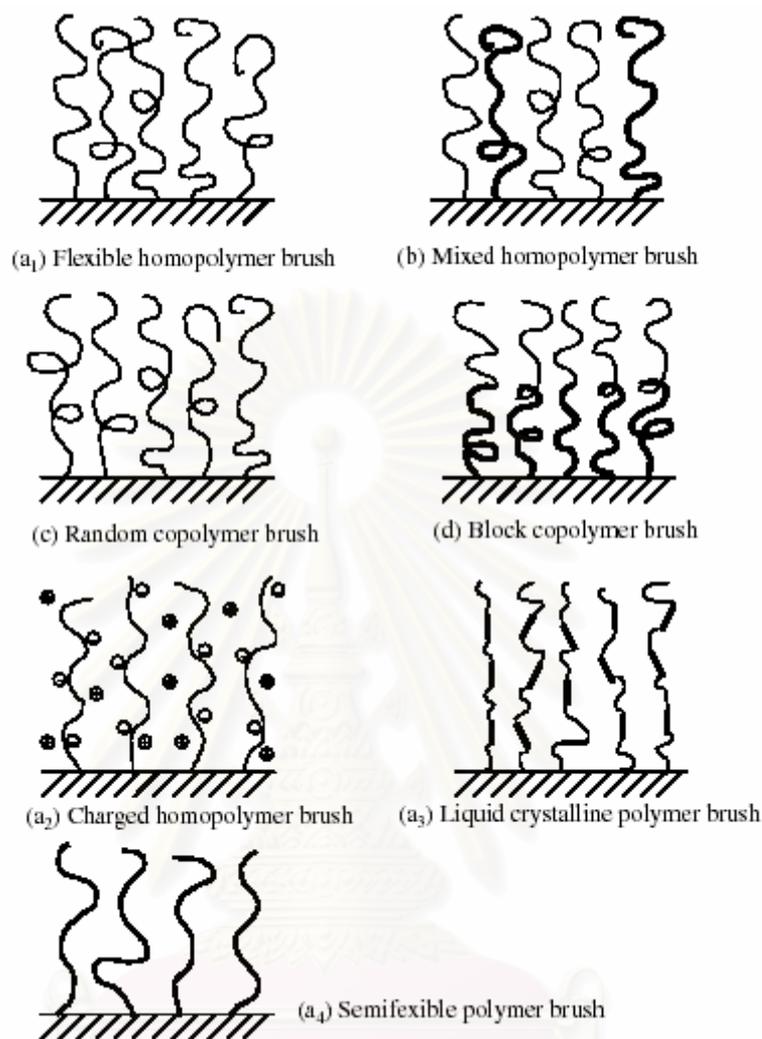
Figure 2.2 Classification of linear polymer brushes, $(a_1–a_4)$ homopolymer brushes; (b) mixed homopolymer brush; (c) random copolymer brush; (d) block copolymer brush.

Generally, there are two ways to fabricate polymer brushes: physisorption and covalent attachment (Figure 2.3). For polymer physisorption, block copolymers adsorb onto a suitable substrate with one block interacting strongly with the surface and the other block interacting weakly with the substrate. The disadvantages of physisorption include thermal and solvolytic instabilities due to the non-covalent nature of the grafting, poor control over polymer chain density and complications in synthesis of suitable block copolymers. Tethering of the polymer chains to the surface is one way to surmount some of these disadvantages. Covalent attachment of polymer

brushes can be accomplished by either "grafting to" or "grafting from" approaches. In a "grafting to" approach, preformed end-functionalized polymer molecules react with an appropriate substrate to form polymer brushes. This technique often leads to low grafting density and low film thickness, as the polymer molecules must diffuse through the existing polymer film to reach the reactive sites on the surface. The steric hindrance for surface attachment increases as the tethered polymer film thickness increases. The "grafting from" approach is a more promising method in the synthesis of polymer brushes with a high grafting density. "Grafting from" can be accomplished by treating a substrate with plasma or glow-discharge to generate immobilized initiators onto the substrate followed by in situ surface-initiated polymerization. However "grafting from" well-defined self-assembled monolayers (SAMs) is more attractive due to a high density of initiators on the surface and a well-defined initiation mechanism. Also progress in polymer synthesis techniques makes it possible to produce polymer chains with controllable lengths. Polymerization methods that have been used to synthesize polymer brushes include cationic, anionic, TEMPO-mediated radical, atom transfer radical polymerization (ATRP) and ring opening polymerization.

Physisorption

"Grafting to"
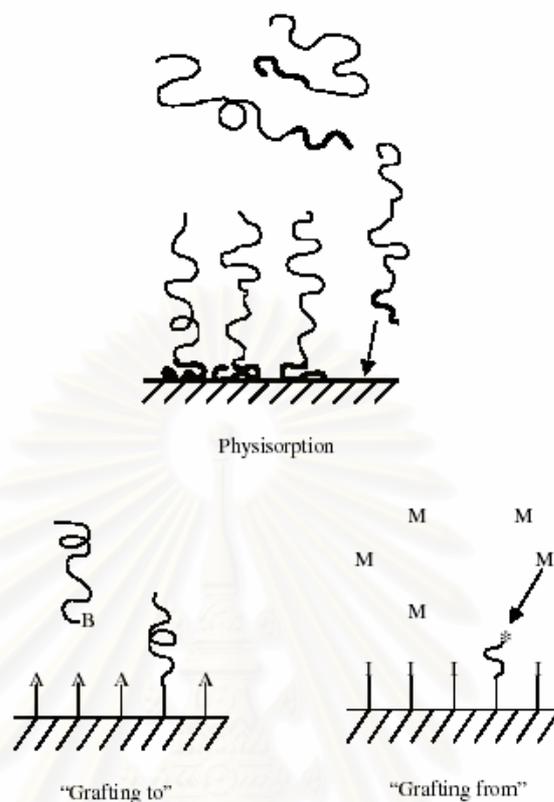
"Grafting from"

Figure 2.3 Preparation of polymer brushes by "physisorption", "grafting to" and "grafting from".

In order to achieve a better control of molecular weight and molecular weight distribution and to obtain novel polymer brushes like block copolymer brushes, controlled radical polymerizations including ATRP, reverse ATRP, TEMPO-mediated and iniferter radical polymerizations have been used to synthesize tethered polymer brushes on solid substrate surfaces [21-26].

In recent years, ATRP has been the most widely empolyed technique for the formation of polymer brushes *via* surface initiated polymerization. ATRP is compatible with a variety of functionalised monomers. The living/controlled character of the ATRP process yields polymers with a low polydispersity ($\overline{M}_w/\overline{M}_n$) that are end-functionalized and so can be used as macroinitiators for the formation of di- and triblock copolymers. Equally important, surface-initiated ATRP is experimentally more accessible than for example, the living anionic and cationic polymerizations, which require rigorously dry conditions. The synthesis of thiol and silane derivatised

surface-bound initiators is easier than AIBN-silane derivative or the nitroxide silane derivative for free radical and NMP polymerizations. In 1998, Fukuda and coworkers prepared poly(methyl methacrylate) brushes on silicon surface *via* surface-initiated atom transfer radical polymerization. The addition of free initiator to the polymerization solution yields free polymer which can be characterised by conventional methods. The relatively narrow polydispersities of these polymers in conjunction with the molecular weights were proportional to monomer conversion points towards the surface polymerization being controlled. The thickness of the polymer brushes was related to the concentration of the free initiator added, the lower concentration of free initiator the thicker the films being achieved [27].

Husseman and coworkers [23] applied ATRP in the synthesis of tethered polymer brushes on silicon wafers and achieved great success. They prepared SAMs of 5-trichlorosilylpentyl-2-bromo-2-methylpropionate on silicate substrates. The α-bromoester is a good initiator for ATRP. They have successfully synthesized PMMA brushes by the polymerization of MMA initiated from the SAMs. It has also been reported that tethered polyacrylamide has been obtained from surface initiated ATRP of acrylamide on a porous silica gel surface [24].

Matyjaszewski and coworkers [28] reported a detailed study of polymer brush synthesis using ATRP in controlled growth of homopolymer and block copolymers from silicon surfaces. They described that the persistent radical effect must be considered in controlled radical polymerizations. In other words, a sufficient concentration of deactivation must be available to provide control over chain lengths and distributions. The Cu (II) can be supplied by termination of initiator molecules in the early stages of the polymerization or by addition of the transition metal complex prior to commencement of the reaction. Moreover, the only factor affected is the kinetics of the reaction; in the former case, first-order consumption of monomer is dictated by the chains generated from the free initiator while in the latter, due to the extremely low concentration of alkyl halide bound to the surface and low monomer conversion, growth of polymer chains scales linearly with reaction time. Their conclusion suggested that the design of such complex structures whether in solution

or at an interface, understanding of the relative rates of chain propagation, equilibrium constants, and the influences of the end group, metal, and ligand in crossover reaction are important. Factors such as initiator functionality and blocking efficiency can have a profound influence on the physical properties of the resulting material.

In 2001, Werne and Patten [29] reported the preparation of structurally well-defined polymer-nanoparticle hybrids by modifying the surface of silica nanoparticles with initiators for ATRP and by using these initiator-modified nanoparticles as macroinitiators. They found that polymerizations of styrene and methyl methacrylate (MMA) using the nanoparticle initiators displayed the diagnostic criteria for a controlled / "living" radical polymerization: an increase in the molecular weight of the pendant polymer chains with monomer conversion and a narrow molecular weight distribution for the grafted chains. Polymerization of styrene from smaller silica nanoparticles (75-nm-diameter) exhibited good molecular weight control, while polymerization of MMA from the same nanoparticles exhibited good molecular weight control only when a small amount of free initiator was added to the polymerization solution. For the polymerizaiton of both styrene and MMA from larger silica nanoparticles (300-nm-diameter) did not exhibit molecular weight control. Molecular weight control was induced by the addition of a small amount of free initiator to the polymerization but was not induced when 5-15 mol% of deactivator (Cu(II) complex) was added. These findings provide guidance for efforts in using ATRP for the controlled grafting of polymers from high and low surface area substrates.

2.2 Branched polymer brushes

Highly branched polymers are of considerable scientific and industrial interest, due to their low intrinsic viscosity, high solubility and miscibility, and their potential as polyfunctional carriers. The interest in hyperbranched polymers arises from the fact that they combine some feature of dendrimers, for example, an increasing number of end groups and a compact structure in solution- with the ease of preparation of linear polymer by means of a one-pot reaction. However, the polydispersities are usually

high and their structures are less regular than those of dendrimers, which are monodisperse molecules with well-defined, perfectly branched architectures. Dendrimers have a highly compact and globular shape, and are produced in a multi-step organic synthesis. During the past decade, the field of arborescent polymers (dendrimer, hyperbranched, and highly branched polymers) has become well established, with a large of synthetic approaches, fundamental studies on the structure and properties of these unique materials, and the identification of possible applications for these materials.
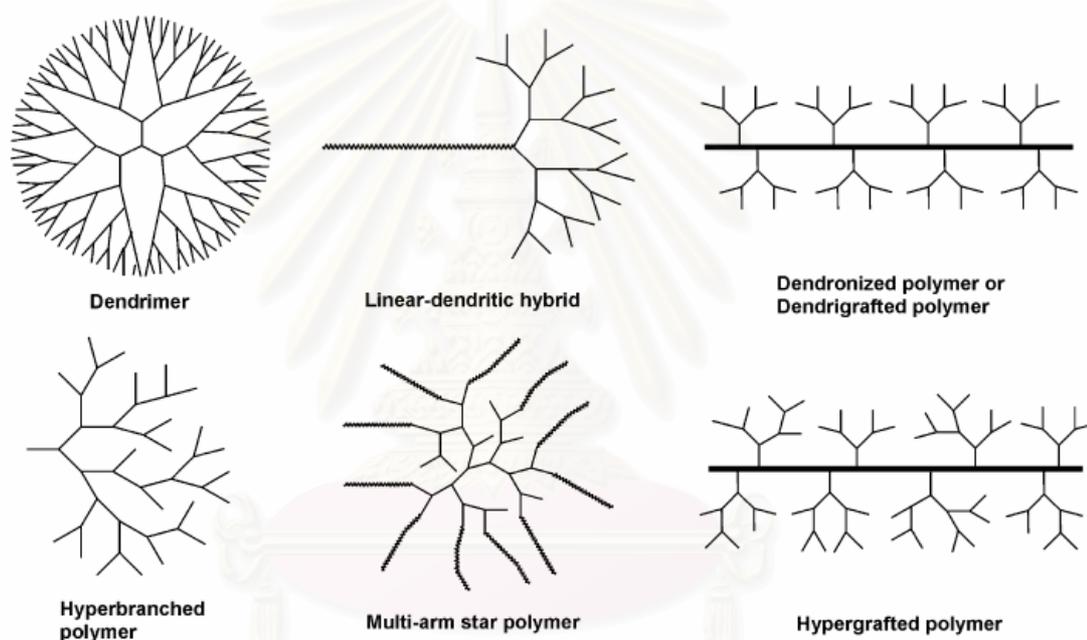
Figure 2.4 Schematic description of dendritic polymers.

.

Several strategies for the preparation of the hyperbranched polymers are currently employed, the most common method being the polycondensation of AB_n monomers. The recent discovery of self-condensing vinyl polymerization (SCVP) by Frechet et al. made it possible to use vinyl monomers for the one-step synthesis of hyperbranched structures with degree of branching (DB) ≤ 0.5. This reaction is based on an initiator-monomer ("inimer") of the general structure AB^*, where the double bond is disignated A and B^* is a group capable of initiating the polymerization of

vinyl groups. Living cationic and radical polymerizations, group transfer polymerization, and ring opening polymerization have been applied to SCVP. The activated B[*] adds across the double bond A, to form the dimer. Scheme 2.1 shows the idealized case of one addition of monomer followed by deactivation to form the new group A[*]. The dimer, 2, can now be reactivated at either B[*] or A[*]. Addition of monomer at A[*] results in 3a, while addition at B[*] yields 3b. Further addition of monomer, or *n*-mer, to either 3a or 3b, can result in a polymer that is branched.
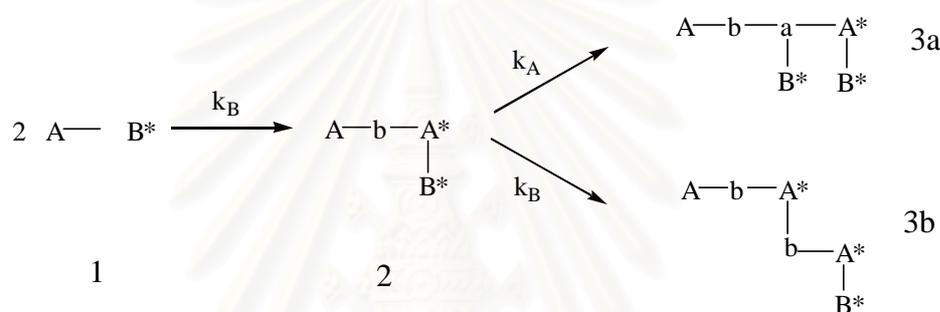
Scheme 2.1 Self-condensing vinyl polymerization (SCVP) of an AB[*] inimer

Since the disclosure of the above reaction, it has also been shown that the copolymerization of AB[*] inimers with conventional vinyl monomers (M), this technique was extended to self-condensing vinyl copolymerization (SCVCP), leading to highly branched polymer, allowing to control molecular weight, molecular weight distribution, and degree of branching by the comonomer ratio. The copolymerization method is a facile approach to obtain functional branched polymers, because different types of functional groups can be incorporated into a polymer depending on the chemical nature of the comonomer. In addition, the chain architecture can be modified easily by a suitable choice of the comonomer ratio in the feed. The polymerization can be initiated in two ways (Scheme 2.2): (i) the addition of the active B[*] group to the vinyl group of monomer (M) forming a dimer with one active site, M*, and (ii) the addition of a B[*] group to the vinyl group (A) of the AB[*] inimer forming a dimer with

two active sites, A^* and B^*. Both the initiating B^* group and the newly created propagating centers A^* and M^* can react with any vinyl group in the system.
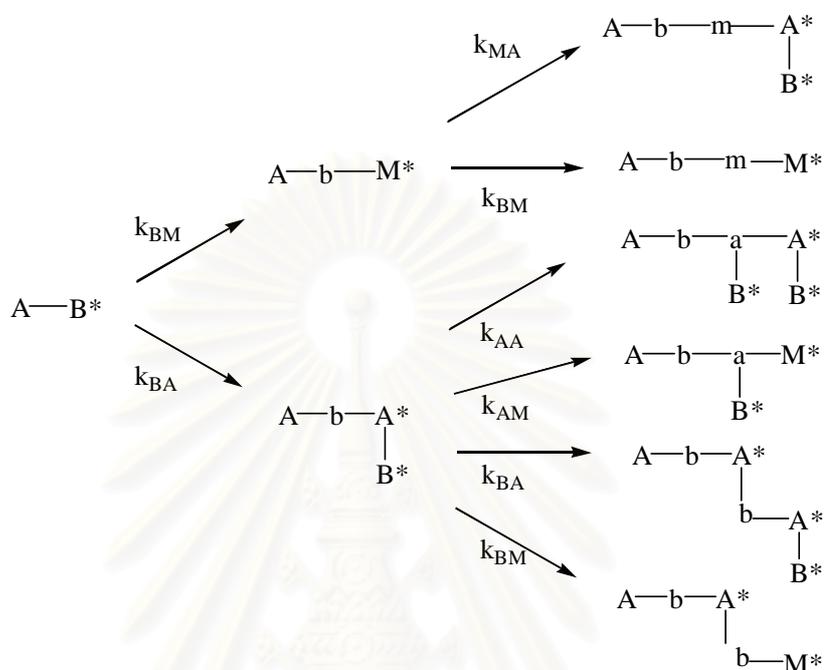
Scheme 2.2 Self-condensing vinyl copolymerization (SCVCP) of an AB^* inimer with a conventional vinyl monomers (M)

Atom transfer radical polymerization (ATRP) has been applied to SCVP and SCVCP, because of (a) the feasibility of attaining conrolled polymerization of conventional monomers, (b) the significant influence of various factors on the degree of branching, molecular weight and polydispersity of a branched polymer, (c) compatibility with a wide variety of monomers (e.g., acrylates, styrenes, acrylonitrile, and derivatives) and (d) easy handling compared to other living systems. For AB^* monomers to be used in ATRP, they must contain a halogen atom capable of reacting with the copper (I). In a general description, the double bond (A) is separated from the B^* group by a spacer, R. Curently, the types of monomers that can be polymerized by ATRP and consequently the type of A group, include styrenes, acrylates and methacrylates. The B^* group can be a (2-halopropionyl)oxy, (2-haloisobutyryl)oxy, 2-halopropionitrile or benzyl halide. The versatility of this approach is enhanced by the wide variety of R groups that can be inserted between the double bond, A, and the

functional group, B*. By changing the various groups, A, R or B*, numerous monomers/materials can be developed. The example of AB* monomers shown in Figure 2.5.
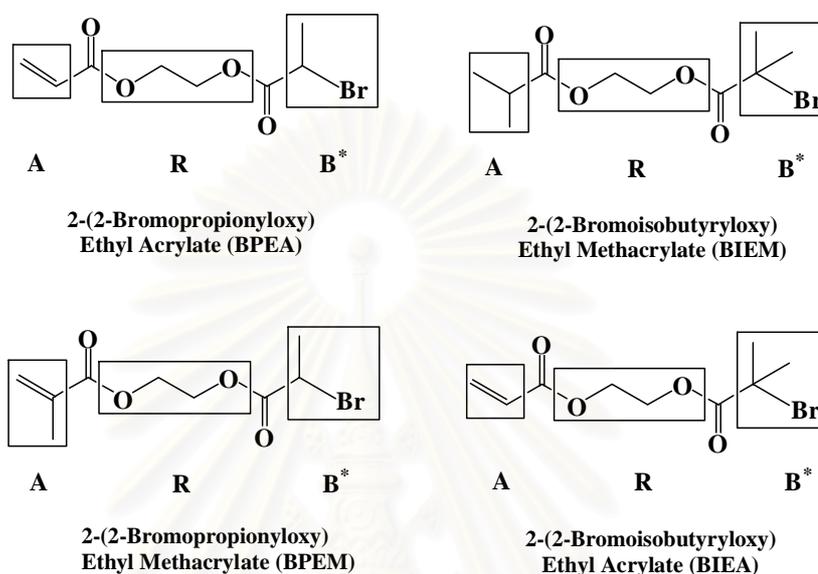
Figure 2.5 AB* monomers synthesized for polymerization by ATRP to prepare hyperbranched acrylic polymers.

The surface chemistry and interfacial properties of hyperbranched polymers have also become a field of growing interest. In recent years, must interest has been paid to highly branched polymers grafted chemically onto surfaces, as their distinctive chemical and physical properties can be used advantageously as functional surfaces and as interfacial materials. Such surface-grafted hyperbranched polymer can be regarded as a type of polymer brush, as they refer to an assembly of polymer chains which are tethered by one end to a surface or an interface. The typical structures of hyperbranched, branched, and linear polymers grafted onto surface are summarized in Figure 2.6. Depending upon the substrates, it can be divided into 3D, 2D and 1D hybrids, which correspond to products grafted on spherical particles, planar surface and linear polymers, respectively.
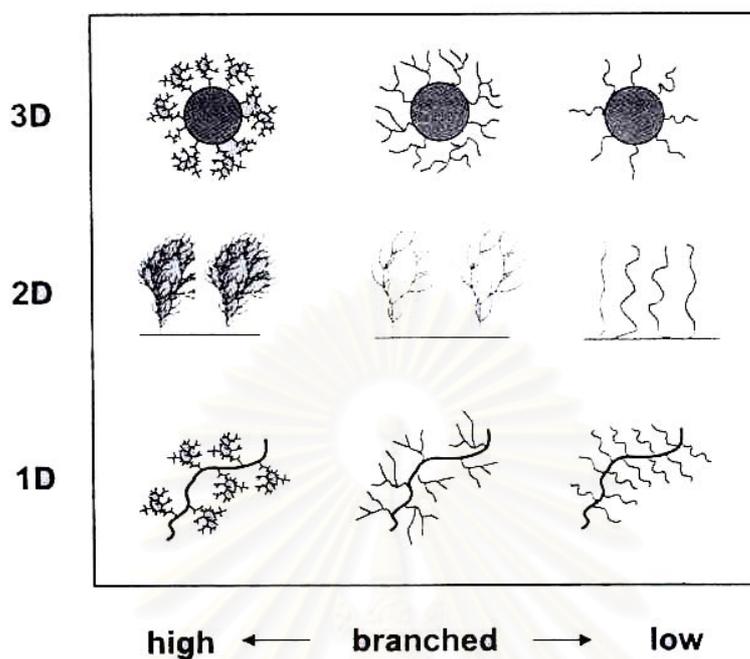
Figure 2.6 Surface-grafted hyperbranched, highly branched, and linear polymers: from one- dimensional (1D) to three-dimensional (3D).

By using self-condensing vinyl polymerization (SCVP) and self-condensing vinyl copolymerization (SCVCP) in combination with surface-initiated polymerization via atom transfer radical polymerization (ATRP), a varity of surface-grafted hyperbranched polymers have been syntheized. Scheme 2.3 shows the convenient synthetic approach for preparing hyperbranched on 2D and 3D surface in wich a silicon wafer or silica nanoparticles grafted with an initiator layer were used for SCVP via atom transfer radical polymerization (ATRP). SCVCP was also applied as a method for the synthesis of highly branched polymers grafted from surfaces. In contrast, surface-initiated ATRP resulted in the preparation of linear polymer brushes.
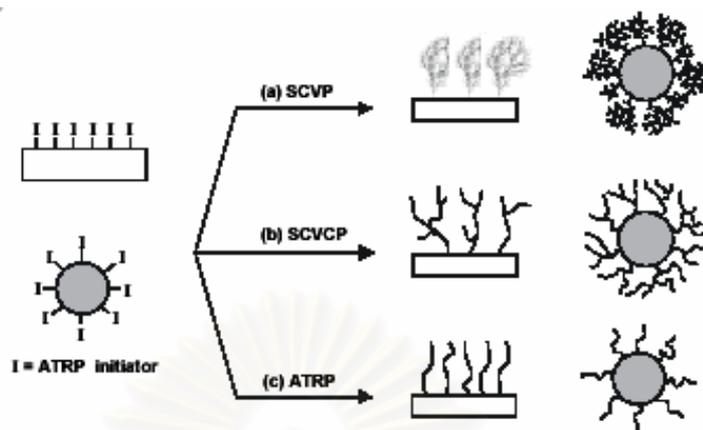
Scheme 2.3 Synthesis of hyperbranched, highly branched, and linear polymer brushes from planar surfaces and spherical particles via surface-initiated polymerization. a) self-condensing vinyl polymerization (SCVP), b) self-condensing vinyl copolymerization (SCVCP), c) atom transfer radical polymerization (ATRP).

In 2001, Mori and coworkers synthesized hyperbranched, (highly) branched, and linear polymers grafted from a planar surface. A silicon wafer grafted with an initiator layer composed of an α–bromoester fragment is used for a self-condensing vinyl polymerization (SCVP) via atom transfer radical polymerization (ATRP). Suface-initiated SCVP of BPEA was found to yield polymer films with a high degree of branching, and a characteristic surface topography. The size and density of nanoscale protrusions obtained on the surface and the film thickness were observed to depend on the polymerization conditons, such as the ratio $[BPEA]_0:[catalyst]_0$. The chain architecture and chemical structure could be modified by SCVCP, leading to a facial, one-pot synthesis of surface-grafted branched polymers. The copolymerization gave an intermediate surface topography and film thickness between the polymer protrusions obtained from SCVP of AB^* inimer and the polymer brushes obtained by ATRP of a conventional monomer. The difference in the Br content at the surface between hyperbranched, branched, and linear polymers suggested the feasibility of controlling the surface chemical functionality. The principle result of this work is a demonstration of utility of the surface-initiated SCVCP via ATRP to prepare surface-grafted hyperbranched and branched polymers having characteristic architecture and topography [30].

The hyperbranched polymer with (meth)acrylic acid segments grafted on surfaces has been extensively investigated, owing to many scientific and industrial applications, such as biomaterial carriers, intelligent environment responsive surface, and optical chemical sensing. In 2002, Mori and coworkers synthesis hyperbranched polymer and banched poly(acylic acid) on silica nanoparticle by SCVP and SCVCP via ATRP, respectively. Surface-initiated SCVP of BPEA (hyperbranched polymer) gave the result as in the case of the synthesis on silicon wafer. SCVCP of BPEA and *tert*-butyl acrylate (*t*BuA) from the functionalized silica nanoparticles created branched P*t*BuA-silica nanoparticle. The functionality of the end groups on the surface, and the chemical composition as well as the structure of branched polymers grafted on the silica nanoparticles, could be controlled by composition in the feed during the SCVCP. The hybrid nanoparticles with branched poly(acrylic acid) were obtained after hydrolysis of linear segments of the branched P*t*BuA. SCVCP was also applied for the synthesis of branched PAAs having different molecular weights and degree of branching [31].

2.3 Living polymerization

Synthetic polymers are long-chain molecules possessing uniform repeat units (mers). The chains are not all the same length. These giant molecules are of interest because of their physical properties, in contrast to low molecular weight molecules, which are of interest due to their chemical properties. Possibly the most useful physical property of polymers is their low density versus strength.

When synthetic polymers were first introduced, they were made by free radical initiation of single vinyl monomers or by chemical condensation of small difunctional molecules. The range of their properties was understandably merger. Random copolymers are greatly expanding in the range of useful physical properties such as toughness, hardness, elasticity, compressibility, and strength, however, polymer chemists realized that their materials could not compare with the properties of natural polymers, such as wool, silk, cotton, rubber, tendons and spider webbing.

The natural polymers are generally condensation polymers made by addition of monomer units one at a time to the ends of growing polymer chains. Polymerization of all chains stops at identical molecular weights. For some time polymer chemists have realized that to approach nature's degree of sophistication, new synthetic techniques would be needed.

Conventional chain-growth polymerizations, for example, free radical synthesis, consist of four elementary steps: initiation, propagation, chain transfer, and termination. As early as 1936, Ziegler proposed that anionic polymerization of styrene and butadiene, consecutive addition of monomer to an alkyl lithium initiator occured without chain transfer or termination. During transferless polymerization, the number of polymer molecules remains contant. Since there is no termination, active anionic chain ends remain after all of the monomer has been polymerized. When fresh monomer is added, polymerization resumes. The name "living polymerization" was coined for the method by Szwarc [32]. because the chain ends remain active until killed. The term has nothing to do with living in the biological sense. Before Szwarc's classic work, Flory [33] had described the properties associated with living polymerization of ethylene oxide initiated with alkoxides. Flory noted that since all of the chain ends grow at the same rate, the molecular weight is determined by the amount of initiator used versus monomer (Eq. 2.1).

$$\text{Degree of polymerization} = [\text{monomer}]/[\text{initiator}] \qquad (2.1)$$

Another property of polymers produced by living polymerization is the very narrow molecular weight distribution. The polydispersity (D) has a Poisson distribution, $D = \overline{M}_w/\overline{M}_n = 1 + (1/dp)$; $\overline{M}_w$ is the average molecular weight determined by light scattering, $\overline{M}_n$ is the average molecular weight determined by osmometry, and dp is the degree of polymerization (the number of monomer units per chain). The values of $\overline{M}_w$ and $\overline{M}_n$ can also be determined by gel permeation chromatography (GPC). A living polymerization can be distinguished from free radical polymerization or from a condensation polymerization by plotting the molecular weight of the polymer versus conversion. In a living polymerization, the molecular weight is directly proportional to conversion (Figure 2.7, line A). In a free

radical or other nonliving polymerization, high molecular weight polymer is formed in the initial stages (line B), and in a condensation polymerization, high molecular weight polymer is formed only as the conversion approaches 100% (line C).
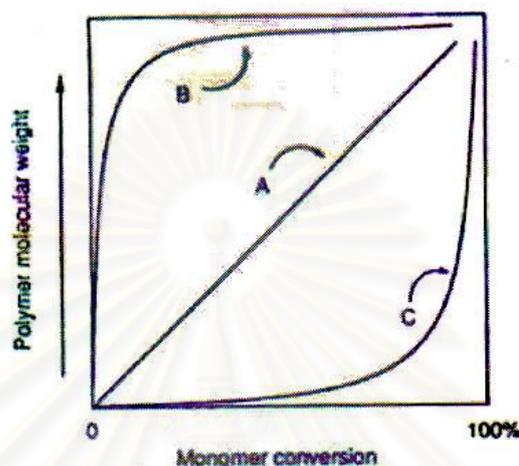
Figure 2.7 Molecular weight conversion curves for various kinds of polymerization methods: (A) living polymerization; (B) free radical polymerization; and (C) condensation polymerization.

Living polymerization techniques give the synthetic chemist two particularly powerful tools for polymer chain design: the synthesis of block copolymers by sequential addition of monomers and the synthesis of functional-ended polymers by selective termination of living ends with appropriate reagents. The main architectural features available starting with these two basic themes are listed in Figure 2.8 along with applications for the various polymer types. Although living polymerization of only a few monomers is nearly perfect, a large number of other systems fit theory close enough to be useful for synthesis of the wide variety of different polymer chain structures. In general, the well-behaved living systems need only an initiator and monomer, as occurs in the anionic polymerization of styrene, dienes, and ethylene oxide. For an increasing number of monomers, more complex processes are needed to retard chain transfer and termination. These systems use initiators, catalysts, and sometimes chain-end stabilizers. The initiator begins chain growth and in all systems is attached (or part of it, at least) to the nongrowing chain end. The catalyst is necessary for initiation and propagation but is not consumed. The chain-end stabilizer

usually decreases the polymerization rate. When the catalyst is a Lewis acid (electron-pair acceptor), the stabilizer will likely be a Lewis base (electron-pair donor), and vice versa. In all systems, the initiation step must be faster than or the same rate as chain propagation to obtain molecular weight control. If the initiation rate is slower than the propagation rate, the first chains formed will be longer than the last chains formed. If an initiator with a structure similar to that of the growing chain is chosen, the initiation rate is assured of being comparable to the propagation rate. A number of living systems operate better if excess monomer is present. A possible explanation is that the living end is stabilized by complexation with monomer [34]. Large counterions tend to be more effective than small counterions in living polymerization systems even when the ionic center is only indirectly involved.
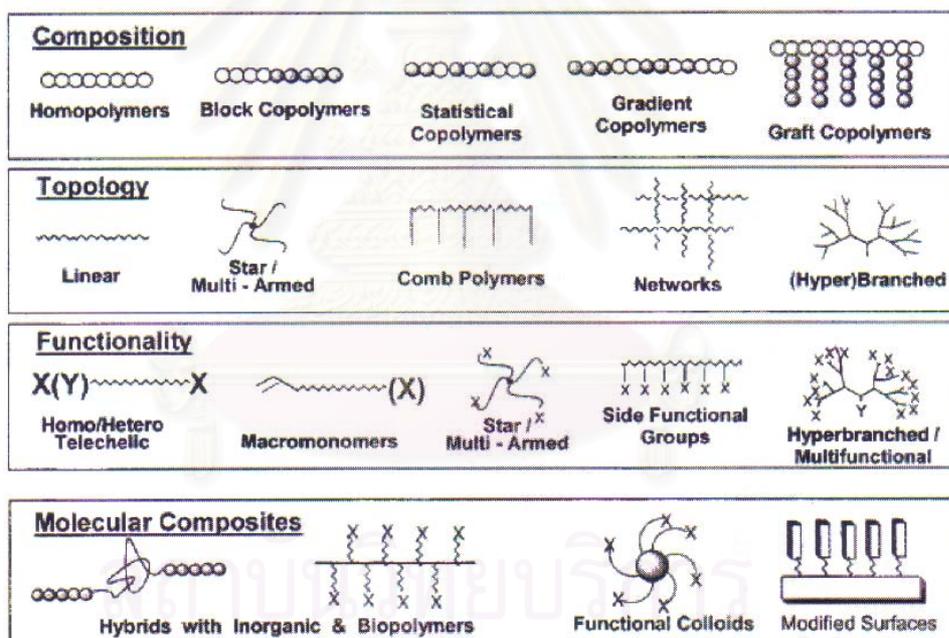
Figure 2.8 Architectural forms of polymers available by living polymerization techniques.

In this research, free radical process for living polymerization is selected and described. The concept of using stable free radicals, such as nitroxides, to reversibly react with the growing polymer radical chain end can be traced back to the pioneering work of Rizzardo and Mozd [35]. After further refinement by Georges [36], the basic blueprint for all subsequent work in the area of "living" free radical polymerization

was developed. Subsequently, the groups of Sawamoto [37], Matyjaszewski [38], Percec [39] and others [40-41] have replaced the stable nitroxide free radical with transition metal species to obtain a variety of copper-, nickel-, or ruthenium-mediated "living" free radical systems. These systems were called atom transfer radical polymerization (ATRP). This mechanism is an efficient method for carbon-carbon bond formation in organic synthesis. In some of these reactions, a transition-metal catalyst acts as a carrier of the halogen atom in a reversible redox process (Figure 2.5). Initially, the transition-metal species, M_t^n, abstracts halogen atom X from the organic halide, RX, to form the oxidized species, $M_t^{n+1}X$, and the carbon-centered radical $R^\bullet$. In the subsequent step, the radical $R^\bullet$ participates in an inter- or intramolecular radical addition to alkene, Y, with the formation of the intermediate radical species, $RY^\bullet$. The reaction between $M_t^{n+1}X$ and $RY^\bullet$ results in a target product, RYX, and regenerates the reduced transition-metal species, M_t^n, which further promotes a new redox process. The fast reaction between $RY^\bullet$ and $M_t^{n+1}X$ apparently suppresses biomolecular termination between alkyl radicals and efficiently introduces a halogen functional group X into the final product in good to excellent yields.
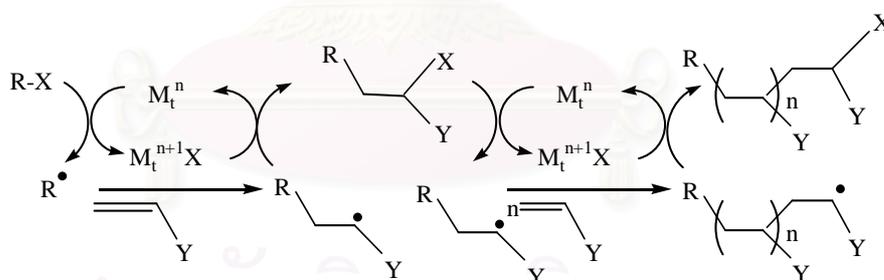
Figure 2.9 Mechanism of ATRP.

The ATRP system relies on one equilibrium reaction in addition to the classical free-radical polymerization scheme (Figure 2.10). In this equilibrium, a dormant species, RX, reacts with the activator, M_t^n, to form a radical $R^\bullet$ and deactivating species, $M_t^{n+1}X$. The activation and deactivation rate parameters are k_{act} and k_{deact}, respectively. Since deactivation of growing radicals is reversible, control over the molecular weight distribution and, in the case of copolymers, over chemical composition can be obtained if the equilibrium meets several requirements [42-43].

1. The equilibrium constant, k_{act}/k_{deact}, must be low in order to maintain a low stationary concentration of radicals. A high value would result in a high stationary radical concentration, and as a result, termination would prevail over reversible deactivation.

2. The dynamics of the equilibrium must be fast; i.e. deactivation must be fast compared to propagation in order to ensure fast interchange of radicals in order to maintain a narrow molecular weight distribution.

$$R\text{-}X \quad + \quad M_t^n \quad \xrightleftharpoons[k_{deact}]{k_{act}} \quad R^\bullet \quad + \quad M_t^{n+1}X$$
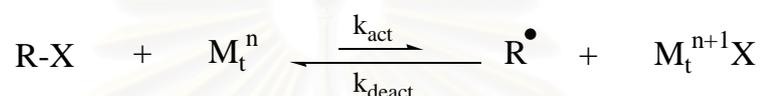
Figure 2.10 Equilibrium reaction in ATRP [44].

Transition metal complexes (catalyst) are perhaps the most important components of ATRP. It is the key to ATRP since it determines the position of the atom transfer equilibrium and the dynamics of exchange between the dormant and active apecies. There are several prerequisites for an efficient transition metal catalyst. First, the metal center must have at least two readily accessible oxidation states separated by one electron. Second, the metal center should have reasonable affinity toward a halogen. Third, the coordination sphere around the metal should be expandable upon oxidation to selectively accommodate a (pseudo)-halogen. Fourth, the ligand should complex the metal relatively strongly. Eventually, the position and dynamics of the ATRP equilibrium should be appropriate for the particular system. A variety of transition-metal complexes have been studied as ATRP catalysts.

Copper catalysts are superior in ATRP in terms of versatility and cost. Styrenes, (meth)acrylate esters and amides, and acrylonitrile have been successfully polymerized using copper-mediated ATRP. Examples of copper complexes used in ATRP are shown in Figure 2.11.
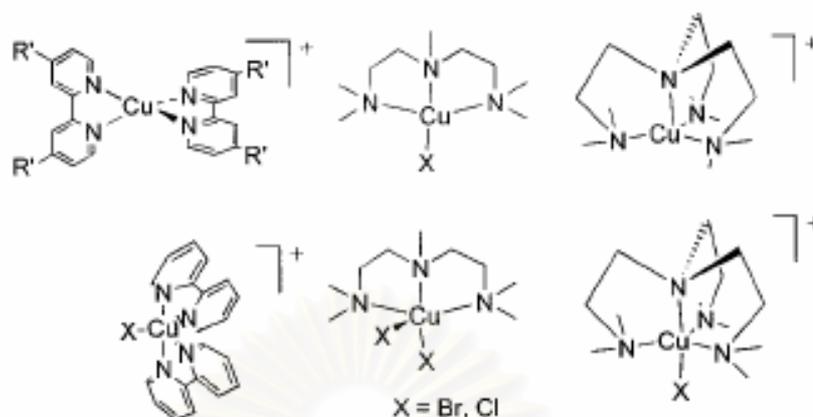
Figure 2.11 Copper complexes used as ATRP catalysts [45].

Nitrogen ligands have been used in copper-mediated ATRP. The monodentate (e.g., N(nBu)3), bidentate(e.g., dNbpy), and multidentate nitrogen ligands have been applied to copper-based ATRP. The electronic and steric effects of the ligands are important. Reduced catalytic activity or efficiency is observed when there is excessive steric hindrance around the metal center or the ligand has strongly electron-withdrawing substituents. A recent survey summarized different ligands employed in copper-mediated ATRP. The effect of the ligands and guidelines for ligand design were reviewed. Activity of N-based ligands in ATRP decreases with the number of coordinating sites N4 > N3 >N2, N1 and with the number of linking C-atoms C2 > C3, C4. It also decreases in the order R_2N- ≈ PyrEnDash-> R-N= > Ph-N=> Ph-NR-. Activity is usually higher for bridged and cyclic systems than for linear analogues. Examples of some N-based ligands used successfully in Cu-based ATRP are shown in Figure 2.12.

Figure 2.12 Example of ligands used in copper-mediated ATRP [45].

In 1995, Matyjaszewski has described the use of Cu^IX (X = Br, Cl) with 2,2'-bipyridine (bpy) as a "solubilizing" ligand. The active species has been described as "CuBr·bpy". This system is active toward styrene, acrylates, and methacrylates under the appropriate condition [38]. Percec has also described the role of bpy as partially solubilizing the Cu(I)/Cu(II) catalyst [26]. The role of the bpy is to co-ordinate to Cu(I) to give a *pseudo*-tetrahedral Cu(I) center in solution (Figure 2.13).

Figure 2.13 Rotation of the bpy ligands from the tetrahedral and co-ordination of halide at the Cu center.

Furthermore, in 1997 Matyjaszewski and coworkers [46] have described the use of simple amines as ligands for the copper mediated atom transfer radical polymerization (ATRP) of styrene, methyl acrylate and methyl methacrylate. The simple amines are of interest in ATRP for three general reasons. First, most of the simple amines are less expensive, more accessible and more tunable than 2,2'-

bipyridine (bpy) ligands. Second, due to the absence of the extensive π-bonding in the simple amines, the subsequent copper complexes are less colored. Third, since the coordination complexes between copper and simple amines tend to have lower redox potentials than the copper-bipy complex, the employment of simple amines as the ligand in ATRP may lead to faster polymerization rates. The example of simple amine ligand is *N,N,N',N'',N''*-pentamethyldiethylenetriamine (PMDETA). When this ligand was empolyed in ATRP, all the polymerizations were well controlled with a linear increase of molecular weights with conversion and relatively low polydispersities throughout the reactions. The rate of polymerization showed a significant increase, as compared to the corresponding bipy system. The higher polymerization rate of PMDETA as the ligand is partially attributed to the lower redox potential of the copper(I)-PMDETA complex than the copper(I)-bipy complex, which shifts the equilibrium from the dormant species toward the active species resulting in the generation of more radicals in the system. The structure of copper complex using PMDETA as the ligand was shown in Figure 2.14.
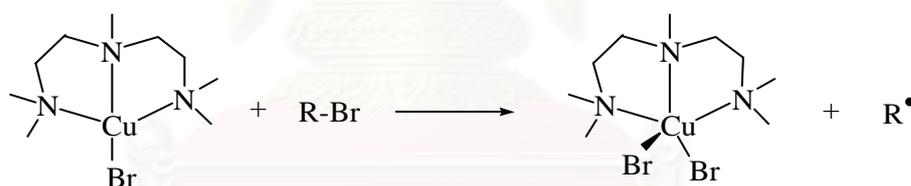
Figure 2.14 Proposed Cu(I) and Cu(II) species using PMDETA as a ligand [45].

2.4 Poly(acrylic acid)

Poly(acrylic acid) (PAA) is weak polyelectrolytes, in which the degree of ionization is governed by the pH and ionic strength of aqueous solution. PAA has been extensively investigated, owing to many scientific and industrial applications, such as intelligent environment-responsive surface [47] optical chemical sensing [48] and biomaterial carriers [49-50]. PAA can be covalently modified with a broad range of functional groups, such as fluorophores, electroactive groups, dyes and other biomolecules. Recent advances of the controlled/living polymerization techniques

made it possible to produce well-defined polymer structures, such as graft copolymers, star polymers, polymer brushes, etc. The interest in synthesis and characterization of such complex polymer systems containing acrylic acid segments has increased enormously.

For the synthesis of well-defined polymers, controlled/living polymerization techniques have been traditionally employed where the polymerizations proceed in the absence of irreversible chain transfer and chain termination. Controlled/living polymerization of acrylic acid by ATRP presents a challenging problem because the acid monomer can poison the catalysts in system of ATRP by coordinating to the transition metal. In addition, nitrogen containing ligands can be protonated, which interferes with the metal complexation ability. Thus, typically, protected monomers have been employed, followed by a polymer-analogous deprotection, e.g. hydrolysis of protecting ester groups. Protected monomers with masked acid groups involve *tert*-butyl acrylate (*t*BuA), *tert*-butyl methacrylate (*t*BuMA), trimethylsilyl methacrylate (TMSMA), benzyl methacrylate (BzMA), 2-tetrahydropyranyl methacrylate (THPMA) and *p*-nitrophenyl methacrylate (PNPMA) (Figure 2.15). After acid hydrolysis, thermolysis, or catalytic hydrogenolysis, these protective groups liberate their original acid functionality. Essential prerequisites for the protected monomer are good 'livingness' under each polymerization condition and selective deprotection under mild conditions.
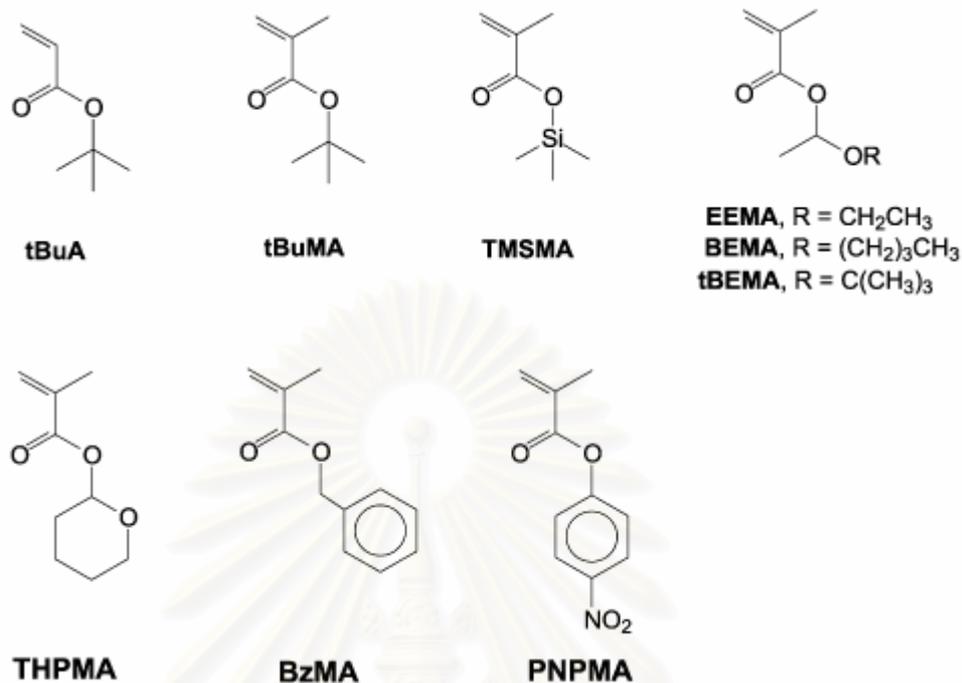
Figure 2.15 Representative examples of protected (meth)acrylic acid monomers with masked acid group.

For the ATRP system, Matyjaszewski et al [51-52] reported controlled polymerization of *t*BuA using methyl 2-bromopropionate, as the initiator and the CuBr/N,N,N$^{'}$,N$^{''}$,N$^{''}$-pentamethyldiethylenetriamine (PMDETA) catalyst system. In most ATRP based syntheses for block and further complex polymer systems, *t*BuA has been employed as a protected monomer, which may be due to the feasibility to control the polymerization and easy hydrolysis.

Recently, branched polyelectrolytes have become of special interest because of their industrial importance and scientifically interesting properties [53]. Due to their different topologies, branched and linear polyelectrolytes should have quite different properties, especially distribution of counterions [54]. Variation in the degree of branching (DB) leads to a continuous change in the properties of branched macromolecules from linear chains to soft nanoparticles with highly compact structures. The recent discovery of self-condensing vinyl polymerization (SCVP) made it possible to use vinyl monomers for a convenient, one-pot synthesis of hyperbranched vinyl polymers with DB ≤ 0.5. Initiator-monomers ('inimers') are used

of the general structure AB*, where the double bond is designated. A and B* is a group capable of being activated to initiate the polymerization of vinyl groups [55] Cationic [56], anionic [57], group transfer [58], controlled radical [59-63], and ring-opening mechanisms [64] have been used. By copolymerizing AB* inimers with conventional monomers, this technique was extended to self-condensing vinyl copolymerization (SCVCP), leading to highly branched copolymers with DB controlled by the comonomer ratio [65-68]. The copolymerization method is a facile approach to obtain functional branched polymers since the DB and MW can be modified easily by a suitable choice of the comonomer ratio in the feed.

The synthesis of randomly branched PAA was conducted by SCVCP of tBuA with an inimer having an acrylate (A) and an α-bromopropionate group (B*), capable to initiate ATRP, followed by hydrolysis of the *tert*-butyl groups [69]. Characterization of the branched Pt BuAs was conducted by multi-detector GPC and NMR analysis, demonstrating that DB, the composition, MW, and MWD can be adjusted by an appropriate choice of the catalyst system, the comonomer composition in the feed, and the polymerization conditions. The water solubility of the branched PAAs decreases with increasing DB and decreasing pH. Aqueous-phase GPC and dynamic light scattering confirm the compact structure of the randomly branched PAAs. Studies at different pH indicate that a marked stretching of the branched chains takes place when going from a virtually uncharged to a highly charged stage.

PAA chains attached to planar and spherical surfaces have recently attracted much interest as academic model systems and as candidates for various industrial applications such as sensing, cellular engineering, and corrosion inhibition, due to an extremely high density of functional groups at the surface. Surface-grafted PAA has been also synthesized by 'grafting from' techniques via conventional radical polymerization [70], achieving higher grafting density. Surface-initiated SCVCP via ATRP has been applied as a facile, one-pot synthesis of branched PtBuA grafted from a surface (Scheme 2.4) [71]. Because both the initiator-monomer ('inimer') and the functionalized silicon wafer with an ATRP initiator layer have groups capable of initiating the polymerization of vinyl groups, the chain growth can be started from both the initiators immobilized on the silicon wafer, and an α-bromopropionate group

in the inimer. The one-step SCVCP of the inimer with a comonomer (*t*-BuA) via ATRP from the surface gave a branched P*t*BuA with characteristic surface topography, which may be due to the branched architectures. The surface topography, branched structure, film thickness, and surface functionality (bromine content) could be modified easily by a suitable choice of the comonomer ratio in the feed and polymerization method. Hence, this method is a novel and convenient approach towards the preparation of smart interfaces.

Surface-initiated SCVCP of an acrylic AB* inimer with *t*BuA from silica nanoparticles functionalized with monolayers of ATRP initiators has been employed as a new method for the synthesis of branched P*t*BuA–silica hybrid nanoparticles [72]. Well-defined polymer chains were grown from the surface to yield nanoparticles comprised of silica cores and branched P*t*BuA shells. Hydrolysis of the ester functionality created branched PAAs grafted on silica nanoparticles. The chemical composition and the architectures of the branched PAAs grafted on the silica nanoparticles were controlled by composition in the feed during the SCVCP. Chain growth of *t*BuA from the surface via ATRP yielded linear P*t*BuA grafted on the silica nanoparticles. These methodologies can be applied to a wide range of inorganic materials for surface-initiated SCVCP to allow the preparation of new 3D branched polyelectrolyte/inorganic hybrid materials.
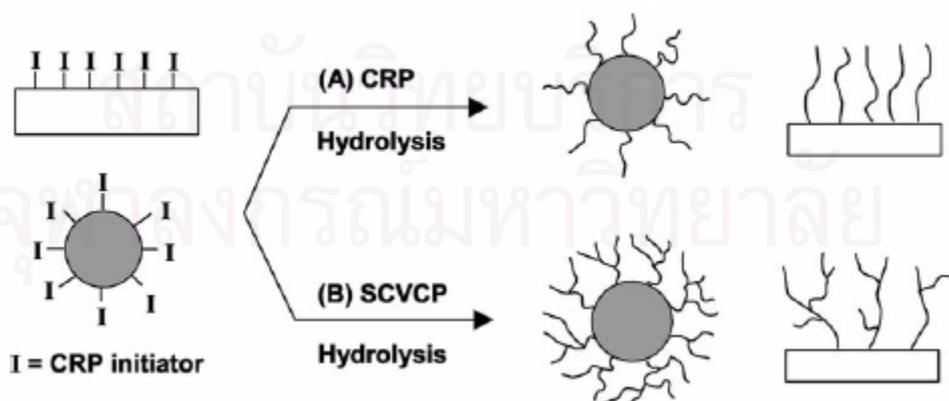
Scheme 2.4 Synthesis of surface-grafted linear and branched PAAs (or their precursors) by (A) CRP and (B) SCVCP from planar surfaces and spherical particles

Boyes and coworkers [73] synthesize diblock copolymer polyelectrolyte brushes of either polystyrene (PS) or poly(methyl acrylate) (PMA) and poly(acrylic acid) (PAA) by ATRP. The polyelectrolyte diblock copolymer brushes were used for the synthesis of metal nanoparticles by treatment the PAA with aqueous metal salt subsequent reduction of the treated PAA.

In 2004, Kai Qi and coworkers [74] used polymer brushes as functional thin film. The functionalized polymer brushes was prepared *via* surface initiated, nitroxide mediated, free radical polymerization (NMP). By using a novel biotinylated alkoxyamine, biotin units were incorporated to the polymer chain termini *via* nitroxide exchange chemistry. The biotin units at the end of polymer brushes were shown to be bio-available and binding underwent with their protein receptors, streptavidin.

2.5 Characterization techniques

2.5.1 Gel Permeation Chromatography [75]

Gel permeation chromatography, more correctly termed *size exclusion chromatography,* is a separation method for high polymers, similar to but advanced in practice over *gel filtration* as carried out by biochemists, that has become a prominent and widely used method for estimating molecular-weight distributions since its discovery just over two decades ago in 1961. The separation takes place in a chromatographic column filled with beads of a rigid porous "gel"; highly cross-linked porous polystyrene and porous glass are preferred column-packing materials. The pores in these gels are of the same size as the dimensions of polymer molecules.

A sample of a dilute polymer solution is introduced into a solvent stream flowing through the column. As the dissolved polymer molecules flow past the porous beads, they can diffuse into the internal pore structure of the gel to an extent depending on their size and the pore-size distribution of the gel. Larger molecules can enter only a small fraction of the internal portion of the gel, or are completely

excluded; smaller polymer molecules penetrate a larger fraction of the interior of the gel. The larger the molecule, therefore, the less time it spends inside the gel, and the sooner it flows through the column. The different molecular species are eluted from the column in order of their molecular size as distinguished from their molecular weight, the largest emerging first.

A complete theory predicting retention times or volumes as a function of molecular size has not been formulated for gel permeation chromatography. A specific column or set of columns (with gels of different pore sizes) is calibrated empirically to give such a relationship, by means of which a plot of amount of solute versus retention volume can be converted into a molecular-size-distribution curve.

As in all chromatographic processes, the band of solute emerging from the column is broadened by a number of processes, including contributions from the apparatus, flow of the solution through the packed bed of gel particles, and the permeation process itself. Corrections for this zone broadening can be made empirically; it usually becomes unimportant when the sample has $\overline{M}_w/\overline{M}_n > 2$.

Gel permeation chromatography is extremely valuable for both analytic and preparative work with a wide variety of systems ranging from low to very high molecular weights. The method can be applied to a wide variety of solvents and polymers, depending on the type of gel used. With polystyrene gels, relatively nonpolar polymers can be measured in solvents such as tetrahydrofuran, toluene, or (at high temperatures) o-dichlorobenzene; with porous glass gels, more polar systems, including aqueous solvents, can be used. A few milligrams of sample suffices for analytic work, and the determination is complete in as short a time as a few minutes using modern high-pressure, high-speed equipment.

The results of careful gel permeation chromatography experiments for molecular-weight distribution agree so well with results from other techniques that there is serious doubt as to which is correct when residual discrepancies occur.
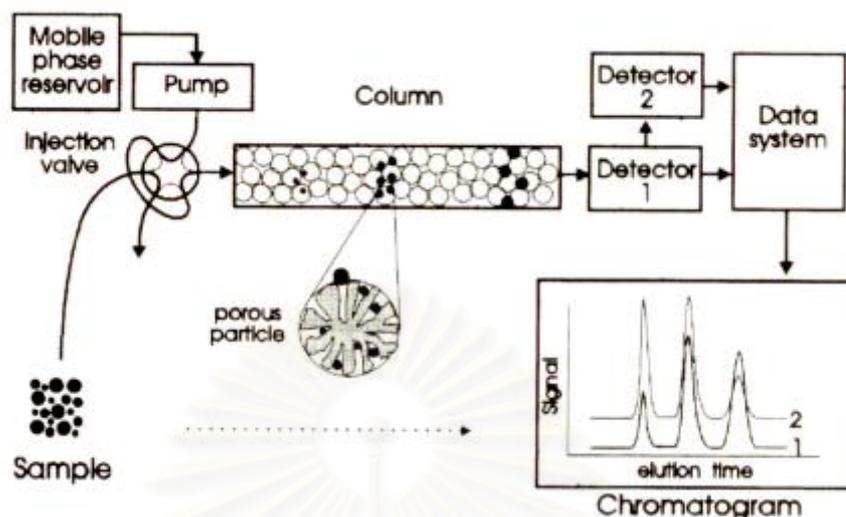
Figure 2.16 Schematic representation of the gel permeation chromatography.

2.5.2 Ellipsometry [76]

Ellipsometry is a sensitive optical technique for determining properties of surfaces and thin films. If linearly polarized light of a known orientation is reflected at oblique incidence from a surface then the reflected light is elliptically polarized. The shape and orientation of the ellipse depend on the angle of incidence, the direction of the polarization of the incident light, and the reflection properties of the surface. Ellipsometry measures the polarization of the reflected light with a quarter-wave plate followed by an analyzer; the orientations of the quarter-wave plate and the analyzer are varied until no light passes though the analyzer. From these orientations and the direction of polarization of incident light are expressed as the relative phase change, Δ, and the relative amplitude change, Ψ, introduced by reflection from the surface. These values are related to the ratio of Fresnel reflection coefficients, R_p and R_s for p and s- polarized light, respectively.

$$\text{Tan}(\Psi)\,e^{i\Delta} = \frac{R_p}{R_s} \tag{2.2}$$

An ellipsomer measures the changes in the polarization state of light when it is reflected from a sample. If the sample undergoes a change, for example, a thin film on the surface changes its thickness, then its reflection properties is also changed. Measuring these changes in the reflection properties allow us to deduce the actual change in the film's thickness.
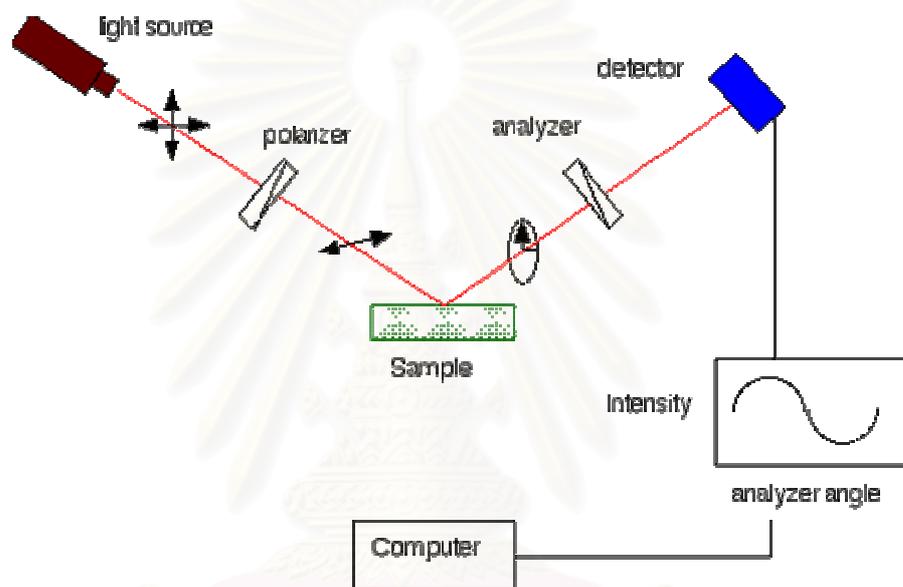
Figure 2.17 Schematic of the geometry of an ellipsometry experiment.

2.5.3 Contact angle measurement [77]

Contact angle measurements are often used to assess changes in the wetting characteristics of a surface and hence indicate a change in surface energy. The technique is based on the three-phase boundary equilibrium described by Young's equation.
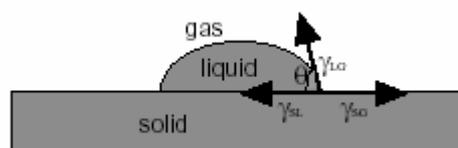
Figure 2.18 Schematic representation of the Young's equation.

$$\gamma_{LG}\cos\theta = \gamma_{SG} - \gamma_{SL} \tag{2.3}$$

where γ_{LG}, γ_{SG} and γ_{SL} are the interfacial tension between the phases with subscripts L, G, S corresponding to liquid, gas, and solid phase respectively and θ refers to the equilibrium contact angle. The Young's equation applies for a perfectly homogeneous atomically flat and rigid surface and therefore supposes many simplifications. In the case of real surfaces, the contact angle value is affected by surface roughness, heterogeneity, vapor spreading pressure, and chemical contamination of the wetting liquid. Although the technique to measure contact angles is easy, data interpretation is not straightforward and the nature of different contributions to the surface is a matter of discussion. Generally, we can define the complete wetting, wetting, partial wetting, and nonwetting according to Figure 2.19.
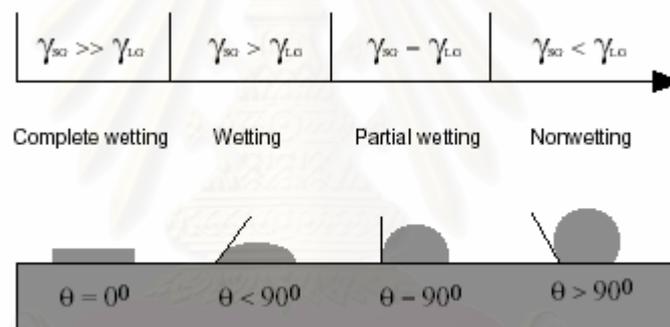
Figure 2.19 Schematic representation of wettability.

2.5.4 Atomic force microscopy (AFM) [78]

AFM is a type of scanning probe microscopy, allowing three-dimensional topographical imaging of surface. The AFM probe is in physical contact with the surface as it moves over the sample. Because it may be used on any surface, AFM is much more suited to polymer surface analysis. The essential features of AFM are shown in Figure 2.20. The tip of the probe, which is commonly made of silicon nitride, is attached to a cantilever bearing a reflective surface upon which is a laser beam is directed. The sample is mounted on a piezoelectric support, which moves in response to surface variations sensed by the probe. As the tip is scanned (or "rastered") over the surface, topological variations cause deflections in the cantilever

that are monitored by recording the path of the reflected laser beam. A computer interprets the deflections as a three-dimensional profile of the polymer surface with resolution in the angstrom range, which is several orders of magnitude better than that obtained by SEM.
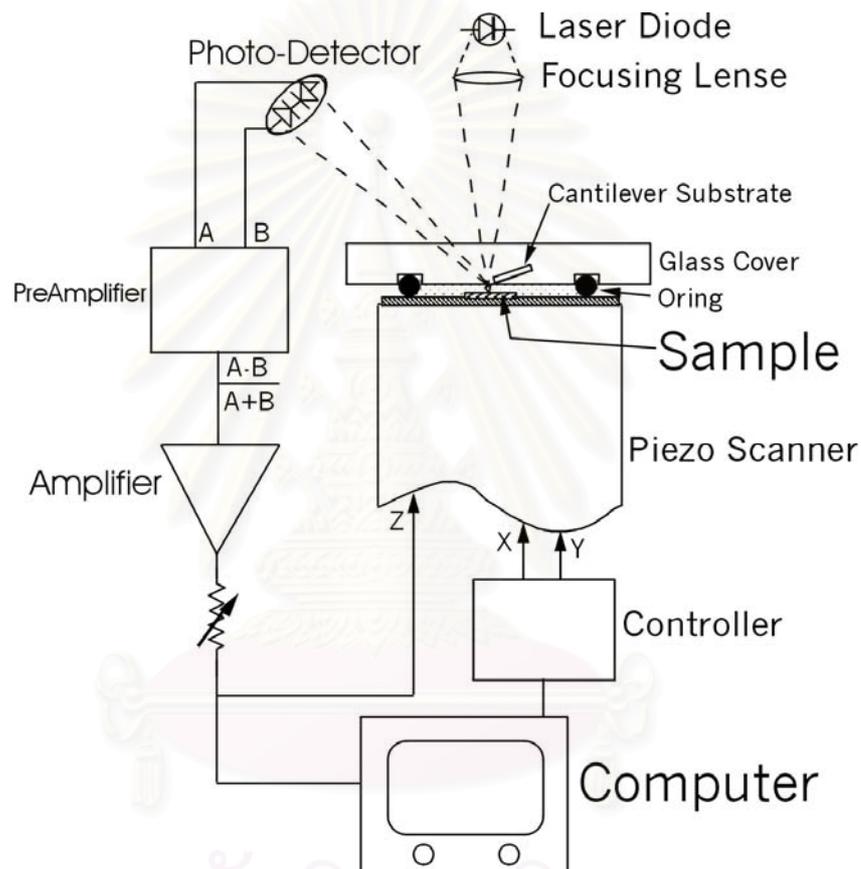
Figure 2.20 Schematic diagram of an atomic force microscope.

The Atomic Force Microscope (AFM) is being used to solve processing and materials problems in a wide range of technologies affecting the electronics, telecommunications, biological, chemical, automotive, aerospace, and energy industries. The materials being investigated include thin and thick film coatings, ceramics, composites, glasses, synthetic and biological membranes, metals, polymers, and semiconductors. The AFM is being applied to studies of phenomena such as abrasion, adhesion, cleaning, corrosion, etching, friction, lubrication, plating, and polishing. By using AFM, one cannot only image the surface in atomic resolution but

also measure the force at nano-newton scale. The publications related to the AFM are growing speedily since its birth.

The first AFM was made by meticulously gluing a tiny shard of diamond onto one end of a tiny strip of gold foil. In 1985 Binnig and Gerber used the cantilever to examine insulating surfaces. A small hook at the end of the cantilever was pressed against the surface while the sample was scanned beneath the tip. The force between tip and sample was measured by tracking the deflection of the cantilever. This was done by monitoring the tunneling current to a second tip positioned above the cantilever. They could delineate lateral features as small as 300 Å. The force microscope emerged in this way. In fact, without the breakthrough in tip manufacture, the AFM probably would have remained a curiosity in many research groups. It was Albrecht, a fresh graduate student, who fabricated the first silicon microcantilever and measured the atomic structure of boron nitride. Today the tip-cantilever assembly typically is microfabricated from Si or Si_3N_4. The era of AFM came finally when the Zurich group released the image of a silicon (111) 7X7 pattern. The world of surface science knew that a new tool for surface microscope was at hand. After several years the microcantilevers have been perfected, and the instrument has been embraced by scientists and technologists.

The force between the tip and the sample surface is very small, usually less than 10^{-9} N. How to monitor such small forces is another story. The detection system does not measure force directly. It senses the deflection of the microcantilever. The detecting systems for monitoring the deflection fall into several categories. The first device introduced by Binnig was a tunneling tip placed above the metallized surface of the cantilever. This is a sensitive system where a change in spacing of 1 Å between tip and cantilever changes the tunneling current by an order of magnitude. It is straightforward to measure deflections smaller than 0.01 Å. Subsequent systems were based on the optical techniques. The interferometer is the most sensitive of the optical methods, but it is somewhat more complicated than the beam-bounce method which was introduced by Meyer and Amer. The beam-bounce method is now widely used as a result of the excellent work by Alexander and colleagues. In this system an optical beam is reflected from the mirrored surface on the back side of the cantilever onto a

position-sensitive photodetector. In this arrangement, a small deflection of the cantilever will tilt the reflected beam and change the position of beam on the photodetector. A third optical system introduced by Sarid uses the cantilever as one of the mirrors in the cavity of a diode laser. Motion of the cantilever has a strong effect on the laser output, and this is exploited as a motion detector

The principles on how the AFM works are very simple. An atomically sharp tip is scanned over a surface with feedback mechanisms that enable the piezo-electric scanners to maintain the tip at a constant force (to obtain height information), or height (to obtain force information) above the sample surface. Tips are typically made from Si_3N_4 or Si, and extended down from the end of a cantilever. The nanoscope AFM head employs an optical detection system in which the tip is attached to the underside of a reflective cantilever. A diode laser is focused onto the back of a reflective cantilever. As the tip scans the surface of the sample, moving up and down with the contour of the surface, the laser beam is deflected off the attached cantilever into a dual element photodiode. The photodetector measures the difference in light intensities between the upper and lower photodetectors, and then converts to voltage. Feedback from the photodiode difference signal, through software control from the computer, enables the tip to maintain either a constant force or constant height above the sample. In the constant force mode, the piezo-electric transducer monitors real time height deviation. In the constant height mode, the deflection force on the sample is recorded. The latter mode of operation requires calibration parameters of the scanning tip to be inserted in the sensitivity of the AFM head during force calibration of the microscope.

Some AFM's can accept full 200 mm wafers. The primary purpose of these instruments is to quantitatively measure surface roughness with a nominal 5 nm lateral and 0.01nm vertical resolution on all types of samples. Depending on the AFM design, scanners are used to translate either the sample under the cantilever or the cantilever over the sample. By scanning in either way, the local height of the sample is measured. Three dimensional topographical maps of the surface are then constructed by plotting the local sample height versus horizontal probe tip position.

The concept of resolution in AFM is different from radiation based microscopies because AFM imaging is a three dimensional imaging technique. The ability to distinguish two separate points on an image is the standard by which lateral resolution is usually defined. There is clearly an important distinction between images resolved by wave optics and scanning probe techniques. The former is limited by diffraction, and later primarily by apical probe geometry and sample geometry. Indeed, many authors have seen that it is the radius of curvature that significantly influences the resolving ability of the AFM. Even greater improvements in resolution have been attained with Tapping mode but contact imaging still is capable of high resolution imaging. The brief discussion on resolution was published by Keller

In order to obtain good AFM results, the vibration isolation platform is needed. The vibration isolation consists of a large mass attached to bungy cords firmly anchored to the building. Damping of the oscillation is believed to result from rubbing of the rubber fibres inside of the bungy cord against the outside lining material. Between the low resonance frequency of the bungy cord system and the high resonance frequency of the microscope hardware itself (>10 kHz), the AFM effectively comprises a band pass filter. This allows the microscopists to safely image their samples in the intermediate range of about 1-100 Hz and obtain atomic resolution.

CHAPTER III

EXPERIMENTAL

3.1 Materials

All reagents and materials are analytical grade

1. Acrylic acid 2-hydroxyethyl ester	: Fluka
2. (+)-biotinyl-3,6,9-trioxaundecanediamine	: Bioactive
3. 2-Bromo-2-methylpropionyl bromide	: Fluka
4. 2-Bromo-2-propionyl bromide	: Fluka
5. *tert*-Butyl acrylate	: Aldrich
6. Copper (I) bromide	: Fluka
7. Dichloromethane	: Merck
8. Dimethoxyethane	: Fluka
9. 1-(3-Dimethylaminopropyl)-3-ethylcarbodiimide hydrochloride	: Fluka
10. Ethanol	: Merck
11. Ethoxydimethylsilane	: Gelest
12. Ethyl acetate	: Merck
13. Ethyldiisopropylamine	: Fluka
14. Hexane	: Merck

15. Hydrogen hexachloroplatinate (IV) hexahydrate : Aldrich

16. Hydrogen peroxide   : Univar

17. *N*-Hydroxysuccinimide   : Fluka

18. Magnesium sulfate anhydrous   : Unilab

19. Methanol   : Merck

20. *N, N, N′, N″, N″*-pentamethyldiethylenetriamine : Aldrich

21. Propan-1-ol   : Univar

22. Pro-2-en-1-ol   : Merck

23. Silica gel 60 (0.063-0.200 mm)   : Merck

24. Silicon wafer (Single-sided)   : Siltron Inc. Korea

25. Sodium dodecyl sulfate   : Fluka

26. Sodium sulfate anhydrous   : Fluka

27. Streptavidin, fluorescein conjugated   : Bioactive

28. Sulfuric acid   : Merck

29. Tetrahydrofuran   : Carlo

30. Toluene   : Carlo

31. Triethylamine   : Carlo

32. Trifluoroacetic acid   : Fluka

33. Toluene anhydrous 99 %   : Aldrich

34. Ultrapure distilled water   : Mill-Q Lab system

3.2 Equipments

3.2.1 Ellipsometry

The ellipsometry was studied by using Gaertner Ellipsometer L117. The thicknesses were determined in air with a 70° of incidence angle at 632.8 nm. The thickness of the adsorbed film was calculated by using the software "Dafibm" Rudolph Research, Double Absorbing Films Calculations. The calculation was based on a refractive index $N_{initiator}$ = 1.443, $N_{t\text{-}BuA}$ = 1.460, $N_{hydroxyl}$ = 1.462 and a silicon substrate refractive index $N_{substrate}$ = 3.858. At least five different locations on each sample were measured and the average thickness was calculated.

3.2.2 Nuclear magnetic resonance spectroscopy (NMR)

The ^{1}H NMR spectra was recorded in $CDCl_3$ using Varian, model Mercury-400 nuclear magnetic resonance spectrometer operating at 400 MHz. Chemical shifts (δ) are reported in part per million (ppm) relative to tetramethylsilane (TMS) or using the residual protonated solvent signal as a reference.

3.2.3 Fourier transform infrared (FT-IR)

The FT-IR spectra were recorded with a FT-IR spectrometer (Perkin Elmer), model system 2000, with 32 scans at resolution 4 cm^{-1}. A frequency of 400-4000 cm^{-1} was collected by using TGS detector. The sample containing silica particles were prepared as KBr pellets.

3.2.4 Contact angle measurements

Contact angle goniometer model 100-00 and a Gilmont syringe with a 24-gauge flat-tipped needle (Ramé-Hart, Inc., USA) was used for the determination of water contact angles. The measurements were carried out in air at the room temperature. Dynamic advancing and receding angles were recorded while water was added to and withdrawn from the drop, respectively. The reported angle is an average of 5 measurements on different area of each sample.

3.2.5 Atomic force microscopy (AFM)

AFM images were recorded with Atomic Force Microscope model SPI-3800, Seiko I, Tokyo, Japan. Measurements were performed in air using tapping mode. Silicon nitride tip with a resonance frequency of 13 kHz and a spring constant 0.02-0.1 N/m were used.

3.2.6 Gel permeation chromatography (GPC)

The molecular weight and molecular weight distributions of the PtBuA homopolymer and copolymer were determined by gel permeation chromatography (GPC) using THF as eluent, Water E600 column connected to the RI detector. The flow rate was 1 mL/min. Narrow PS standards were used for the calibration curve. In case of the PAA, aqueous gel permeation chromatogram obtained from Water 600 controller chromatograph equipped with ultrahydrogel linear and guard column at 30 °C. Water was used as eluent with the flow rate of 0.6 mL/min. Poly(ethylene glycol)(PEG) was used standards for calibration. The molecular weight as determined by a reflactive index detector, waters 2410.

3.2.7 UV-spectroscopy

UV spectroscopy Model Techna, specgene was used for determination the amount of carboxylic groups of poly(acrylic acid) brushes on surface by reading the absorbance at 633 nm.

3.3 Synthesis of α-bromoester to be used as initiator

3.3.1 Synthesis of 2-bromo-2-methylpropionic acid allyl ester (1)

Prop-2-en-1-ol   2-Bromo-2-methylpropionyl bromide   2-Bromo-2-methylpropionic acid allyl ester

(1)

To a solution of 1.70 mL (25 mmol) of prop-2-en-ol in 25 mL of dry tetrahydrofuran, pyridine 2.1 mL (26.5 mmol) was added, followed by a dropwise addition of 2-bromo-2-methylpropionyl bromide (3.10 mL, 25 mmol). The mixture was stirred at room temperature overnight and then diluted with hexane and then washed once with 2N HCl and twice with deionized water. The organic phase was dried over sodium sulfate and filtered. The solvent was removed from the filtrate under reduced pressure, the colorless oily residue was purified by filtering through a silica gel column chromatography to give the product in 90% yield.

^{1}**H NMR (CDCl$_3$) of (1):** δ 1.98 (6H, C(C$\underline{H}_3$)$_2$, s), 4.71 (2H, OC$\underline{H}_2$, d, J = 5.46 Hz), 5.30-5.44 (2H, =C$\underline{H}_2$, complex m), 5.93-6.0 (1H, =C$\underline{H}$, complex m).

3.3.2 Synthesis of 2-bromo-2-methylpropionic acid 3-(ethoxydimethyl silanyl)propyl ester (2)

Ethoxydimethyl silane   2-Bromo-2-methylpropionic acid allyl ester   2-Bromo-2-methylpropionic acid 3-(ethoxydimethylsilanyl)propyl ester

(1)   **(2)**

To a solution of the alkene derivative (1) (2.07 g, 10 mmol) in ethoxydimethylsilane (1.2 mL, 10 mmol), a 1:1 ethanol/dimethoxyethane solution of chloroplatinic acid, H_2PtCl_6 (1.1 mg, 0.2 mL) was added. The reaction mixture was stirred at room temperature under nitrogen in the dark for 14 h. Dry toluene (3 mL) was then added and the excess ethoxydimethylsilane was removed under reduced pressure. Dry dichloromethane was added and then removed under reduced pressure. The crude product was passed through a short column of dry sodium sulfate, the column was washed with dry dichloromethane and the dichloromethane was removed under reduced pressure to give the desired product as a yellow viscous liquid (2) (2.17 g, 70 % yield).

^{1}H NMR (CDCl$_3$): δ 0.04 (6H, Si(C$\underline{H}_3$)$_2$, s), 0.931 (2H, OCH$_2$CH$_2$C$\underline{H}_2$, t, J = 7.04 Hz), 1.20 (3H, SiOCH$_2$C$\underline{H}_3$, t, J = 7.04 Hz), 1.66 (2H, OCH$_2$C$\underline{H}_2$CH$_2$, complex m), 1.90 (6H, C(C$\underline{H}_3$)$_2$, s), 3.69 (2H, SiOC$\underline{H}_2$CH$_3$, q, J = 7.04 Hz), 4.09 (2H, OC$\underline{H}_2$CH$_2$CH$_2$, t, J = 7.04 Hz).

3.3.3 Synthesis of 2-bromo-2-methylpropionic acid propyl ester as a "sacrificial" initiator (3)

| Propan-1-ol | 2-Bromo-2-methylpropionyl bromide | 2-Bromo-2-methylpropionic acid propyl ester (3) |
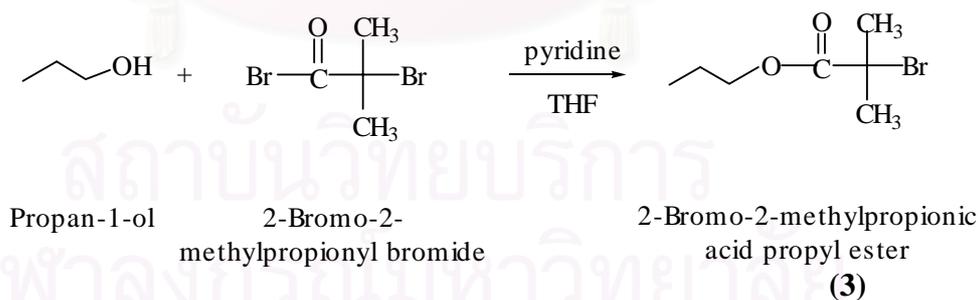
To a solution of propan-1-ol (1.5 g, 25 mmol) in 25 mL of tetrahydrofuran, pyridine (3.1 mL, 26.5 mmol) was added, followed by a dropwise addition of 2-bromo-2-methylpropionyl bromide (3.10 mL, 25 mmol). The mixture was stirred at room temperature overnight and then diluted with hexane and washed once with 2N HCl and twice with deionized water. The organic phase was dried over sodium sulfate and filtered. The solvent was removed from the filtrate under reduced pressure, and

the colorless oily residue was purified by filtering through a silica gel column chromatography to give the desired product in 90% yield.

^{1}H NMR (CDCl$_3$) of (3): δ 1.0 (3H, OCH$_2$CH$_2$C$\underline{H}_3$, t, J = 7.02 Hz), 1.72 (2H, OCH$_2$C$\underline{H}_2$CH$_3$, complex m), 1.95 (6H, C(C$\underline{H}_3$)$_2$, s), 4.15 (2H, OC$\underline{H}_2$CH$_2$CH$_3$, t, J = 6.24 Hz).

3.4 Synthesis of acrylic acid 2-(2-bromopropionyloxy)ethyl ester (BPEA) (4) to be used as comomomer for copolymerization of branched P(*t*BuA)

Acrylic acid 2-hydroxy ethyl ester   2-Bromopropionyl bromide   Acrylic acid 2-(2-bromo-propionyloxy) ethyl ester (BPEA)

(4)
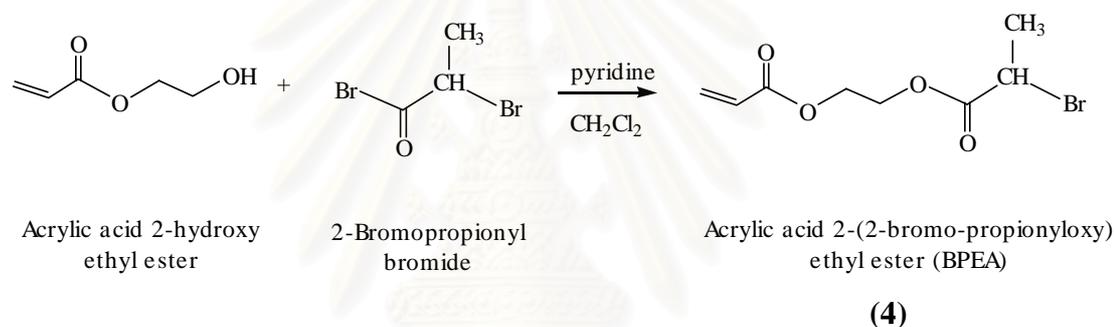
Under nitrogen, a solution of 2-bromopropionyl bromide (36.5 mL, 348 mmol) in 50 mL of CH$_2$Cl$_2$, was added dropwise to a stirring solution of acrylic acid 2-hydroxyethyl ester (40.0 mL, 348 mmol) and pyridine (31.0 mL, 383 mmol) in 250 mL of CH$_2$Cl$_2$. The reaction was cooled in an ice bath. During the addition, a white precipitate formed (pyridine-HBr). After the complete addition of 2-bromopropionyl bromide, 1 h, the reaction was stirred at room temperature for 3 h. The precipitate was then filtered. Additional precipitate and the yellow oil were obtained after CH$_2$Cl$_2$ was evaporated. The precipitate was filtered and washed with CH$_2$Cl$_2$. The oil and CH$_2$Cl$_2$ wash were combined and washed with water (50 mL, 3x) and then dried over MgSO$_4$ and treated with decolorizing carbon. The CH$_2$Cl$_2$ was evaporated to give the yellow oil. Distillation of the oil gave a colorless liquid.

^{1}H NMR (CDCl$_3$): δ 6.43 (1H, d), 6.14 (1H, dd), 5.89 (1H, d), 4.39 (5H, m), 1.82 (3H, d).

3.5 Pretreatment of silicon substrates

Silicon wafers were cut into 1.5 x 1.5 cm^2 substrates. The substrates held in a slotted hollow glass cylinder (custom designed holder) were put in a freshly prepared mixture of 7 parts of concentrated sulfuric acid and 3 parts of 30% hydrogen peroxide. Substrates were submerged in the solution at room temperature for 2 h, rinsed with five to seven aliquots of deionized water and placed in a clean oven at 120°C for 2 h. Silanization reaction was carried out immediately after treating the substrates in this fashion.

3.6 Preparation of surface grafted α-bromoester initiator (5)

(2)   (5)

Freshly cleaned silicon substrates were placed into a dried Schlenk tube, followed by anhydrous toluene (30 mL) containing 4 mmol (33 μl) of 2-bromo-2-methylpropionic acid 3-(ethoxydimethylsilanyl)propyl ester (2). Reactions were carried out under nitrogen atmosphere at ambient temperature for 18 h. The substrates were rinsed with 1x10 mL of toluene, 2x10 mL of 2-propanol, 2x10 mL of ethanol, 1x10 mL of ethanol-water (1:1), 1x10 mL of water, 1x10 mL of ethanol and 1x10 mL of water and dried under vacuum.

3.7 Preparation of polymer brushes

3.7.1 Surface-initiated homopolymerization of *tert*-butyl acrylate
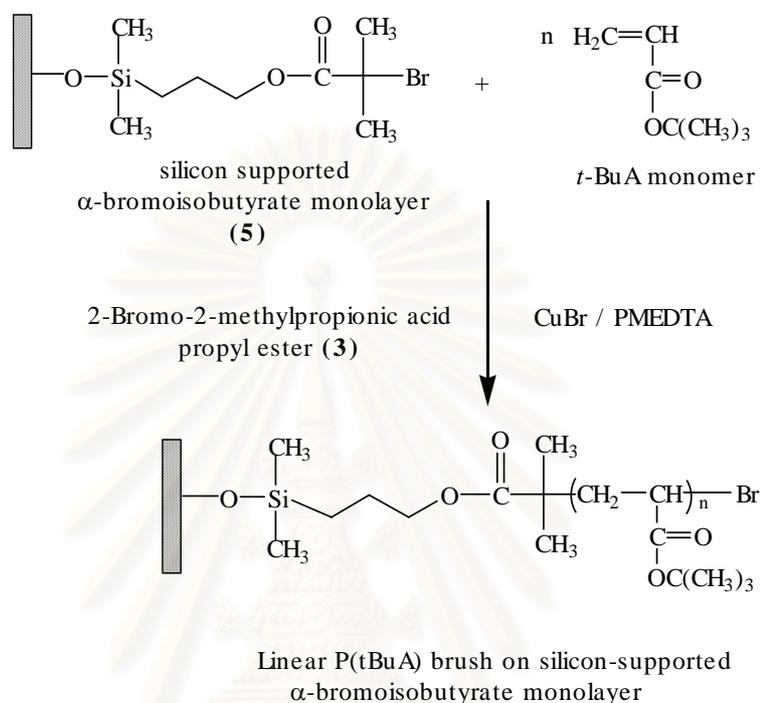
Silicon substrates were placed in a Schlenk flask and sealed with a rubber septum. The flask was evacuated and back-filled with nitrogen three times and left under a nitrogen atmosphere. CuBr (49.3 mg, 0.34 mmol), *t*BuA monomer (10 ml, 68 mmol), and acetone (15 mL) were added to a separate Schlenk flask with a magnetic stirrer bar, sealed with a rubber septum, and degassed by purging with nitrogen for 1 h. PMDETA (71.8 μL, 0.34 mmol) was added to the mixture via a syringe, and the solution was stirred 60°C until it became homogeneous (approximately 5 min). The solution was then transferred to the flask containing the silicon wafer via cannula, followed by the addition of "sacrificial" initiator (2-bromo-2-methylpropionic acid propyl ester (3), 71.8 mg, 0.34 mmol) via syringe. The polymerization was allowed to proceed at 60°C. After a set reaction time, the silicon substrates were removed and rinsed with THF. To remove untethered polymer, the silicon substrates were placed in a Soxhlet extractor and extracted with THF for 24 h and dried under vacuum. The substrates bearing polymer brushes were then analyzed by contact angle measurement, ellipsometry and AFM. Free polymer from the polymerization solution

was isolated by first evaporating residual monomer and solvent, dissolving in THF, and then passing the THF/polymer solution through a short column of silica to remove any residual catalyst and analyzed by GPC.

3.7.2 Surface-initiated copolymerization of *tert*-butyl acrylate and acrylic acid 2-(2-bromopropionyloxy)ethyl ester

silicon supported
α-bromoisobutyrate monolayer
(5)

t-BuA monomer

BPEA monomer (4)

CuBr/PMDETA

Branched P*t*BuA brush on silicon-supported
α-bromoisobutyrate monolayer
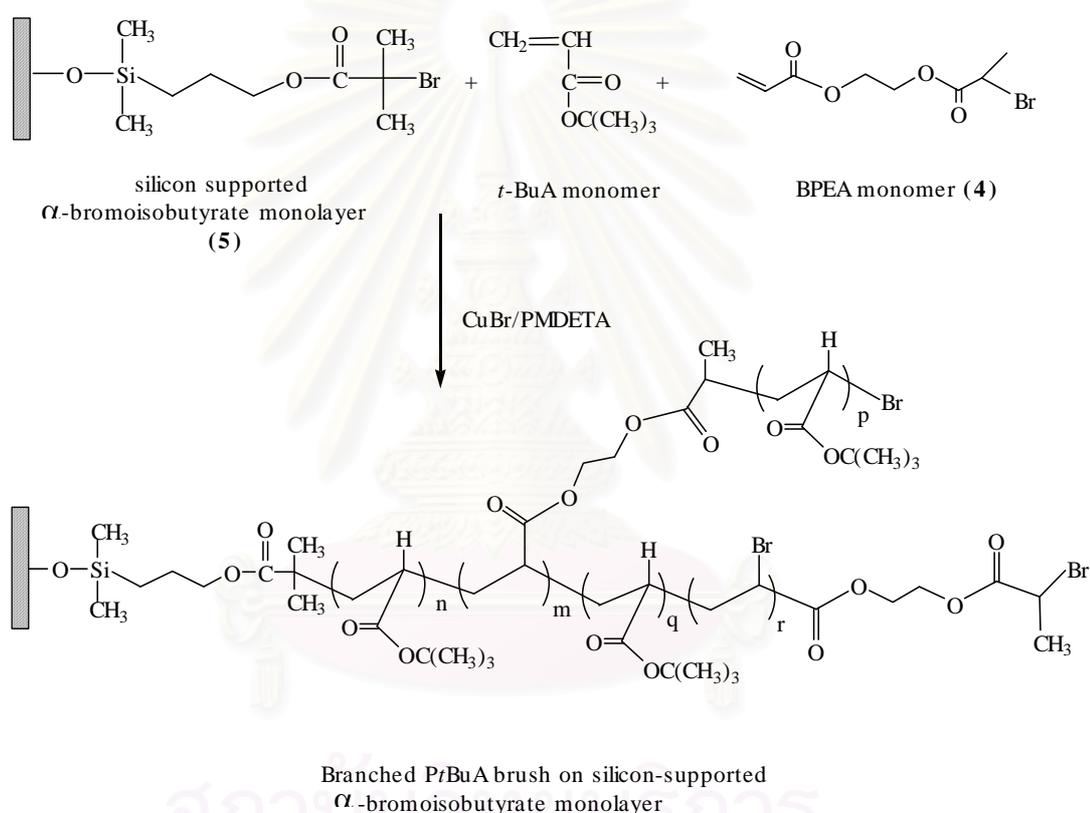
Silicon substrates were placed in a Schlenk flask and sealed with a rubber septum. The flask was evacuated and back-filled with nitrogen three times and left under a nitrogen atmosphere. CuBr (53.8 mg, 0.375 mmol), *t*BuA monomer and acetone (15 mL) were added to a separate Schlenk flask with a magnetic stirrer bar, sealed with a rubber septum, and degassed by purging with nitrogen for 1 h. PMDETA (78.4 μL, 0.375 mmol) was added to the mixture via a syringe, and the solution was stirred at 60°C until it became homogeneous (approximately 5 min). The solution was then transferred to the flask containing the silicon substrates via cannula, followed by the addition of acrylic acid 2-(2-bromopropionyloxy)ethyl ester (BPEA)

monomer via syringe. The polymerization was allowed to proceed at 60°C. After a set reaction time, the silicon substrates was removed and rinsed with THF. To remove untethered copolymer, the silicon substrates were placed in a Soxhlet extractor and extracted with THF for 24 h and dried under vacuum. The substrates bearing polymer brushes were then analyzed by contact angle measurement, ellipsometry and AFM. Free copolymer from the polymerization solution was isolated by first evaporating residual monomer and solvent, dissolving in THF, and then passing the THF/polymer solution through a short column of silica to remove any residual catalyst and analyzed by GPC.

3.8. Hydrolysis of linear and branched poly(*tert*-butyl acrylate) grafted on silicon substrates

Linear poly(acrylic acid) brushes
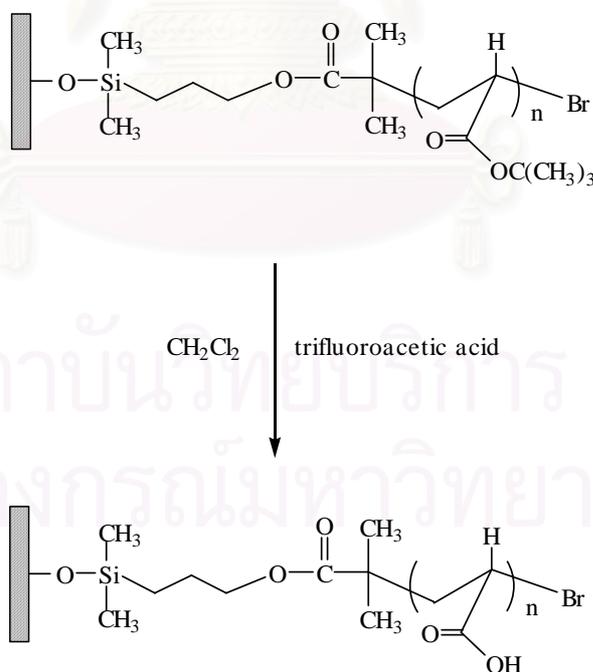
Branched poly(acrylic acid) brushes
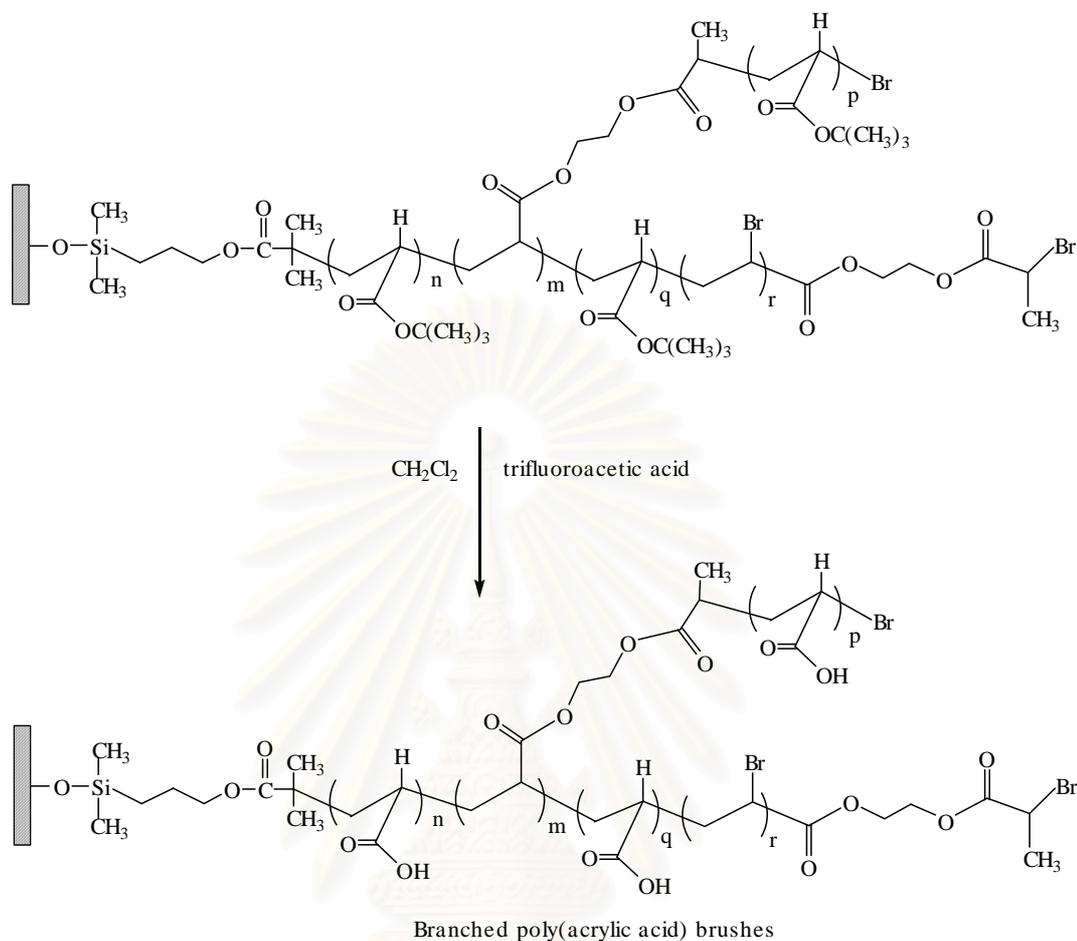
The silicon wafer containing the tethered linear and branched poly(*tert*-butyl acrylate) were placed in Schlenk flask. The mixture of trifluoroacetic acid (2.9 mL, 37.5 mmol) and dichloromethane (15 mL) were added and stirred at room temperature for 6 h. The wafer was removed and rinsed with dichloromethane, and then dried under vacuum.

3.8.1 Determination of carboxyl groups of poly(acrylic acid) brushes grafted on silicon substrate.

The toluidine blue o staining method was employed to determine the amount of carboxyl groups on PAA brushes. A 0.5 mM dye aqueous solution was prepared at pH 10. The silicon substrates bearing PAA brushes were placed in the dye solution for 6 h at 30°C. The substrates were then removed and thoroughly washed with a sodium

hydroxide solution of pH 9 for 24 h to remove any noncomplexed dye adhering to the substrates. The dye that was complexed with carboxyl groups was desorbed from the surface by soaking the substrates in a 50% acetic acid solution for 16 h. The desorbed dye content was obtained by measuring of the optical density of the solution at 633 nm with an UV-vis spectrophotometer. The PAA content was obtained from a calibration plot of the optical density versus dye concentration assuming one carboxyl group reacted with one dye molecule.

3.9 Attachment of biotin to carboxyl group of poly(acrylic acid) brushes

linear and branched PAA
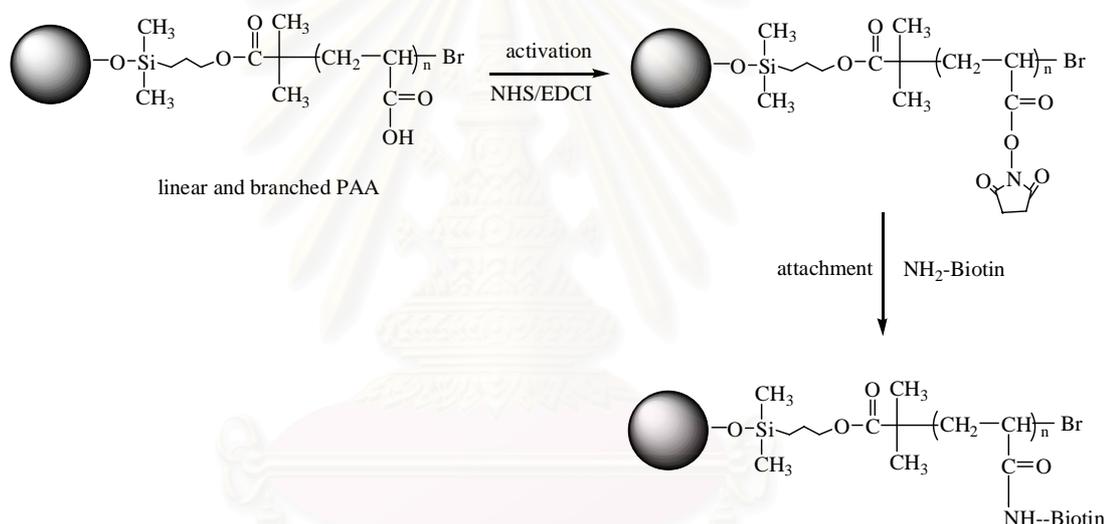
Carboxyl groups of PAA brushes were activated by suspending the silicon particles bearing PAA brushes in an aqueous solution of EDCI (0.05 M) and NHS (0.1 M) for 30 min. The substrates were washed with water. Then, the samples were suspended in a solution of (+)-biotinyl-3,6,9-trioxaundecanediamine (10 mM) in phosphate-buffered saline (PBS, pH 7.4) for 2 h at room temperature and washed thoroughly with PBS solution.

3.10 Streptavidin binding to biotin-attached PAA brushes.

The silicon particles bearing biotin-attached PAA brushes obtained from 3.9 were suspended in a solution of PBS containing 0.1% (w/v) bovine serum albumin (BSA) for 60 min. The particles were then incubated with a solution of fluorescein-conjugated streptavidin (0.1 mg/mL) in PBS at room temperature. After 14 h, the particles were washed several times with PBS and distilled water. The particles were spread on a glass slide and covered with a thin cover slip. Fluorescence microscope equipped with a digital camera was used to examine the streptavidin bound on the particles.

CHAPTER IV

RESULTS AND DISCUSSION

In this chapter, the results are divided into three sections. The first section mainly focuses on the synthesis of linear and branched poly(*tert*-butyl acrylate)(P*t*BuA) brushes from silicon-supported ∝-bromoisobutyrate monolayer by surface-initiated atom transfer radical polymerization (ATRP) of *tert*-butyl acrylate (tBuA) and self-condensing vinyl copolymerization (SCVCP) of acrylic acid 2-(2-bromopropionyloxy)ethyl ester (BPEA) with *tert*-butyl acrylate (tBuA) *via* atom transfer radical polymerization (ATRP), respectively. The second section explains the synthesis of linear and branched poly(acrylic acid) (PAA) brushes by hydrolysis of P*t*BuA brushes to remove *tert*-butyl groups. The final section involves the attachment of biotin to the carboxyl group of both linear and branched poly(acrylic acid) brushes.

4.1 Synthesis of α-bromoester to be used as initiators

4.1.1 Synthesis of 2-bromo-2-methylpropionic acid allyl ester (1)

Prop-2-en-1-ol   2-Bromo-2-methylpropionyl bromide   2-Bromo-2-methylpropionic acid allyl ester

(1)
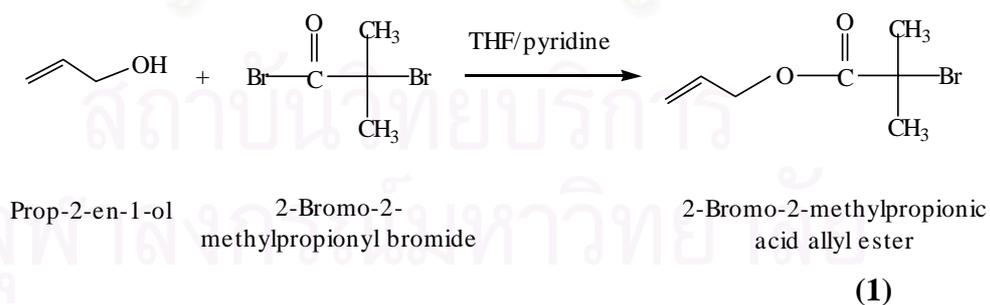
The nucleophilic substitution of prop-2en-1-ol with 2-bromo-2-methylpropionyl bromide in tetrahydrofuran gave 2-bromo-2-methylpropionic acid allyl ester **(1)** as a colorless liquid product which was sufficiently pure for the next synthesis without further purification after the work-up process. The ^{1}H NMR (Figure A-1) of product **(1)** shows a multiplet peaks of alkene protons (C$\underline{H}_2$=CH) at 5.25-5.40

ppm and (CH_2=C$\underline{H}$) at 5.88-5.98 ppm. The doublet signal of methylene proton (OCH_2) at 4.71 ppm and a singlet signal of the methyl proton of C(C$\underline{H}_3$)$_2$ at 1.98 ppm indicating the complete reaction between prop-2en-1-ol and 2-bromo-2-methyl propionyl bromide.

4.1.2 Synthesis of 2-bromo-2-methylpropionic acid 3-(ethoxydimethyl silanyl)propyl ester (2)

Ethoxydimethyl silane	2-Bromo-2-methylpropionic acid allyl ester	2-Bromo-2-methylpropionic acid 3-(ethoxydimethylsilanyl)propyl ester
	(1)	(2)
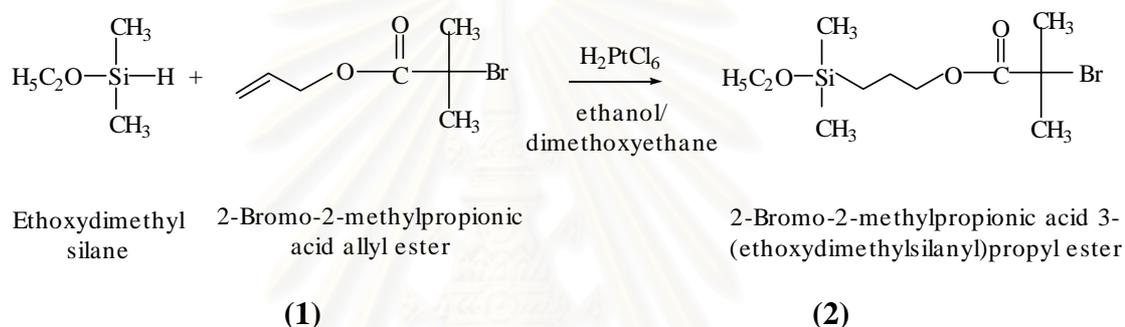
Hydrosilylation of ethoxydimethylsilane with (1) was carried out in the dark in the presence of a catalytic amount of chloroplatinic acid, H_2PtCl_6 at room temperature for 24 h. The crude product of 2-bromo-2-methylpropionic acid 3-(ethoxydimethyl silanyl)propyl ester (2) was a yellow viscous liquid, which was sufficiently pure for the next synthesis without further purification after the work-up process. The mechanism of hydrosilylation is shown in Scheme 4.1. The ^{1}H-NMR spectrum (Figure A-2) of product (2) shows a triplet signal and multiplet signal of the methylene proton (SiC$\underline{H}_2$CH$_2$CH$_2$O) and (SiCH$_2$C$\underline{H}_2$CH$_2$O) at 0.93 and 1.66 ppm, respectively. The multiplet peaks of protons ((C$\underline{H}_2$=CH) at 5.25-5.40 and (CH_2=C$\underline{H}$) at 5.88-5.98 ppm) from the starting alkene derivative (1) disappeared after the reaction indicating the completion of the reaction.
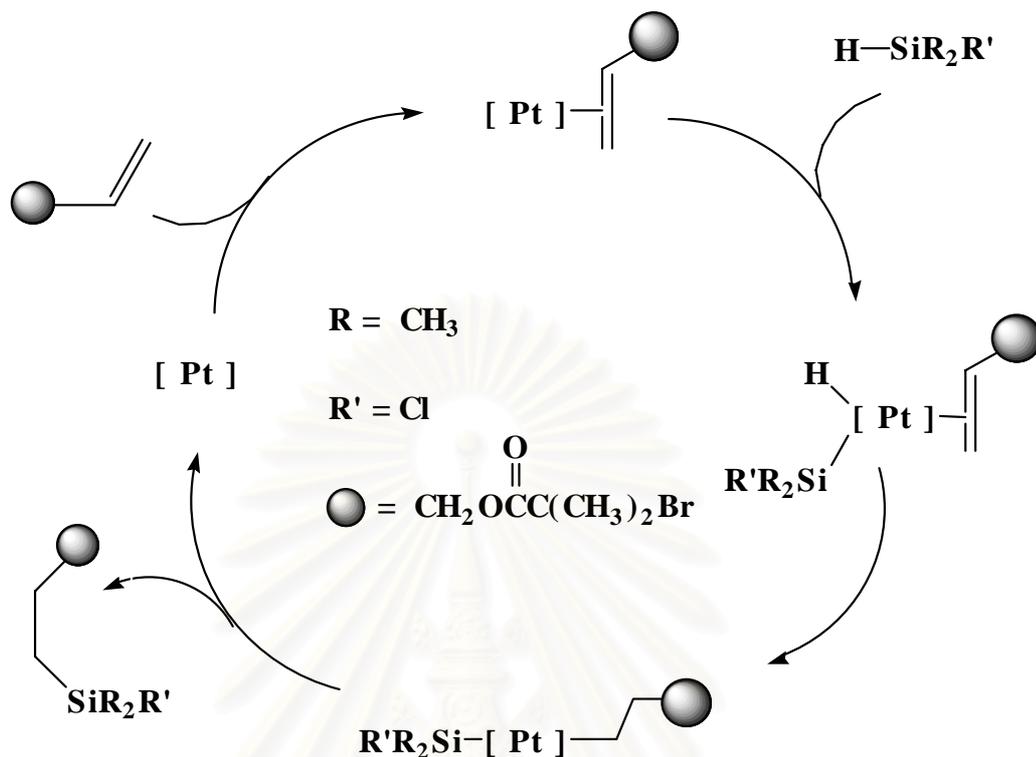
Scheme 4.1 Mechanism of hydrosilylation using chloroplatinic acid as a catalyst

4.1.3 Synthesis of 2-bromo-2-methylpropionic acid propyl ester (3) as a "sacrificial" initiator

Propan-1-ol   2-Bromo-2-   2-Bromo-2-methylpropionic
                  methylpropionyl bromide   acid propyl ester
   **(3)**
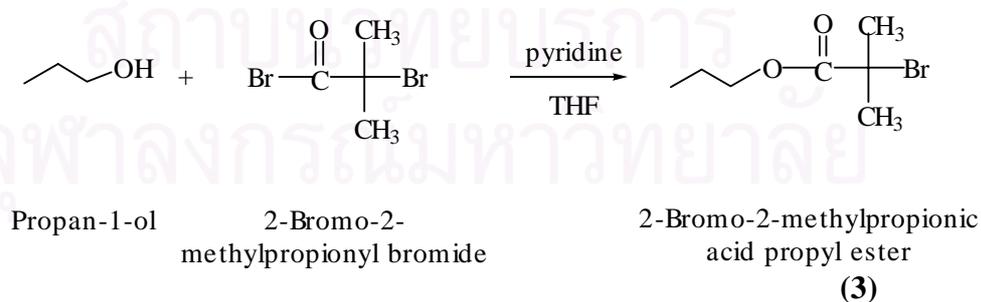
The nucleophilic substitution of propan-1-ol with 2-bromo-2-methylpropionyl bromide in tetrahydrofuran gave 2-bromo-2-methylpropionic acid propyl ester **(3)** as a pale yellow viscous liquid, which was sufficiently pure for the next synthesis without further purification after the work-up process. The ^{1}H-NMR (Figure A-3) of the

product (3) showed a singlet signal of the methyl proton C(C$\underline{H}_3$)$_2$ at 1.96 ppm and a doublet signal of methylene proton (OCH$_2$) at 4.71 ppm indicating the success of the reaction between propan-1-ol and 2-bromo-2-methylpropionyl bromide. This product was used as an "added" or "sacrificial" initiator for the polymerization of polymer brushes.

4.2 Synthesis of acrylic acid 2-(2-bromopropionyloxy)ethyl ester (BPEA) (4) to be used as a comonomer for copolymerization

| Acrylic acid 2-hydroxy ethyl ester | 2-Bromopropionyl bromide | Acrylic acid 2-(2-bromo-propionyloxy) ethyl ester (BPEA) |
| | | **(4)** |
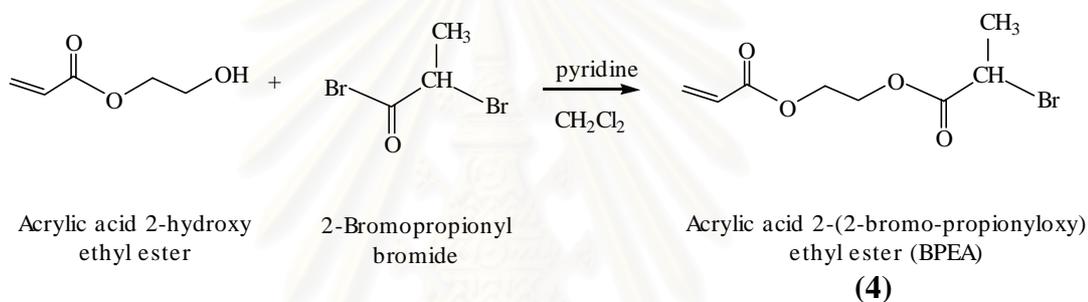
Acrylic acid 2-(2-bromopropionyloxy)ethyl ester (BPEA) is a vinyl monomer containing alkyl halide group that can be activated to initiate a polymerization of double bonds. This monomer was used for the preparation of branched PtBuA by atom transfer radical polymerization. BPEA monomer contained an acrylic group connected to a (2-bromopropionyl)oxy group by an ethylene linkage. ^{1}H NMR spectrum (Figure A-4) of the product (4) shows a doublet signal and doublet of doublet signals of alkene protons (C$\underline{H}_2$=CH) at 6.43, 5.89 ppm and (CH$_2$=C$\underline{H}$) at 6.14 ppm. Also, there are signals of an ethylene linkage and the methylene proton geminal to bromine at 4.39 ppm and a multiplet signal of the methyl protons at 1.82 ppm.

4.3 Preparation of surface grafted ∝-bromoester initiators (5)

(2)   (5)

Using the optimized condition previously reported [79], an α-bromoisobutyrate monolayer having the maximum density was grafted on silicon substrates with a thickness of 9.3 ± 0.1Å as measured by ellipsometry. Advancing/receding water contact angle of the silicon-supported ∝-bromoisobutyrate monolayer was 72°/68° which was significantly different from the value of 30°/15° for the cleaned and dried hydrophilic silicon substrates.

4.4 Preparation of poly(*tert*-butyl acrylate) brushes

This section mainly focuses on the synthesis of linear and branched poly(*tert*-butyl acrylate) (P*t*BuA) brushes. P*t*BuA brushes were grown from the surface grafted α–bromoisobutyrate monolayer *via* ATRP at 60°C in the presence of CuBr/PMEDTA using acetone as a solvent.

4.4.1 Surface-initiated homopolymerization of *tert*-butyl acrylate

silicon supported
α-bromoisobutyrate monolayer
(5)

t-BuA monomer

2-Bromo-2-methylpropionic acid
propyl ester **(3)**

CuBr / PMEDTA

Linear P(tBuA) brush on silicon-supported
α-bromoisobutyrate monolayer

This approach was used for the preparation of linear poly(*tert*-butyl acrylate) (P*t*BuA) brushes.

1) Molecular weight and graft density of linear P*t*BuA brushes

It is rather difficult to obtain the molecular weight of the polymer brush directly since the amount of polymer on the silicon substrate is too small to be degrafted and analyzed. The polymer chains formed by the free initiator ("sacrificial" initiator) in solution were then used to monitor the surface-initiated polymerization process and molecular weight. It has been proven that the molecular weight and polydispersity of the graft polymer were nearly equal to those of the free polymer produced in the solution, meaning that the free polymer in the solution is a good measure of the characteristics of the graft polymer [80]. The free initiator plays a role not only as an indicator of the polymerization but also as a controller for the ATRP on the surface. The concentration of the Cu^{II} complex produced from the reaction at the substrate surface is too low to reversibly deactivate polymer radicals with a sufficiently high rate. The addition of the free initiator creates the necessary

concentration of the Cu(II) complex, which in turn controls the polymerization on the substrate as well as in solution (Scheme 4.2).

$$P_m{-}X \; + \; Cu(I)X/\,Ligand \; \underset{k_{deact}}{\overset{k_{act}}{\rightleftharpoons}} \; P_m^{\cdot} \; + \; X\text{-}Cu(II)X/\,Ligand$$

Scheme 4.2 Activation/deactivation cycles of ATRP process

The ^{1}H-NMR spectra shown in Figure 4.1 indicates that the signals of the double bond of monomer disappeared while the CH proton of the polymer appeared at 2.16 ppm and the CH$_3$ protons shift from 1.49 ppm to 1.37 ppm.

Figure 4.1 ^{1}H-NMR spectra of (A) *t*BuA and (B) P*t*BuA in solution.

Figure 4.2 shows the change in the molecular weight ($\overline{M}_n$) and molecular weight distribution ($\overline{M}_w/\overline{M}_n$) of free P*t*BuA as a function of polymerization time at two targeted degrees of polymerization (DP) of 100 and 200. The monomer concentration ([*t*BuA]) of 4.6 M and the [I]/[CuBr]/[PMDETA] mole ratio of 1:1:1 were fixed in these experiments. The amount of free initiator was varied to obtain the targeted DP. The molecular weight increased with an increase of targeted DP. For both targeted DPs, the molecular weight increased linearly with increasing polymerization time. The highest molecular weight obtained was in accord with the targeted Molecular weight. The molecular weight distribution being close to 1.0 suggested that the polymerization mechanism is living.
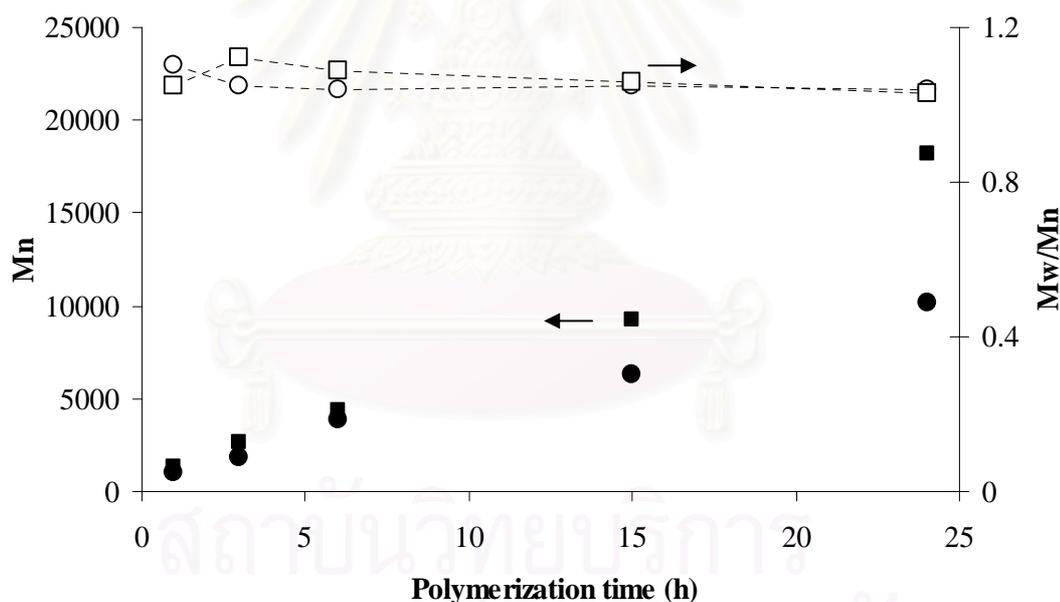
**Figure 4.2** Molecular weight ($\overline{M}_n$): targeted DP = 100 (●), 200 (■) and molecular weight distribution ($\overline{M}_w/\overline{M}_n$): targeted DP = 100 (○), 200 (□) of P*t*BuA as a function of polymerization time.

Figure 4.3 shows the development of P*t*BuA brushes thickness as a function of time at two targeted DPs. It was found that the thickness of P*t*BuA brushes linearly

increased as a function of polymerization time suggesting that the polymerization is living and can be well controlled.
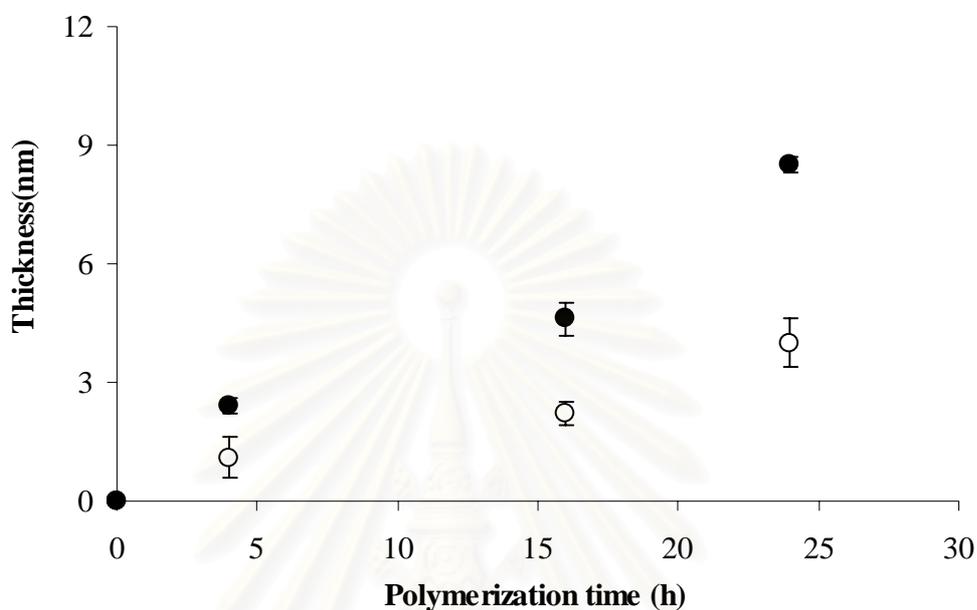
Figure 4.3 Thickness of P*t*BuA brushes versus polymerization time for targeted DP = 200 (●) and 100 (○).

The information related to the molecular weight and thickness can be used to calculate a grafting density of polymer brushes. The grafting density (σ) which is a reciprocal unit of cross-sectional area (A_x) per chain can be determined from the corresponding film thickness (t) and the molecular weight of the chain ($\overline{M}_n$) from the following equation

$$\sigma = \frac{t\rho N_A}{M_n} = \frac{1}{A_x} \tag{4.1}$$

Where ρ is the mass density (1.1 g/cm^3 for P*t*BuA) and N_A is Avogadro's number. Using slopes obtained from the plots in Figures 4.4 and 4.5 which correspond to t/M$_n$, the calculated grafting density is 0.25 and 0.32 chains/nm^2 for the targeted DP = 100 and 200, respectively. These results agree quite well with the data previously reported that the grafting densities for various polymers prepared by surface-initiated ATRP were also ranged from 0.1 to 0.6 chains/nm^2 [81].
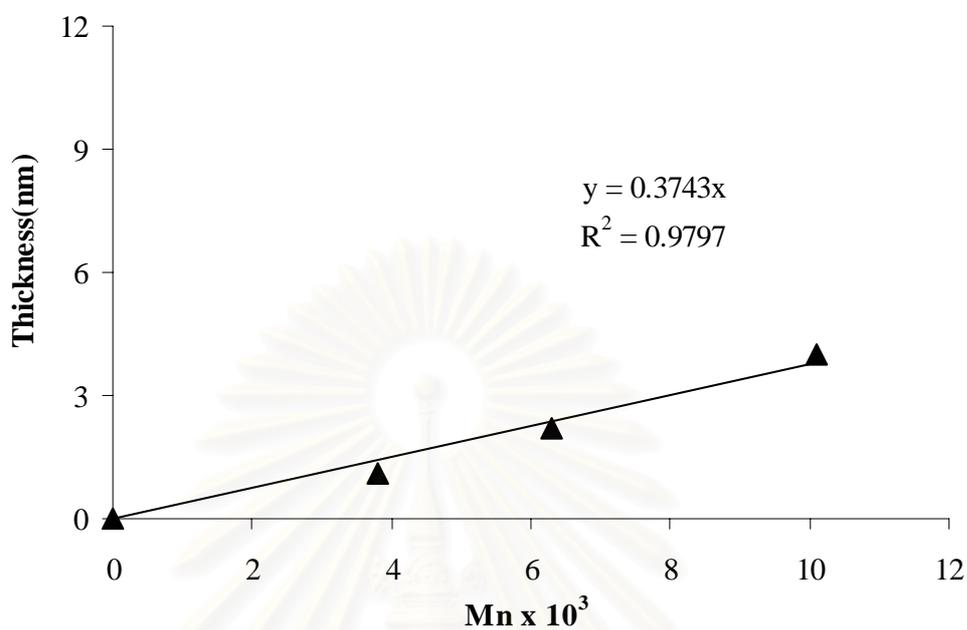
Figure 4.4 Relationship between the ellipsometric thickness of P*t*BuA brushes with the molecular weight ($\overline{M}_n$) of free P*t*BuA for targeted DP = 100.
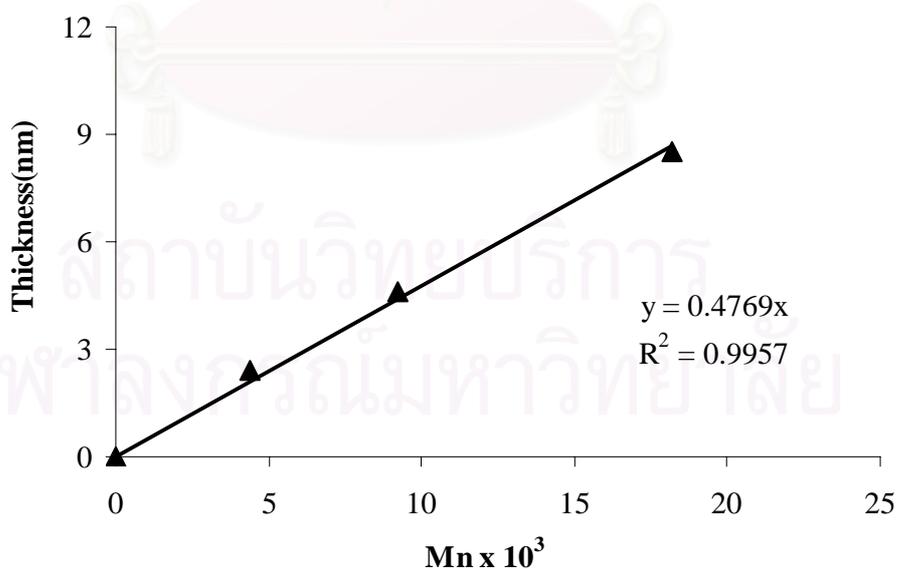
**Figure 4.5** Relationship between the ellipsometric thickness of P*t*BuA brushes with the molecular weight ($\overline{M}_n$) of free P*t*BuA for targeted DP = 200.

2) Confirmation of linear P*t*BuA brushes formation

Formation of linear P*t*BuA brushes on the silicon substrate was confirmed by FT-IR and water contact angle measurements. The FT-IR spectra of linear P*t*BuA brushes obtained by ATRP from the α-bromoisobutyrate functionalized silica particles are depicted in Figure 4.6. The spectra showed the C-H stretching at 2936 and 2978 cm^{-1}, CH$_3$ bending at 1370 cm^{-1} and a peak at 1727 cm^{-1} due to the carbonyl stretching of ester.
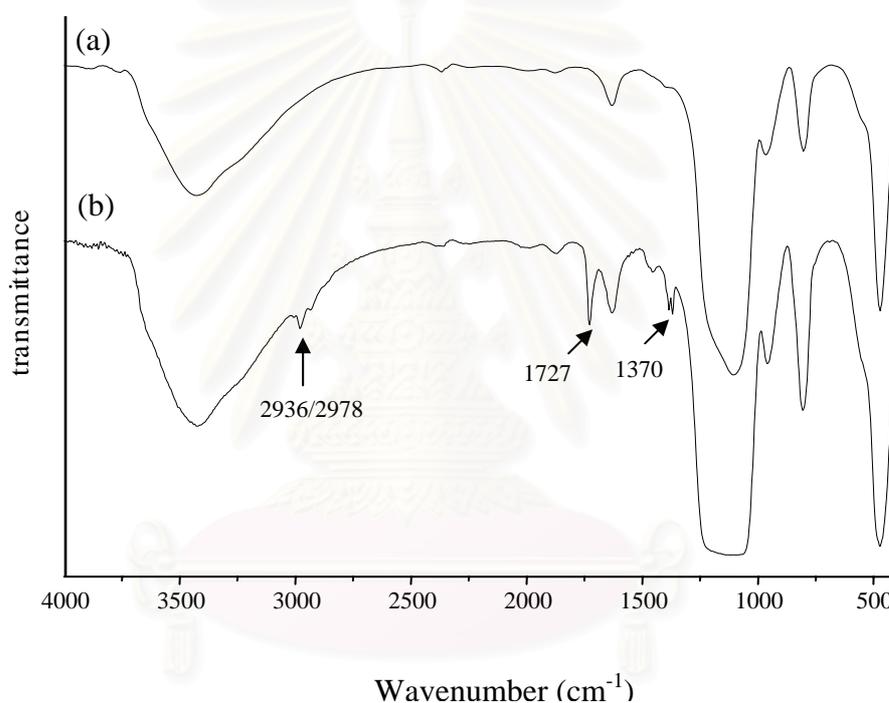
Figure 4.6 FT-IR spectra of (a) silica particles and (b) P*t*BuA brushes on silica particles having targeted DP = 200.

The growth of linear P*t*BuA brushes can also be monitored by water contact angle analysis. Figure 4.7 illustrates advancing (θ_A) and receding (θ_R) water contact angles of silicon-supported P*t*BuA brushes as a function of polymerization time. Both advancing (θ_A) and receding (θ_R) contact angles rapidly increased from 72°/58° of the silicon-supported α-bromoisobutyrate monolayer to ~ 92°/71° and ~ 95°/76° for targeted DP = 100 and 200, respectively. This result indicated that more hydrophobic

surface has been obtained as a consequence of linear PtBuA brushes formation. Moreover, the contact angle hysteresis (θ_A - θ_R) being less than 20° also implies that the surface bearing linear PtBuA brushes is quite homogeneous and smooth.
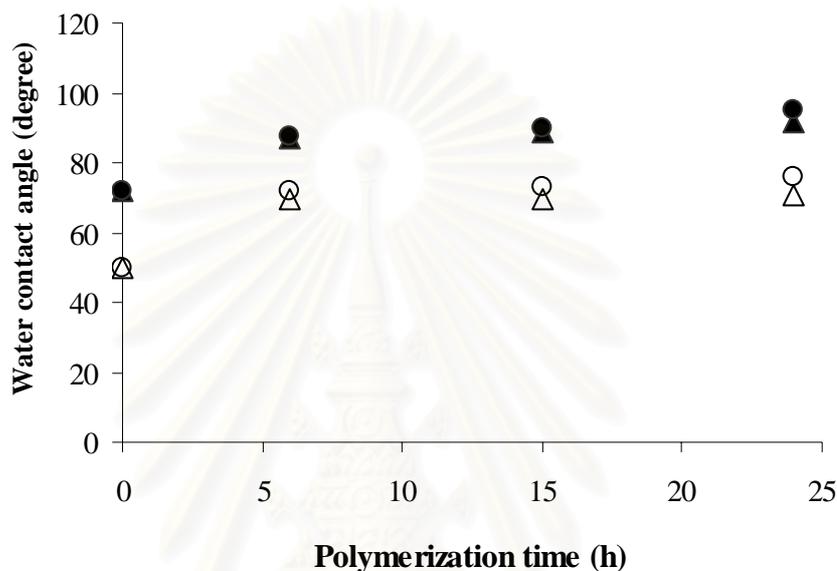
Figure 4.7 Water contact angle data of PtBuA brushes versus polymerization time for targeted DP = 200 (θ_A (●), θ_R (○)) and targeted DP = 100 (θ_A (▲), θ_R (Δ)).

4.4.2 Surface-initiated copolymerization of *tert*-butyl acrylate and acrylic acid 2-(2-bromopropionyloxy)ethyl ester (BPEA)

This approach was used for the preparation of branched poly(*tert*-butyl acrylate) (PtBuA) brushes.

Branched P*t*BuA brush on silicon-supported
α-bromoisobutyrate monolayer

1) Molecular weight and molecular weight distribution

The self-condensing vinyl copolymerization (SCVCP) of the AB* inimer, acrylic acid 2-(2-bromopropionyloxy)ethyl ester (BPEA), with *t*BuA was conducted with CuBr/PMDETA using acetone as a solvent at 60 °C. The $[tBuA]_0/[BPEA]_0$ comonomer ratio (γ) was varied between 2.5 and 100 whereas the comonomer $([tBuA]_0 + [BPEA]_0)$-to-catalyst $([CuBr]_0)$ ratio (μ) was kept at a constant value of 200. Polymerization was conducted for 24 h. The broad GPC traces of the resulting polymers shown in Figure 4.8 imply that the molecular weight distributions of all polymers are broad signifying the characteristics of branched polymer. The elution curve shifts toward higher molecular weight with increasing comonomer ratio.

Figure 4.8 GPC traces of branched P*t*BuA having different comonomer ratio obtained by SCVCP of BPEA and *t*BuA.

Figure 4.9 represents the dependences of the molecular weight distribution ($\overline{M}_w/\overline{M}_n$) and average molecular weights ($\overline{M}_n$ and $\overline{M}_w$) of polymers as a function of the comonomer ratio in the range of $100 > \gamma > 2.5$. The $\overline{M}_n$ and $\overline{M}_w$ of the branched P*t*BuA consistently increase with γ, whereas there is no significant difference in the molecular weight distribution when the comonomer ratio was greater than 10.
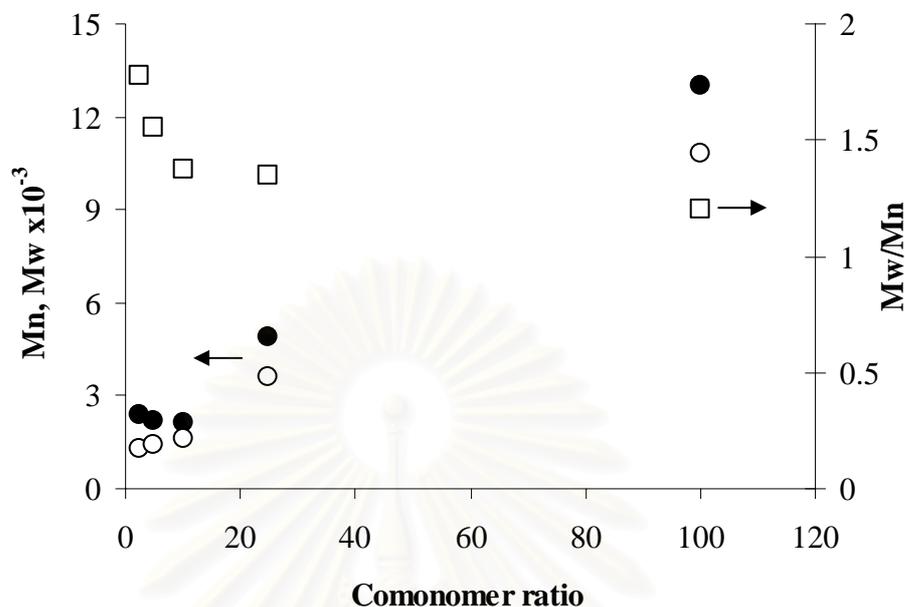
Figure 4.9 Dependence of molecular weights ($\overline{M}_w, \overline{M}_n$) and molecular weight distribution ($\overline{M}_w/\overline{M}_n$) on the comonomer ratio (γ): $\overline{M}_n$ (○), $\overline{M}_w$ (●), and $\overline{M}_w/\overline{M}_n$ (□).

2) Degree of branching

^{1}H-NMR spectra of the branched P*t*BuA shown in Figure 4.10 exhibit a broad peak at 4.1-4.4 ppm (region 1) corresponding to the protons of the ethylene linkage and the protons germinal to bromine in either A* (polymer), B* (monomer or polymer), or M* (polymer), all of which are derived from BPEA. The symbol descriptions are explained in Chapter II. Hence, the sum of proton of the ethylene linkage and the ones germinal to bromine is proportional to the fraction of BPEA in the copolymer. The peak at 1.4 ppm (region 4) is assigned to the *tert*-butyl group of P*t*BuA segment. The comonomer composition calculated from the ratio of these peaks is in good agreement with the comonomer composition in the feed which corresponds to the γ value. The agreement demonstrates complete inimer incorporation. The broad peaks at 1.2-2.8 ppm are attributed to the polymer backbone (methylene and methine protons). The large doublet at 1.8 ppm (region 2) is assigned to CH_3 of the 2-bromopropionyloxy group, B* (corresponding to an end group), while the broad peak

at 1.1-1.3 ppm (region 3) is assigned to the methyl protons, b, which is formed by the activation of the B* and subsequent addition of monomer. For the copolymer obtained by SCVCP, these peaks should be related to the degree of branching and the comonomer composition. The proportion of b calculated by the equation of $b =$ (region 3)/(sum of region 2 and region 3). For equal reactivity of active sites, the degree of branching determined by NMR, DB_{NMR}, is given as.

$$DB_{NMR} = 2\left(\frac{b}{\gamma + 1}\right)\left\{1 - \left(\frac{b}{\gamma + 1}\right)\right\} \tag{4.2}$$

According to the theory of SCVCP, the comonomer ratio, γ can be directly related to the degree of branching. Assuming equal reactivity of all active sites, the degree of branching obtained from the theory, DB_{theo}, can be represented as [82].

$$DB_{theo} = \frac{2(1 - e^{-(\gamma+1)})(\gamma + e^{-(\gamma+1)})}{(\gamma + 1)^2} \tag{4.3}$$

From this approach, DB_{NMR} decreases with γ, as shown in Figure 4.11. And the values are in good agreement with the theoretical ones calculated from Eq. 4.3. Although NMR experiments afford a conclusive measurement of the degree of branching for lower γ value, the low concentration of branching points in the copolymer having $\gamma >$ 10 does not permit the determination of the degree of branching directly by the spectroscopic method, because of low intensities of the peaks in regions 2 and 3. However, for the case of high comonomer ratio the relation between DB_{NMR} and γ becomes very simple and dose not depend on the reactivity ratios of the various active centers. In this copolymerization system, BPEA used as an AB* inimer contains the acrylate and bromopropionate groups, both of which form secondary radicals, and tBuA used as a comonomer also generates a secondary radical. The secondary α-bromoester dormant species formed during the reaction should have a reactivity similar to the 2-bromopropionate found on the AB* inimer. Hence, the difference in the rate constants is considered to be small.
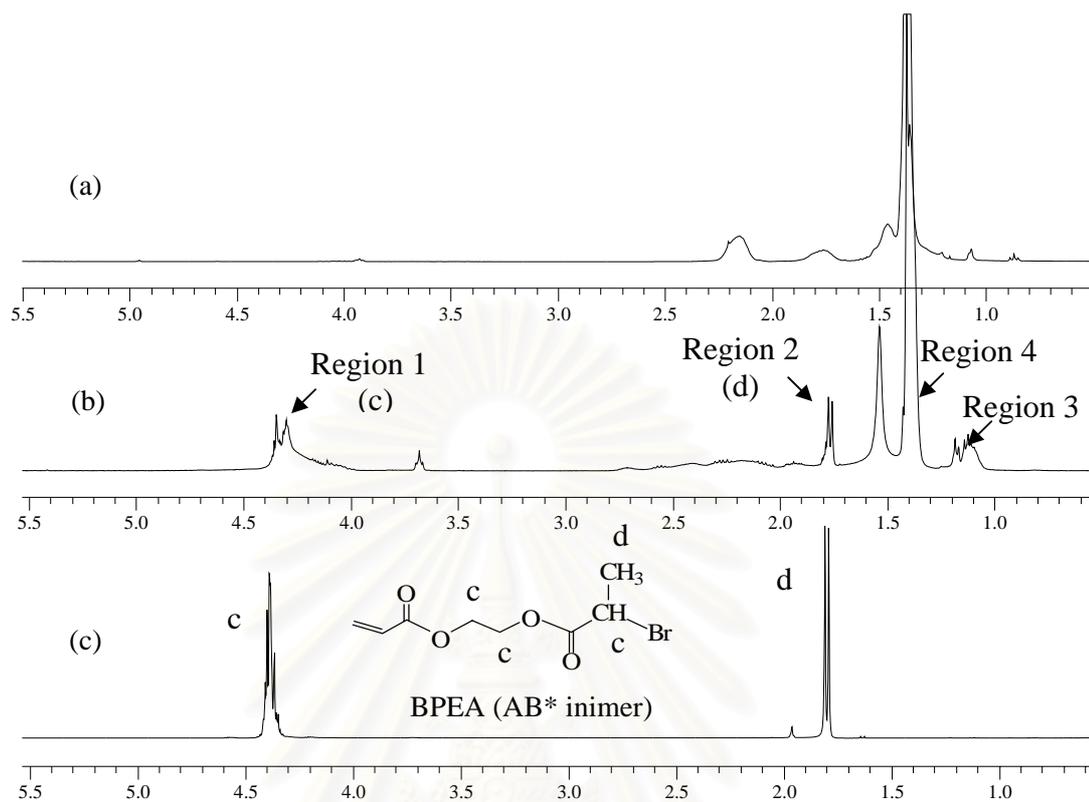
Figure 4.10 ^{1}H-NMR spectra of (a) *t*BuA, (b) branched P*t*BuA: $\gamma = 2.5$ and (c) BPEA.
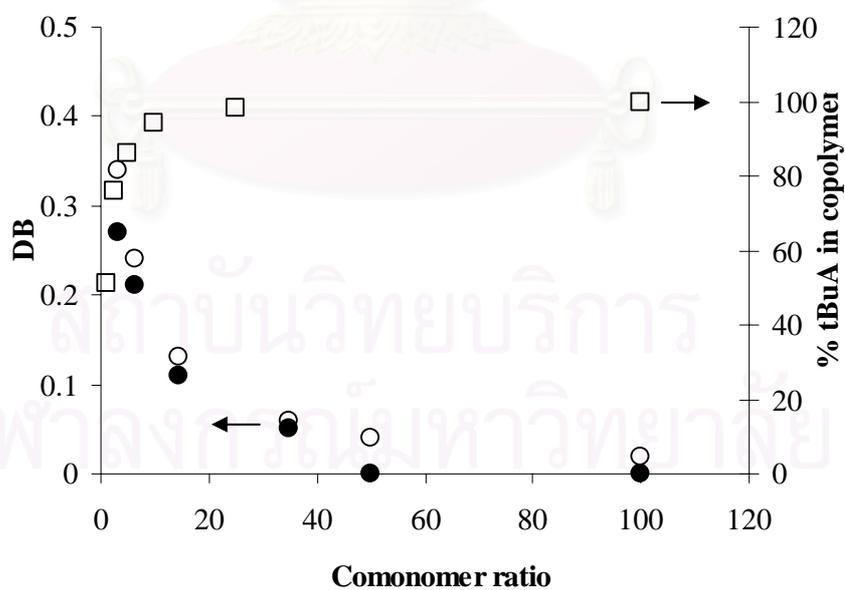
Figure 4.11 Degree of branching of branched P*t*BuA as a function of comonomer ratio: DB_{theo} (○), DB_{NMR} (●).

3) Confirmation of branched P*t*BuA brushes formation

Figure 4.12 shows the FT-IR spectra of branched P*t*BuA grafted on silica particles. The absorption bands due to the carbonyl (1730 cm^{-1}) and the C-H stretching vibrations (2800-3050 cm^{-1}) are clearly visible in the grafted branched P*t*BuA. The intensities of carbonyl and CH$_3$ bending vibration (1370 cm^{-1}) peaks increase with increasing comonomer ratio owing to the elevated ratio of P*t*BuA in copolymer.
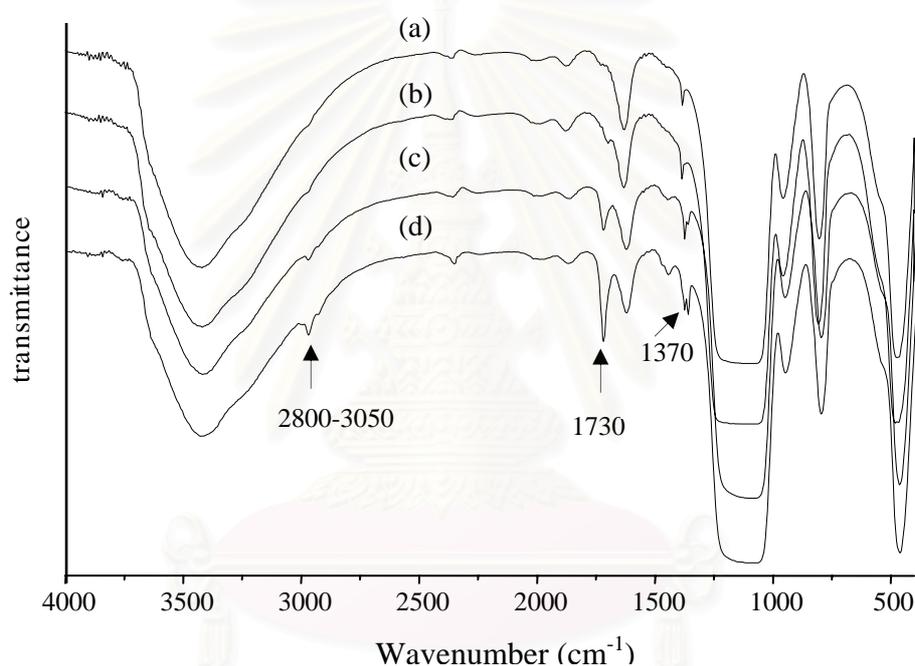
Figure 4.12 FT-IR spectra of branched P*t*BuA: (a) $\gamma = 2.5$, (b) $\gamma = 10$, (c) $\gamma = 25$, and (d) $\gamma = 100$.

The growth of branched P*t*BuA brushes can also be monitored by water contact angle analysis. Figure 4.13 illustrates advancing (θ_A) and receding (θ_R) water contact angles of silicon-supported branched P*t*BuA brushes as a function of comonomer ratio. θ_A/θ_R rapidly increased from 74°/52° of the silicon-supported α-bromoisobutyrate monolayer to ~102°/74° indicating the formation of the more hydrophobic silicon-supported branched P*t*BuA brushes.
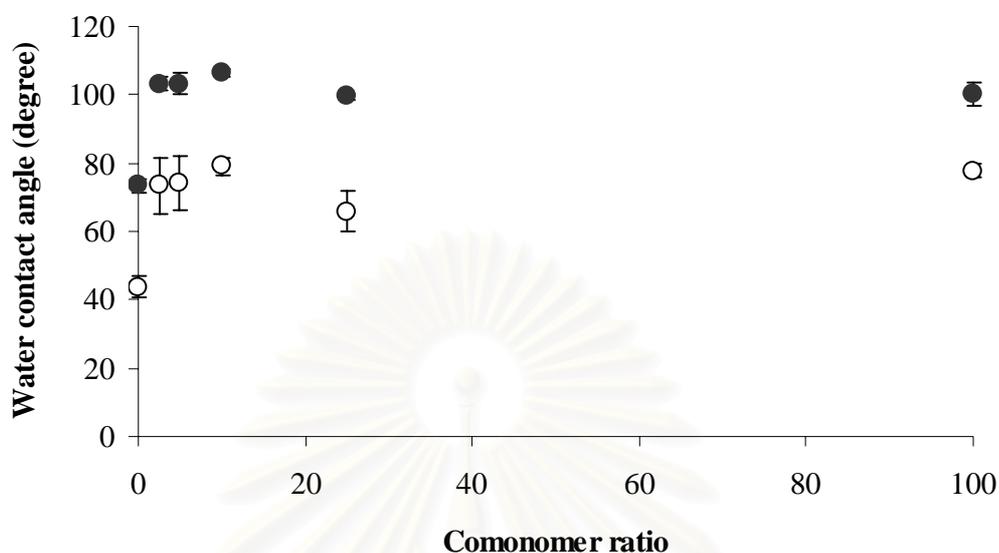
Figure 4.13 Water contact angle of branched P*t*BuA brushes versus comonomer ratio: $\theta_A(\bullet)$ and θ_R (○).

The fact that the contact angle hysteresis $(\theta_A-\theta_R)$ of the silicon-supported branched P*t*BuA brushes was slightly greater than that of the silicon-supported linear P*t*BuA brushes also implied that the surface bearing branched P*t*BuA brushes may be rougher than the surface covered by linear P*t*BuA. In fact, this speculation can be confirmed by atomic force microscopy. Figure 4.14 shows AFM images of linear and branched P*t*BuA brushes. Large protrusions are irregularly distributed on the branched polymer with a mean roughness (Ra) of about 3.2 nm, while the linear polymer shows a relatively uniform and smooth surface with a mean roughness (Ra) of about 1.5 nm.
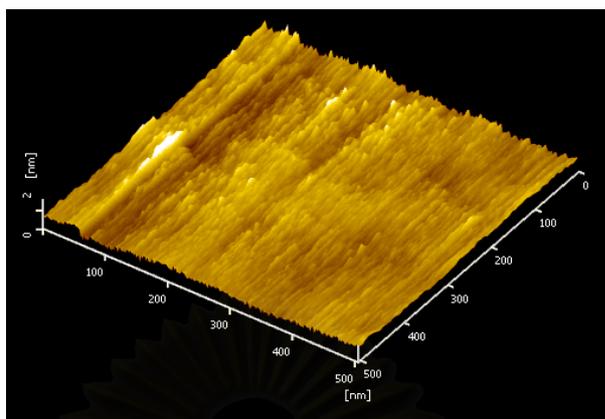
(a)
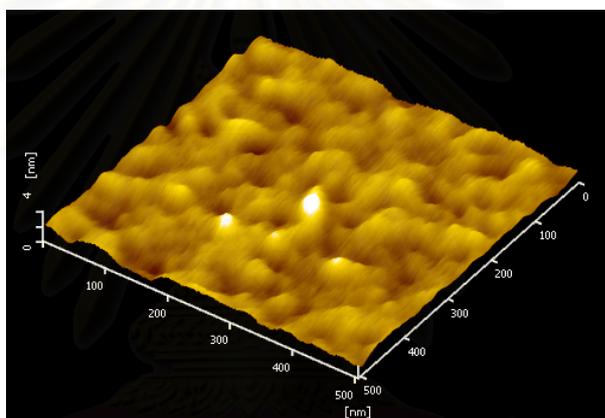
(b)

Figure 4.14 AFM images of (a) linear P*t*BuA brushes and (b) branched P*t*BuA brushes.

4.5 Preparation of linear and branched poly(acrylic acid) brushes

Poly(acrylic acid) (PAA) brushes can be prepared by hydrolysis of poly(*tert*-butyl acrylate) (P*t*BuA) brushes using trifluoroacetic acid (TFA) in dichloromethane at room temperature. An influence of TFA concentration and reaction time was investigated in order to identify an optimal condition for hydrolysis.

4.5.1 Determination of optimal condition for hydrolysis

Linear poly(acrylic acid) brushes
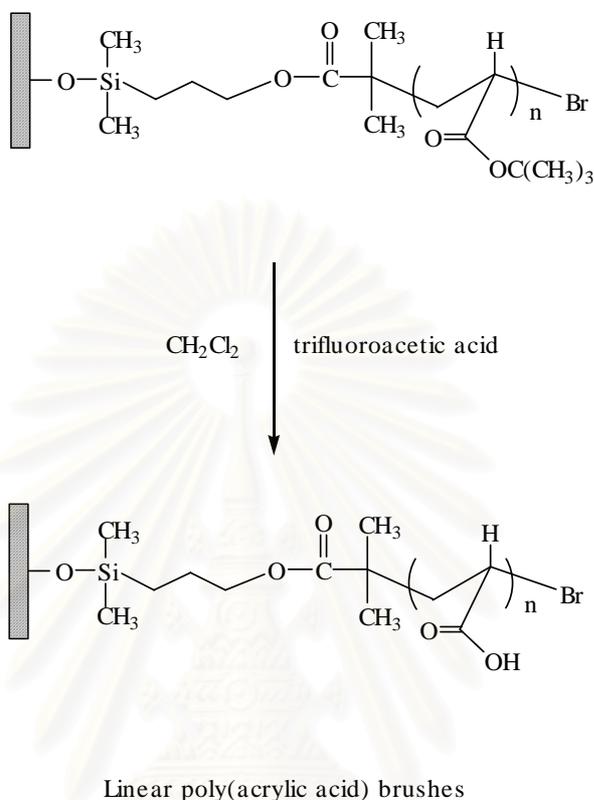
Linear PtBuA brushes (targeted DP = 200, $\overline{M}_n$ =18207, thickness = 8.5 nm) were firstly hydrolyzed by TFA solution having varied concentration at a fixed reaction time of 3 h. According to Figure 4.15, the water contact angles (θ_A and θ_R) decreased as a function of TFA concentration. No further reduction of the contact angles was observed when the TFA concentration was beyond 2.5 M.
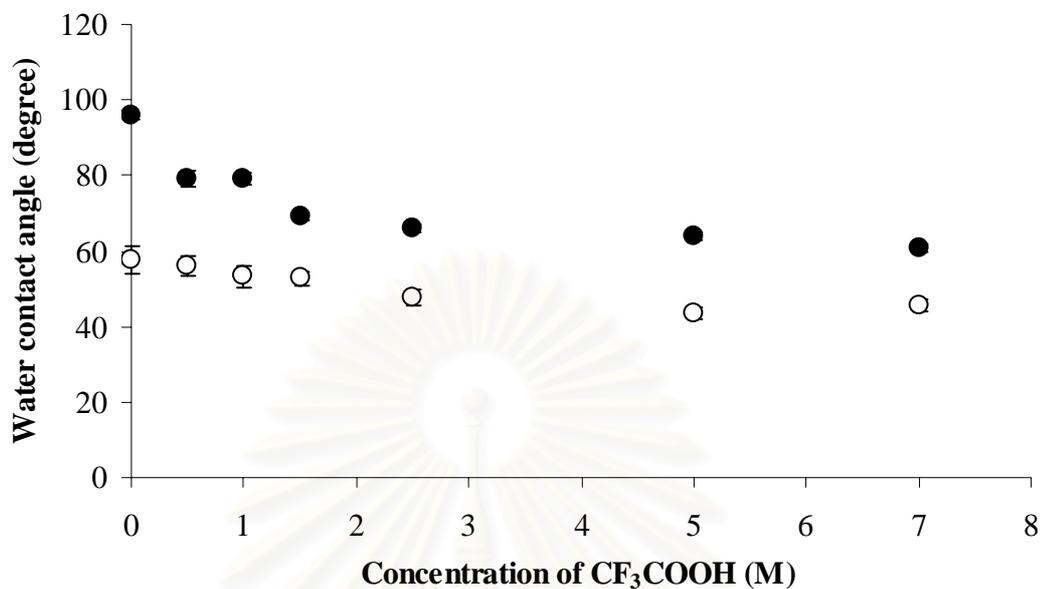
Figure 4.15 Water contact angle of P*t*BuA brushes after hydrolysis for 3h as a function of TFA concentration: θ_A(●) and θ_R (○).

By choosing TFA concentration of 2.5 M, the influence of reaction time on water contact angles was determined. Both θ_A and θ_R decreased rapidly within 1 h from $96^o/58^o$ of PtBuA brushes to $66^o/45^o$ implying that PAA brushes have been formed as a result of hydrolysis (Figure 4.16). The θ_R remained almost unchanged throughout the period of investigation. The θ_A, on the other hand, continued to decrease and reached 72° after 6h then increased again as the longer hydrolysis time was applied. The greater contact angle hysteresis observed in this particular case was possibly caused by the partial degrafting of the polymer chains from the surface upon extensive hydrolysis. Thus, the optimal condition for hydrolysis of P*t*BuA was to use 2.5 M TFA at room temperature for 6 h.
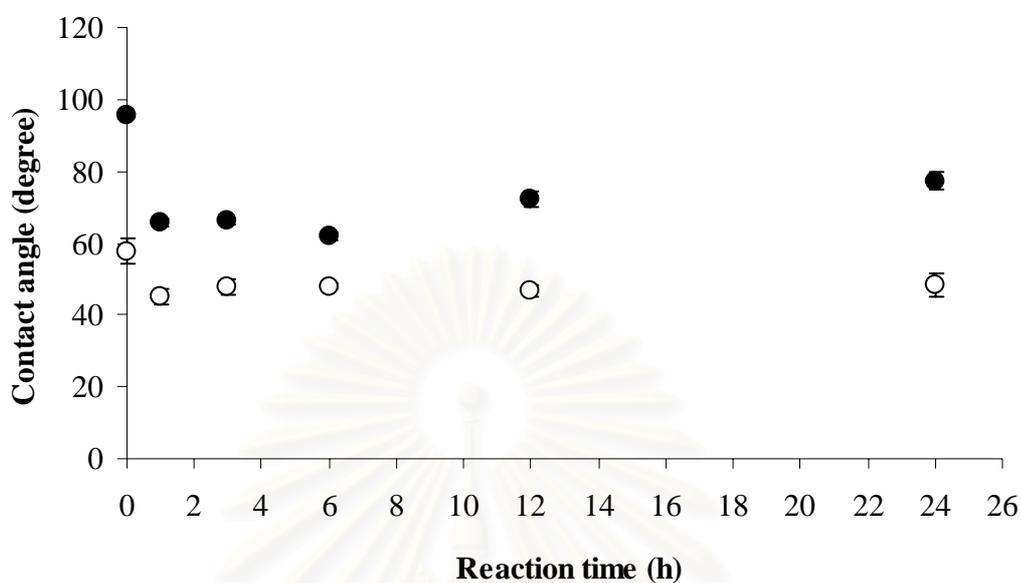
Figure 4.16 Water contact angle of of P*t*BuA brushes after hydrolysis by 2.5 M TFA as a function of reaction time: $\theta_A(\bullet)$ and θ_R (○).

4.5.2 Confirmation of linear and branched PAA brushes formation

Upon hydrolysis using the optimized condition previously identified, the hydrophobic surfaces of linear and branched P*t*BuA brushes were transformed to the hydrophilic surfaces of linear and branched PAA brushes. The contact angle data are outlined in Table 4.1.

Table 4.1 Advancing (θ_A) and receding (θ_R) water contact angle of P*t*BuA before and after hydrolysis by 2.5 M TFA for 6 h

Sample	Water contact angle (°)	
	θ_A	θ_R
Linear P*t*BuA	95 ± 1.7	76 ± 4.0
Linear PAA	60 ± 1.7	43 ± 0.8
Branched P*t*BuA	99 ± 0.9	66 ± 6.0
Branched PAA	68 ± 0.8	47 ± 4.7

Figure 4.17 shows FT-IR spectra of linear and branched P*t*BuA before and after hydrolysis. After hydrolysis, the acid functionality is clearly visible as the broad peak from 2800 to 3800 cm^{-1} which was assigned to H-bonded carboxyl groups of PAA brushes. The carbonyl stretching of the ester group from P*t*BuA brushes at 1728 cm^{-1} shifted slightly to 1720 cm^{-1} which belongs to the carbonyl stretching of the carboxyl group from PAA brushes and the CH$_3$ bending vibration (from *t*-butyl group of P*t*BuA brushes) at 1370 cm^{-1} simultaneously disappeared after P*t*BuA brushes were transformed to PAA brushes.
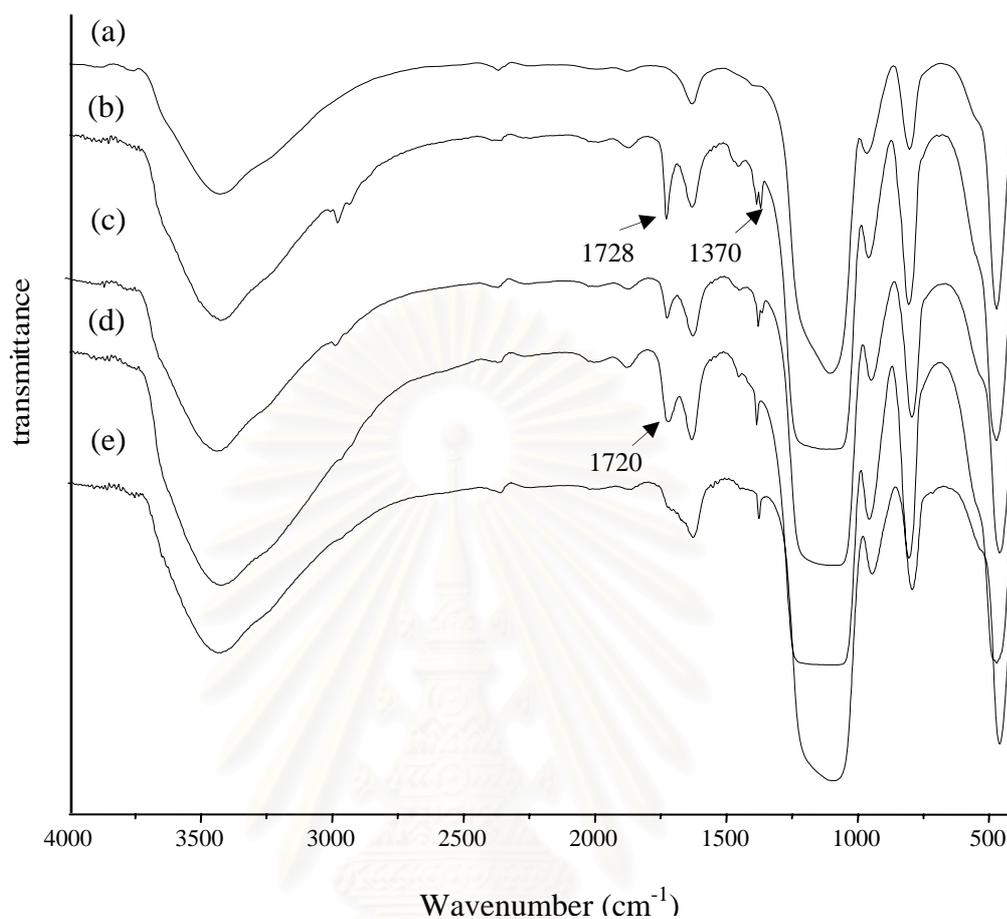
Figure 4.17 FT-IR spectra of (a) unmodified silica particle, (b) linear P*t*BuA brushes , (c) branched P*t*BuA brushes, (d) linear PAA brushes and (e) branched PAA brushes.

4.5.3 Determination of carboxyl group density of PAA brushes

The density of carboxyl group (COOH) on PAA brushes was quantitatively determined by using toluidine blue o assay. The carboxyl groups of PAA brushes can form a complex with toluidine blue o. The absorbance of the solution containing the desorbed complex was measured at 633 nm. The COOH content was obtained from a calibration plot of the optical density versus dye concentration which is displayed in Appendix C.

From Figure 4.18, it was found that the density of carboxyl group increased as a function of the molecular weight or chain length of the linear PAA brushes for both

targeted DPs. The density was ranged from 2.2 to 7.0 ($\times 10^{-9}$ mol/cm^2) for the linear PAA brushes having $\overline{M}_n$ and thickness in the range of 3.8×10^3 to 14.0×10^3 and 1.1 to 8.5 nm, respectively.
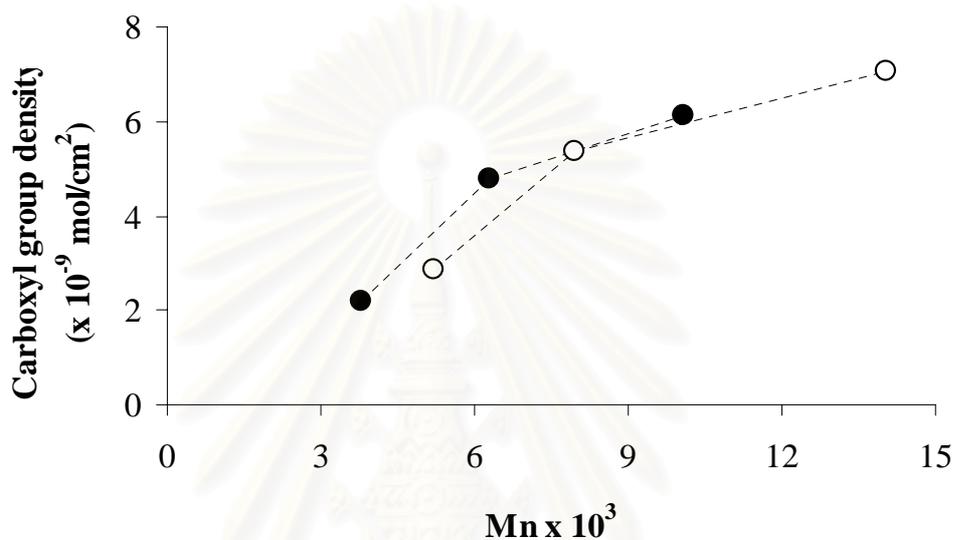
Figure 4.18 Carboxyl group density of linear PAA brushes as a function of molecular weight for targeted DP = 100 (●) and 200 (o).

For branched PAA brushes, the density of carboxyl group decreased with the increasing degree of branching (DB) (Figure 4.19) or increased with the increasing comonomer ratio (γ) (Figure 4.20). The density was ranged from 5.2 to 6.6 ($\times 10^{-9}$ mol/cm^2) for the branched PAA brushes. It should be noted that this range is narrower than that of the linear PAA brushes.
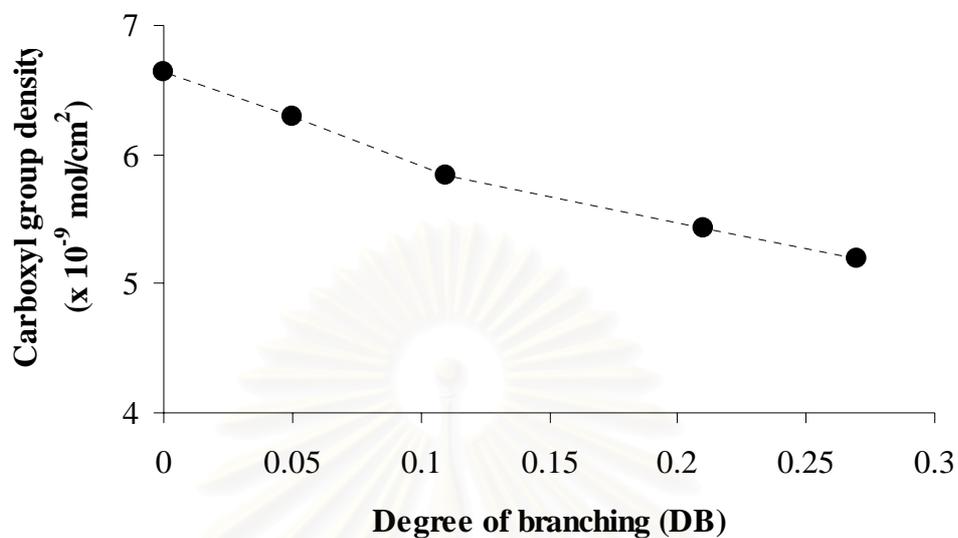
Figure 4.19 Carboxyl group density of branched PAA brushes as a function of degree of branching (DB).
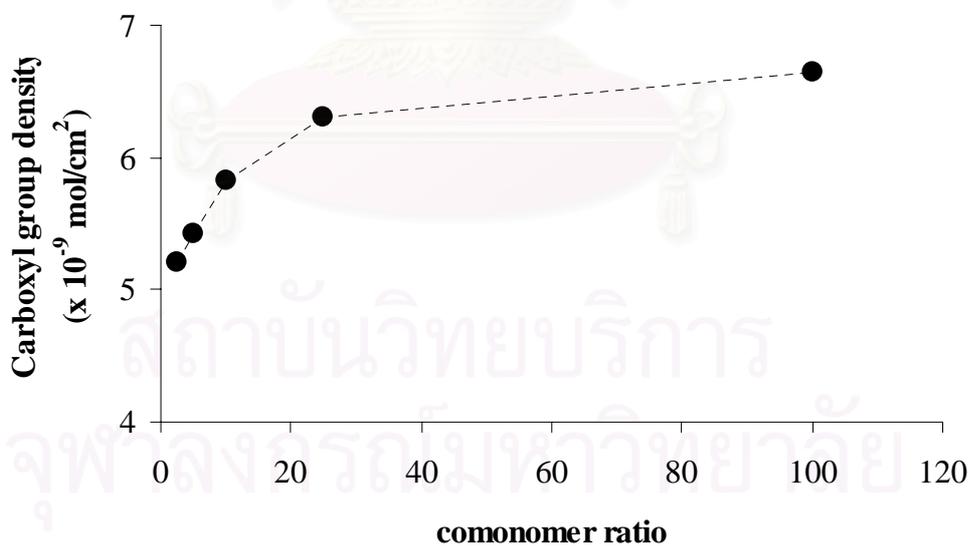
Figure 4.20 Carboxyl group density of branched PAA brushes as a function of comonomer ratio (γ).

4.6 Attachment of biotin to carboxyl group of poly(acrylic acid) brushes

In general, biomolecules are often immobilized on polymer surfaces via an amide bond formation between the carboxyl group and the amine group of biomolecule. A biotin-based ligand was chosen as a model biomolecule to be attached to the carboxyl group of PAA brushes. Biotin-streptavidin system is frequently used for biosensing application due in large part to their strong, biospecific interaction (K_D = 10^{-5}M) [83]. The association between biotin and streptavidin is very rapid and unaffected by extremes of pH, organic solvents and other denaturing agents. To achieve the covalent attachment of biotin to the carboxyl group of PAA brushes, a method of introducing reactive intermediate, *N*-hydroxysuccinimidyl (NHS) ester was used. The carboxyl group of PAA brushes was first activated by a water-soluble carbodiimide, 1-(3-dimethylaminopropyl)-3-ethylcarbodiimide hydrochloride (EDCI) and *N*-hydroxysuccinimide (NHS) to form NHS group. The NHS group was then coupled with amine-terminated biotin (NH$_2$-biotin), leading to amide bond formation.
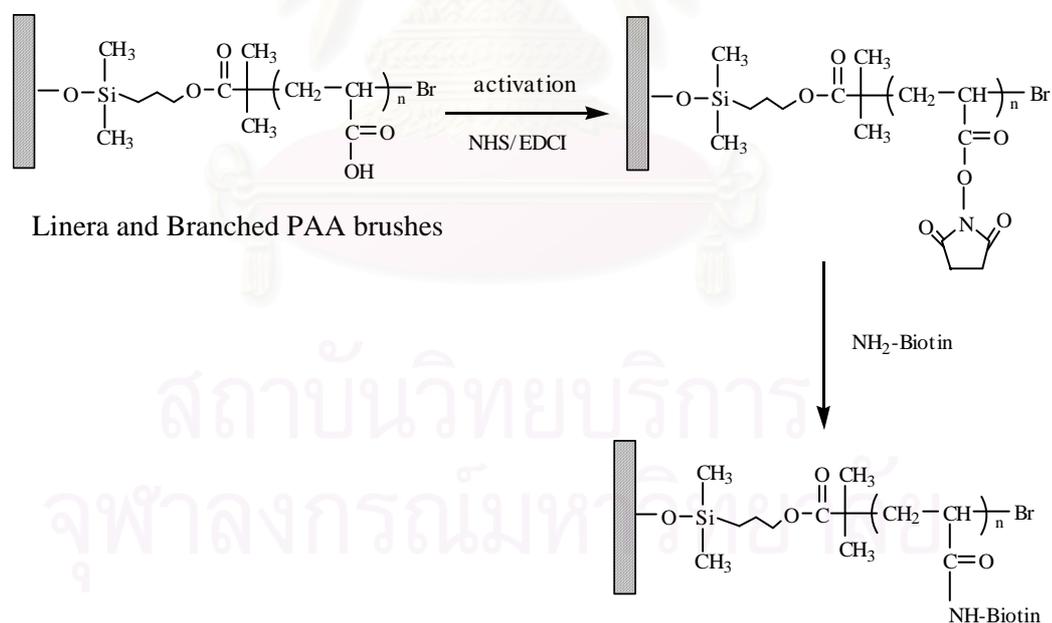
Scheme 4.3 Activation of carboxyl group of PAA brushes followed by binding of NH$_2$-biotin

The increasing of contact angle after the activation (shown in Table 4.2) suggests that the hydrophilic carboxyl groups of PAA brushes have been converted to hydrophobic *N*-succinimidyl groups. The contact angles were not much changed after biotin attachment.

Table 4.2 Advancing (θ_A) and receding (θ_R) water contact angle of PAA brushes before and after the activation by EDCI/NHS followed by the NH$_2$-biotin attachment

Sample	Water contact angle (°)	
	θ_A	θ_R
Linear PAA	60 ± 1.7	43 ± 0.8
Linear PAA-NHS	80 ± 0.8	47 ± 1.4
Linear PAA-biotin	79 ± 0.8	51 ± 1.7
Branched PAA	68 ± 0.8	47 ± 4.7
Branched PAA-NHS	78 ± 0.6	52 ± 1.9
Branched PAA-biotin	80 ± 0.8	53 ± 1.7

The success of activation and biotin attachment was also verified by FT-IR analysis. The shoulder peaks at 1734 and 1778 cm^{-1} assigned to the carbonyl stretching of succinimidyl ester of FT-IR spectrum shown in Figure 4.21 indicated that the carboxyl group was transformed to NHS group after activation by EDCI/NHS. The binding of NH$_2$-biotin can be verified by the presence of amide II band at 1558 cm^{-1} (N-H bending) and the disappearance of signals of succinimidyl ester at 1734 and 1778 cm^{-1}.
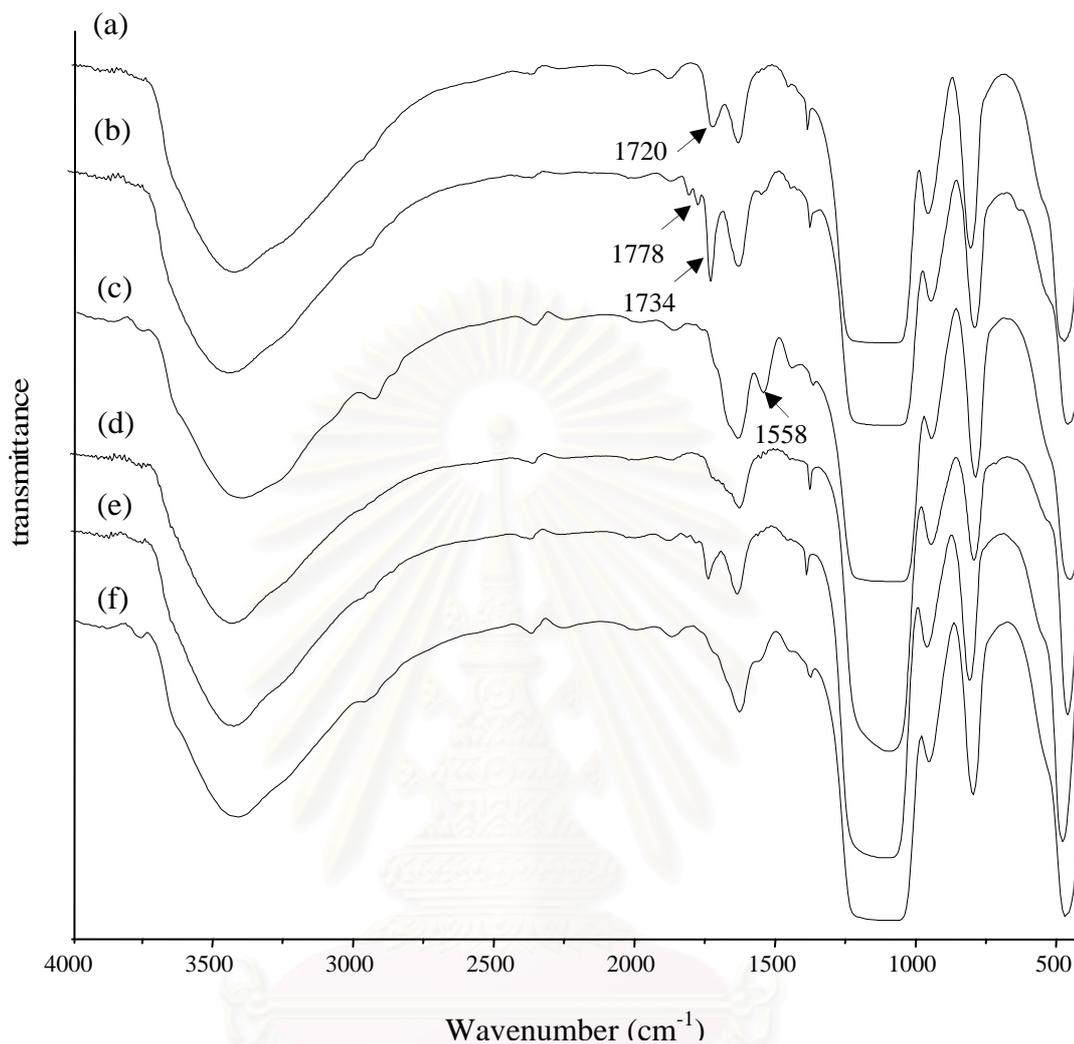
Figure 4.21 FT-IR spectra of (a) linear PAA, (b) linear PAA-NHS, (c) linear PAA-biotin, (d) branched PAA, (e) branched PAA-NHS and (f) branched PAA-biotin.

The extent of activation and NH_2-biotin binding as a function of carboxyl group density of PAA brushes was quantified from the relative ratio of transmittance of the designated peak (C=O stretching of NHS at 1734 cm^{-1} for activation and N-H bending at 1558 cm^{-1} for biotin binding) against the transmittance of Si-O stretching from silica at 794 cm^{-1}. Data in Table 4.3 suggests that the extent of activation and NH_2-biotin attachment proportionally increases as a function of carboxyl group density. The relative ratio of transmittance of the C=O stretching of P*t*BuA at 1727-

1730 cm^{-1} against the transmittance of Si-O stretching from silica at 794 cm^{-1} was also included for comparison.

Table 4.3 Percentage transmittance ratio obtained from FT-IR analysis

Sample	Carboxyl group density (x10^{-9} mol/cm^2)	Transmittance ratio (%)		
		C=O str of PtBuA/ Si-O str	C=O str of NHS/Si-O str	N-H bend/ Si-O str
Linear PAA ($\overline{M}_n$ =6.3x10^3)	4.79	2.10	5.60	-
Linear PAA ($\overline{M}_n$ =10.1x10^3)	6.13	10.80	14.10	5.20
Linear PAA ($\overline{M}_n$ =14.0x10^3)	7.04	17.20	26.40	13.60
Branched PAA ($\overline{M}_n$ =3.6x10^3, γ = 25)	6.30	10.90	12.46	4.70

The attachment of the biotin was qualitatively confirmed by fluorescence microscope. Figures 4.22b and c display optical and fluorescence images of the linear PAA-biotin and branched PAA-biotin grafted on silica particles after incubation in the solution of fluorescein-conjugated streptevidin. The dark area of all optical images in the top row is the area that was covered by the silica particles while the bright area is the empty space on the glass slide. Upon exposure to fluorescence irradiation, the dark area appeared green while the bright area turned dark as can be seen from the images b and c in the bottom row. The bottom image of the control sample (blank silica particles) appeared totally dark indicating there was no fluorescein-conjugated streptevidin adsorbed. This result strongly suggests that NH$_2$-biotin can covalently

attach to the carboxyl group of PAA brushes. And the attached biotin can effectively act as an active binding site for fluorescein-conjugated streptevidin.

Optical images

Fluorescence images

0.1 mm

(a)   (b)   (c)
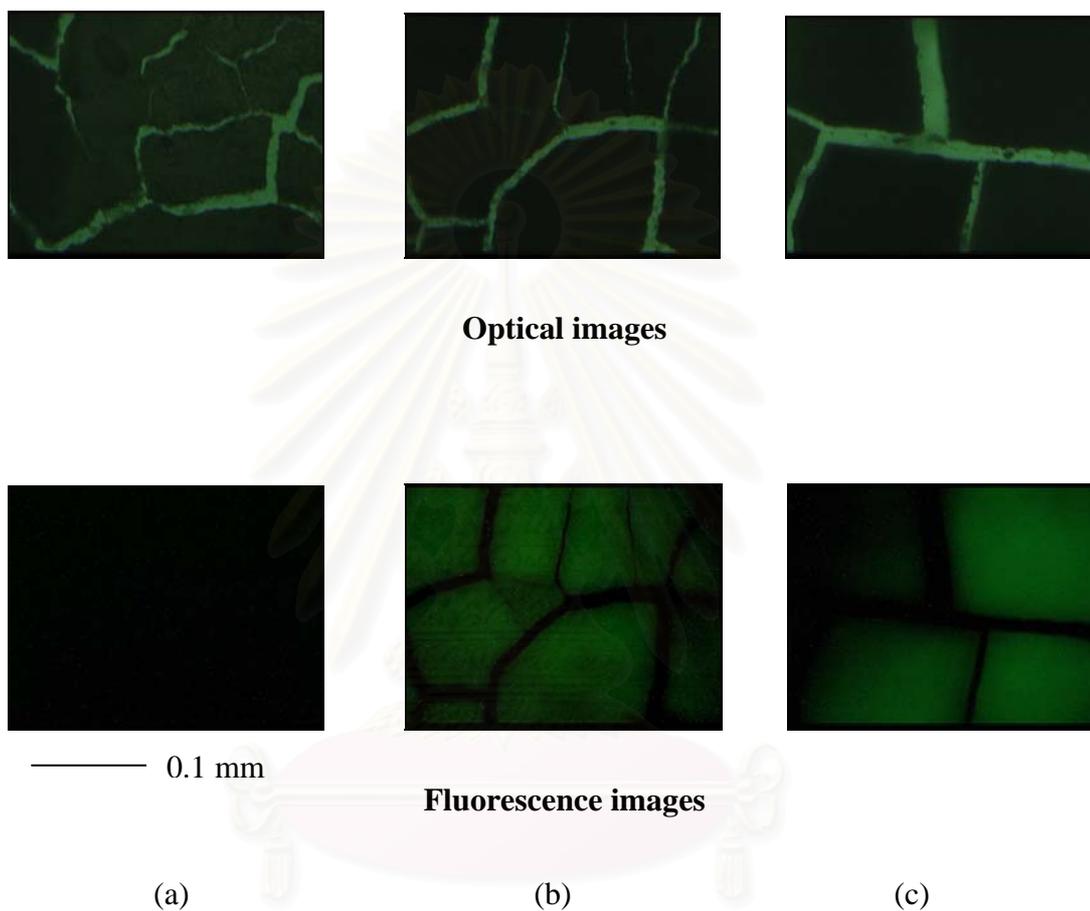
Figure 4.22 Optical (top) and fluorescence (bottom) images of silica particles (spread on glass slide) grafted with biotin-attached linear and branched PAA brushes after binding with fluorescein-conjugated streptevidin: (a) control, (b) linear PAA-biotin (targeted DP = 200, 24 h) and (c) branched PAA-biotin ($\gamma = 25$).

CHAPTER V

CONCLUSION AND SUGGESTION

Linear and branched poly(*tert*-butyl acrylate) (P*t*BuA) brushes can be prepared from the surfaces bearing α-bromoester groups by surface-initiated atom transfer radical polymerization (ATRP) of *tert*-butyl acrylate (*t*BuA) and self-condensing vinyl copolymerization (SCVCP) of acrylic acid 2-(2-bromopropionyl oxy)ethyl ester (BPEA) with *t*BuA via atom transfer radical polymerization (ATRP), respectively. Linear and branched poly(acrylic acid) (PAA) brushes were subsequently obtained after *tert*-butyl groups of P*t*BuA brushes were removed by acid hydrolysis.

In the case of linear polymer brushes, the molecular weight and thickness of polymer brushes can be controlled by reaction time and monomer to initiatior ratio in the solution (targeted degree of polymerization). The graft density of linear P*t*BuA brushes was approximately 0.25 and 0.32 chains/nm^2 for the targeted DP = 100 and 200, respectively. For the branched polymer brushes, the molecular weights, the composition of copolymer and degree of branching (DB) can be adjusted by an appropriate choice of the comonomer composition (γ).

As determined by toluidine blue o assay, the carboxyl group density of the linear PAA brushes was varied as a function of the chain length (MW) while the carboxyl group density of the branched PAA brushes was varied as a function of the comonomer ratio (γ). It has been demonstrated that the carboxyl groups of both linear and branched PAA brushes are readily available for an attachment of biotin-NH$_2$. According to FT-IR analysis, the density of the immobilized biotin relied on the carboxyl group density of the polymer brushes. The fact that the immobilized biotin on polymer can bind effectively with fluorescein-conjugated streptevidin as visualized by fluoroscence microscope suggests that the carboxyl groups of surface-tethered

PAA brushes can potentially served as versatile moieties for immobilization of bioactive species that act as sensing probes of biosensor.

REFERENCES

1. Zhao, B.; Brittain, W. J. "Polymer Brushes: Surface-Immobilized Macromolecules" *Prog. Polym. Sci.* **2000**, *25,* 677-710.

2. Raphael, E.; De Gennes, P. G. "Rubber-Rubber Adhesion with Connector Molecules" *J. Phys Chem* **1992**, *96,* 4002-4007.

3. Ji, H.; De Gennes, P. G. "Adhesion via Connector Molecules: The Many-Stitch Problem" *Macromolecules* **1993**, *26,* 520-525.

4. Amiji, M.; Park, K. J. "Surface Modification of Polymeric Biomaterials with Poly(ethylene oxide), Albumin, and Heparin for Reduced Thrombogenicity" *Biomater. Sci. Polym. Ed.* **1993**, *4,* 217-234.

5. van Zanten, J. H. "Terminally Anchored Chain Interphases: Their Chromatographic Properties" *Macromolecules* **1994**, *27,* 6797-6807.

6. Joanny, J. F. "Lubrication by Molten Polymer Brushes" *Langmuir* **1992**, *8,* 989-995.

7. Takei, Y. G.; Aoki, T.; Sanui, K.; Ogata, N.; Sakurai, Y.; Okano, T. "Dynamic Contact Angle Measurement of Temperature-Responsive Surface Properties for Poly(N-isopropylacrylamide) Grafted Surfaces" *Macromolecules* **1994,** *27,* 6163-6166.

8. Ito, Y.; Ochiai, Y.; Park, Y. S.; Imanishi, Y. "pH-Sensitive Gating by Conformational Change of a Polypeptide Brush Grafted onto a Porous Polymer Membrane" *J. Am. Chem. Soc.* **1997**, *119,* 1619-1623.

9. Ito, Y.; Park, Y. S.; Imanishi, Y. "Visualization of Critical pH-Controlled Gating of a Porous Membrane Grafted with Polyelectrolyte Brushes" *J. Am. Chem. Soc.* **1997**, *119,* 2739-2740.

10. Ito, Y.; Nishi, S.; Park, Y. S.; Imanish, Y. "Oxidoreduction-Sensitive Control of Water Permeation through a Polymer Brushes-Grafted Porous Membrane" *Macromolecules* **1997**, *30,* 5856-5859.

11. Velten, U.; Shelden, R. A.; Caseri, W. R.; Suter, U. W.; Li, Y. "Polymerization of Styrene with Peroxide Initiator Ionically Bound to High Surface Area Mica" *Macromolecules* **1999**, *32,* 3590-3597.

12. Velten, U.; Tossati, S.; Shelden, R. A.; Caseri, W. R.; Suter, U. W.; Hermann, R.; Müller, M. "Graft Polymerization of Styrene on Mica: Formation and Behavior of Molecular Droplets and Thin Films" *Langmuir* **1999**, *15,* 6940-6945.

13. Niu, Q. J.; Fréchet, J. M. J. "Polymers for 193-nm Microlithography: Regioregular 2-Alkoxycarbonylnortricyclene Polymers by Controlled Cyclopolymerization of Bulky Ester Derivatives of Norbornadiene" *Angew Chem, Int Ed Engl* **1998**, *37,* 667-670.

14. Singhvi, R.; Kumar, A.; Lopez, G. P.; Stephanopoulos, G. N.; Wang, D. I. C.; Whitesides, G. M.; Ingber, D. E. "Engineering Cell-Shape and Function" *Science* **1994**, *264,* 696-698.

15. Chen, C. S.; Mrksich, M.; Huang, S.; Whitesides, G. M.; Ingber, D. E. "Geometric Control of Cell Life and Death" *Science* **1997**, *276,* 1425-1428.

16. Aksay, I. A.; Trau, M.; Manne, S.; Honma, I.; Yao, N.; Zhou, L.; Fenter, P.; Eisenberger, P. M.; Gruner, S. M. "Biomimetic Pathways for Assembling Inorganic Thin Films" *Science* **1996**, *273,* 892-898.

17. Balazs, A. C.; Singh, C.; Zhulina, E.; Gersappe, D.; Pickett, G. "Patterned Polymer Films" *MRS Bull* **1997**, *22,* 16-21.

18. Soga, K. G.; Zuckermann, M. J.; Guo, H. "Binary Polymer Brush in a Solvent" *Macromolecules* **1996**, *29,*1998-2005.

19. Mansky, P.; Liu, Y.; Huang, E.; Russell T. P.; Hawker, C. "Controlling Polymer-Surface Interactions with Random Copolymer Brushes" *Science* **1997**, *275,* 1458-1460.

20. Zhao, B.; Brittain, W. J. "Synthesis of Tethered Polystyrene-block-Poly (methyl methacrylate) Monolayer on a Silicate Substrate by Sequential Carbocationic Polymerization and Atom Transfer Radical Polymerization" *J. Am. Chem. Soc.* **1999**, *1219,* 3557-3558.

21. Nakayama, Y.; Matsuda, T. "Surface Macromolecular Architectural Designs Using Photo-Graft Copolymerization Based on Photochemistry of Benzyl N,N-Diethyldithiocarbamate" *Macromolecules* **1996**, *29,* 8622-8630.

22. Ejaz, M.; Yamamoto, S.; Ohno, K.; Tsujii, Y.; Fukuda, T. "Controlled Graft Polymerization of Methyl Methacrylate on Silicon Substrate by the Combined Use of the Langmuir-Blodgett and Atom Transfer Radical Polymerization Techniques" *Macromolecules* **1998**, *31,* 5934-5936.

23. Husseman, M.; Malmström, E. E.; McNamara, M.; Mate, M.; Mecerreyes, D.; Benoit, D. G.; Hedrick, Mansky, P.; Huang, E. ; Russell, T. P.; Hawker, C. J. "Controlled Synthesis of Polymer Brushes by "Living" Free Radical Polymerization Techniques" *Macromolecules* **1999**, *32,* 1424-1431.

24. Huang, X.; Wirth, M. J. "Surface Initiation of Living Radical Polymerization for Growth of Tethered Chains of Low Polydispersity" *Macromolecules* **1999**, *32,* 1694-1696.

25. Sedjo, R. A.; Mirous, B. K.; Brittain, W. J. "Synthesis of Polystyrene-block-poly(methyl methacrylate) Brushes by Reverse Atom Transfer Radical Polymerization" *Macromolecules* **2000**, *33,* 1492-1493.

26. de Boer, B.; Simon, H. K.; Werts, M. P. L.; van der Vegte, E. W.; Hadziioannou, G. ""Living" Free Radical Photopolymerization Initiated

from Surface-Grafted Iniferter Monolayers" *Macromolecules* **2000**, *33*, 349-356.

27. Ejaz, M.; Yamamoto, K.; Ohno, Y. T.; Fukuda, T. "Controlled Graft Polymerization of Mrthyl Mathacrylate on Silicon Substrate by the Combined Use of the Langmuir-Blodgett and Atom Transfer Radical Polymerization Techniques" *Macromolecule* **1998**, 31, 5934-5936.

28. Matyjaszewski, K.; Miller, P. J.; Shukla, N.; Immaraporn, B.; Gelman, A.; Luokala, B. B.; Siclovan, T. M.; Kickelbick, G.; Vallant, T.; Hoffmann, H.; Pakula, T. "Polymers at Interfaces: Using Atom Transfer Radical Polymerization in the Controlled Growth of Homopolymers and Block Copolymers from Silicon Surfaces in the Absence of Untethered Sacrificial Initiator" *Macromolecules* **1999**, *32,* 8716-8724.

29. *von* Werene, T.; Patten, T.E. "Atom Transfer Radical Polymerization from Nanoparticles: A Tool for the Preparation of Well-defined Hybrid Nanostructures and for Understanding the Chemistry of Controlled/"Living" Radical Polymerizations from Surfaces" *J. Am. Chem. Soc.* **2001**, *123*, 7497-7505.

30. Mori, H.; Boker, A.; Krausch, G.; Muller, A. H. E. "Surface-Grafted Hyperbranched Polymer via Self-Condensing Atom Transfer Radical Polymerization from Silicon Surfaces" *Macromolecules* **2001**, 34, 6871-6882.

31. Mori, H.; Seng, D. C.; Zhang, M.; Muller, A. H. E. "Hybrid Nanoparticle with Hyperbranched Polymer Shells via Self-Condensing Atom Transfer Radical Polymerization from Silica surface" *Lungmuir* **2002**, 18, 3682-3693.

32. Szwarc, M.; Levy, M.; Milkovich, R. "Polymerization Initiated by Electron Transfer to Monomer a New Method of Formation of Block Polymers" *J. Am. Chem. Soc.* **1956**, *78,* 2656-2657.

33. Flory, P. J. "Principles of Polymer Chemistry" *Cornell Uni. Press,* Ithaca, NY. **1978**.

34. Webster, O. W. "Living Polymerization Methods" *Science* **1991**, *251,* 887-.

35. Moad, G.; Rizzardo, E.; Solomon D. H. "Selectivity of the Reaction of Free Radicals with Styrene" *Macromolecules* **1982**, *15,* 909-914.

36. Georges, M. K.; Veregin, R. P. N.; Kazmaier, P. M.; Hamer, G. K. "Narrow Molecular Weight Resins by a Free-Radical Polymerization Process" *Macromolecules* **1993**, *26,* 2987-2988.

37. Kato, M.; Kamigaito, M.; Sawamoto, M.; Higashimura, T. "Polymerization of Methyl Methacrylate with the Carbon Tetrachloride/ Dichlorotris-(triphenylphosphine)ruthenium(II)/Methylaluminum Bis(2,6-di-*tert*-butylphenoxide) Initiating System: Possibility of Living Radical Polymerization" *Macromolecules* **1995**, *28,* 1721-1723.

38. Wang, J. S.; Matyjaszewski, K. "Controlled/"Living" Radical Polymerization. Atom Transfer Radical Polymerization in the Presence of Transition-Metal Complexs" *J. Am. Chem. Soc.* **1995**, *117,* 5614-5615.

39. Percec, V.; Barboiu, B. ""Living" Radical Polymerization of Styrene Initiated by Arenesulfonyl Chlorides and CuI(bpy)nCl" *Macromolecules* **1995**, *28,* 7970-7972.

40. Wayland, B. B.; Poszmik, G.; Mukerjee, S. L.; Fryd, M. "Living Radical Polymerization of Acrylates by Organocobalt Porphyrin Complexes" *J. Am. Chem. Soc.* **1994**, *116,* 7943-7944.

41. Granel, C.; DuBois, P.; Jerome, R.; Teyssie, P. "Controlled Radical Polymerization of Methacrylic Monomers in the Presence of a Bis(ortho-chelated) Arylnickel(II) Complex and Different Activated Alkyl Halides" *Macromolecules* **1996**, *29,* 8576-8582.

42. Matyjaszewski, K. "Controlled Radical Polymerization" *ACS Symposium Series NO. 685 American Chemical Society:* Washington, DC, **1997.**

43. Matyjaszewski, K. "Mechanistic and Synthetic Aspects of Atom Transfer Radical Polymerization" *J. Macromol. Sci., Pure Appl. Chem.* **1997**, *A34,* 1785-1801.

44. Chambard, G.; Klumperman, B.; German, A. L. "Effect of Solvent on the Activation Rate Parameters for Polystyrene and Poly(butyl acrylate) Macroinitiators in Atom Transfer Radical Polymerization" *Macromolecules* **2000**, *33,* 4417-4421.

45. Matyjaszewski, K.; Xia, J. "Atom Transfer Radical Polymerization" *Chem. Rev.* **2001**, 101, 2921-2990.

46. Matyjaszewski, K.; Xia, J. "Controlled/"Living" Radical Polymerization. Atom Transfer Radical Polymerization Using Multidentate Amine Ligands" *Macromolecules* **1997**, 30, 7697-7700.

47. Suzuki, K.; Siddiqui, S.; Chappell, C.; Siddiqui, J.A.; Ottenbrite, R. M. *Polym. Adv. Technol.* **2000**, 11, 92.

48. Shi, Y.; Seliskar, C. *J. Chem. Mater.* **1997**, 9, 821.

49. Shimomura, M.; Kikuchi, H.; Matsumoto, H.; Yamauchi, T.; Miyauchi, S. *Polym.J.(Tokyo)* **1995**, 27, 974.

50. Yoshinaga, K.; Kondo, K.; Kondo, A. *Colloid Polym. Sci.* **1997**, 275, 220.

51. Davis, K.A.; Matyjaszewski, K. "Atom Transfer Radical Polymerization of tert-butyl acrylate and Preparation of Block Copolymers" *Macromolecules* **2000**, 33, 4039–4047.

52. Davis, K. A.; Charleux, B.; Matyjaszewski, K. "Preparation of Block Copolymers of Polystyrene and Poly(t-butyl acrylate) of various Molecular weights and Architectures by Atom Transfer Radical

Polymerization" *J Polym Sci, Part A: Polym Chem* **2000**, 38, 2274–2283.

53. Bohrisch, J.; Eisenbach, C. D.; Jaeger, W.; Mori, H.; Muller, A. H. E.; Rehahn, M.; Schaller, C.; Traser, S.; Wittmeyer, P. "New Polyelectrolyte Architectures" *Adv Polym Sci* **2003**, 165, in press.

54. Ballauff, M. "Nanoscopic Polymer Particles with a Welldefined Surface: Synthesis, Characterization, and Properties" *Macromol. Chem. Phys.* **2003**, 204, 220–234.

55. Mori, H.; Muller, A. H. E. "Hyperbranched (meth)acrylates in Solution, in The Melt, and Grafted from Surfaces" *In Dendrimers V, Schalley CA, Vo¨gtle F editors*. Topics in Current Chemistry **2003**, 228, 1–37.

56. Fre´chet, J. M. J.; Henmi, M.; Gitsov, I.; Aoshima, S.; Leduc, M. R.; Grubbs, R. B. "Self-Condensing Vinyl Polymerization: an Approach to Dendritic" *Materials. Science* **1995**, 269, 1080–1083.

57. Baskaran, D. "Synthesis of Hyperbranched Polymers by Anionic Self-Condensing Vinyl Polymerization" *Macromol. Chem. Phys* **2001**, 202, 1569–1575.

58. Simon, P. F. W.; Radke, W.; Muller, A. H. E. "Hyperbranched methacrylates by Self-Condensing Group Transfer Polymerization" *Macromol. Rapid Commun.* **1997**, 18, 865–873.

59. Hawker, C. J.; Fre´chet, J. M. J.; Grubbs, R. B.; Dao, J. "Preparation of Hyperbranched and Star Polymers by a "Living" Self-Condensing Free Radical Polymerization" *J. Am. Chem. Soc.* **1995**, 117, 10763–10764.

60. Weimer, M. W.; Fre´chet, J. M. J.; Gitsov, I. "Importance of Active-Site Reactivity and Reaction Conditions in the Preparation of Hyperbranched Polymers by Self-Condensing Vinyl Polymerization: Highly Branched vs. Linear poly[4-(chloromethyl) styrene] by Metal-Catalyzed "Living"

Radical Polymerization. *J. Polym. Sci. Part A: Polym. Chem.* **1998**, 36, 955–970.

61. Matyjaszewski, K.; Gaynor, S. G.; Kulfan, A.; Podwika, M. "Preparation of Hyperbranched Polyacrylates by Atom Transfer Radical Polymerization. 1. Acrylic AB* Monomers in "Living" Radical Polymerizations" *Macromolecules* **1997**, 30, 5192–5194.

62. Matyjaszewski, K.; Gaynor, S. G.; Mu¨ller, A. H. E. "Preparation of Hyperbranched Polyacrylates by Atom Transfer Radical Polymerization. 2. Kinetics and Mechanism of Chain Growth for the Self-Condensing Vinyl Polymerization of 2-((2-bromopropionyl)oxy) ethyl acrylate" *Macromolecules* **1997**, 30, 7034–7041.

63. Matyjaszewski, K.; Gaynor, S. G. "Preparation of Hyperbranched Polyacrylates by Atom Transfer Radical Polymerization. 3. Effect of Reaction Conditions on the Self-Condensing Vinyl Polymerization of 2-((2-bromopropionyl)oxy)ethyl acrylate" *Macromolecules* **1997**, 30, 7042–7049.

64. Sunder, A.; Hanselmann, R.; Frey, H.; Mu¨lhaupt, R. "Controlled Synthesis of Hyperbranched Polyglycerols by Ring-Opening Multibranching Polymerization" *Macromolecules* **1999**, 32, 4240–4246.

65. Fre´chet, J. M. J, Aoshima, S. "Hyperbranched Copolymers from Bifunctional AB Monomers and Monofunctional Comonomers" *PCT Int. Appl.* **1996**, WO9614345, WO9614346.

66. Gaynor, S. G.; Edelman, S.; Matyjaszewski, K. "Synthesis of Branched and Hyperbranched Polystyrenes" *Macromolecules* **1996**, 29, 1079–1081.

67. Simon, P. F. W.; Mu¨ller, A. H. E. "Synthesis of Hyperbranched and Highly Branched Methacrylates by Self-Condensing Group Transfer Copolymerization" *Macromolecules* **2001**, 34, 6206–6213.

68. Paulo, C.; Puskas, J.E. "Synthesis of Hyperbranched Polyisobutylenes by Inimer-Type Living Polymerization. 1. Investigation of the Effect of Reaction Conditions" *Macromolecules* **2001**, 34, 734–739.

69. Mori H, Chan Seng D, Lechner H, Zhang M, Mu¨ller AHE. Synthesis and Characterization of Branched Polyelectrolytes. 1. Preparation of Hyperbranched Poly(acrylic acid) via Self-Condensing Atom Transfer Radical Copolymerization" *Macromolecules* **2002**, 35, 9270–9281.

70. Biesalski, M.; Johannsmann, D.; Ruhe, J. "Synthesis and Swelling Behavior of a Weak Polyacid Brush" *J. Chem. Phys*. **2002**, 117, 4988–4994.

71. Mori, H.; Bo¨ker, A.; Krausch, G.; Mu¨ller, A. H. E. "Surface-Grafted Hyperbranched Polymers via Self-Condensing Atom Transfer Radical Polymerization from Silicon Surfaces" *Macromolecules* **2001**, 34, 6871–6882.

72. Mori, H.; Chan Seng, D.; Zhang, M.; Mu¨ller, A. H. E. "Hybrid Nanoparticles with Hyperbranched Polymer Shells via Self-Condensing Atom Transfer Radical Polymerization from Silica Surfaces" *Langmuir* **2002**, 18, 3682–3693.

73. Boyes, S. G.; Akgun, B.; Brittain, W. J.; Foster, M. D. "Synthesis, Characterization, and Properties of Polyelectrolyte Block Copolymer Brushes Prepared by Atom Transfer Radical Polymerization and Their Use in the Synthesis of Metal Nanoparticles" *Macromolecules* **2003**, 36, 9539-9548.

74. Qi, K.; Wooley, K. L.; Jhaveri, S. B.; Sogah, D. Y.; Beinhoff, M.; Malkoch, M.; Carter, K. R.; Hawker, C. J. "Nano-patterned and Layered Syntheticbiological Materials Assembled upon Polymer brushes via Biotin/Streptavidin Recognition" *Polymeric Materials: Scince & Engineering* **2004**, 91, 133.

75. Seymour, M. P. "Introduction to Polymers Chemistry" *Tokyo, McGraw-Hill Kogakusha* **1971**

76. www.uta.edu/optics/research/ellipsometry/ellipsometry.htm

77. Xiao, S. J. "Tailored Organic Thin Films on Gold and Titanium: Peptide-Grafting, Protein Resistance and Physical Characterization" *Thesis; M. Sc. Chemistry, Fudan University, Shanghai China* **1999**.7

78. www.chembio.uoguelph.ca/educmat/chm729/afm/introdn.htm

79. *von* Werene, T.; Patten, T.E. "Atom Transfer Radical Polymerization from Nanoparticles: A Tool for the Preparation of Well-defined Hybrid Nanostructures and for Understanding the Chemistry of Controlled/"Living" Radical Polymerizations from Surfaces" *J. Am. Chem. Soc.* **2001**, *123*, 7497-7505.

80. Marutani, E.; Yamamoto, S.; Ninjbadgar, T.; Tsujii, Y.; Fukuda, T.; Takano, M. "Surface-initiated Atom Transfer Radical Polymerization of methyl Methacrylate on magnetite nanoparticles" *Polymer* **2004**, 45, 2231-2235.

81. Husseman, M.; Malmstrom, E. E.; McNamara, M.; Mate, M.; Mecerreyes, D.; Benoit, D. G.; Hedrick, J. L.; Mansky, P.; Huang, E.; Russell, T. P.; Hawker, C. J. "Controlled Synthesis of Polymer Brushes by "Living" Free Radical Polymerization Techniques" *Macromolecules*, **1999**, *32*, 1424-1431.

82. Mori, H.; Chan Seng, D.; Lechner, Hans.; Zhang, M.; Mu¨ller, A. H. E. "Synthesis and Characterization of Branched Polyelectrolytes. 1. Preparation of Hyperbranched Poly(acrylic acid) via Self-Condensing Atom Transfer Radical Copolymerization" *Macromolecule* **2002**, 35, 9270-9281.

83. Lahann, J.; Balcells, M.; Rodon, T.; Lee, J.; Choi, I.S.; Jensen K.F.; Langer, R. "Reactive polymer coatings: A Platfrom for Patterning Proteins and Mammalian Cells onto a Broad Range of Materials" *Langmuir* **2002**, 18, 3632-3638.

APPENDICES

APPENDIX A

A. Proton nuclear magnetic resonance spectroscopy (^{1}H NMR)
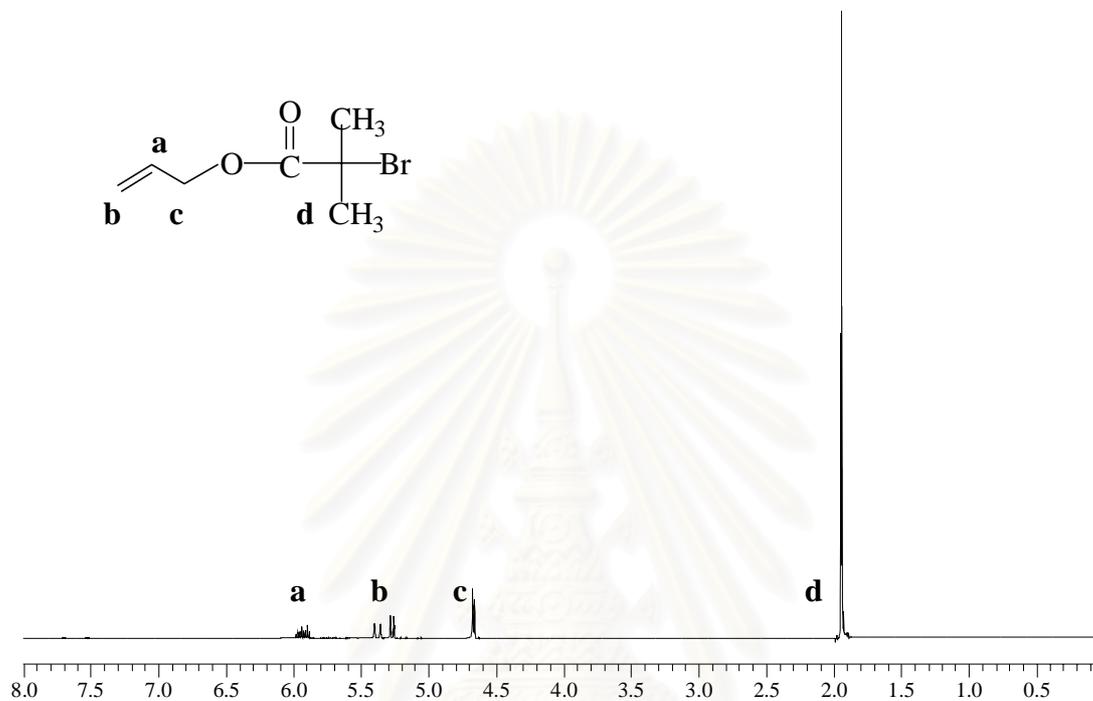
Figure A-1 The ^{1}H-NMR (400 MHz, CDCl$_3$) of 2-bromo-2-methylpropionic acid allyl ester **(1)**.
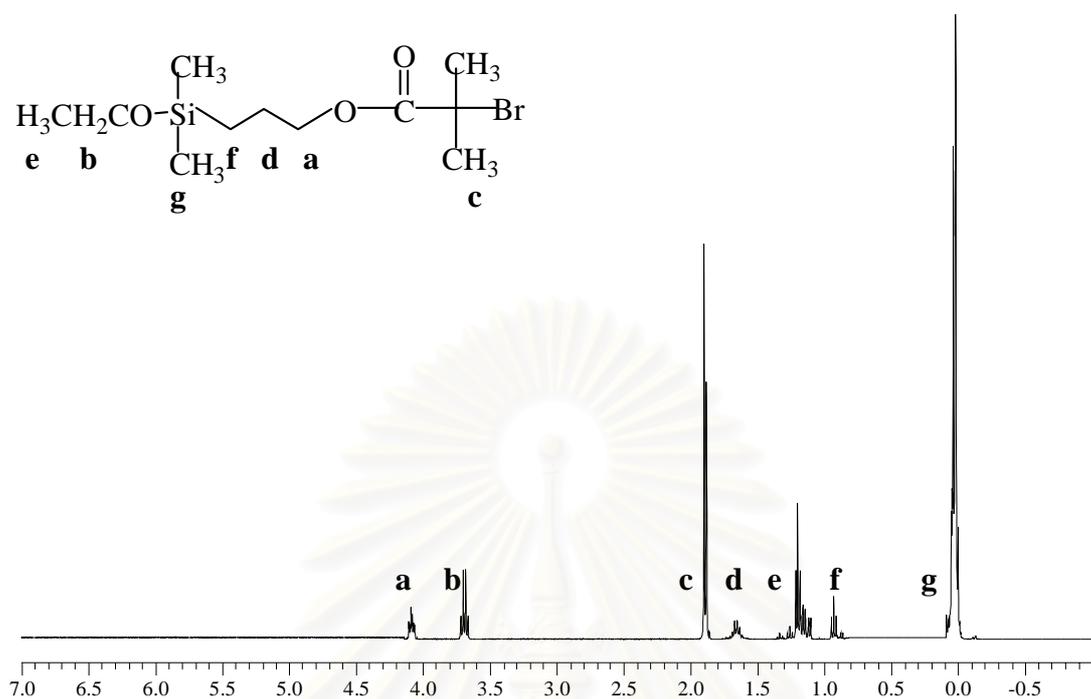
**Figure A-2** The ^{1}H-NMR (400 MHz, CDCl$_3$) of 2-bromo-2-methylpropionic acid 3-(ethoxydimethyl silanyl)propyl ester **(2)**.
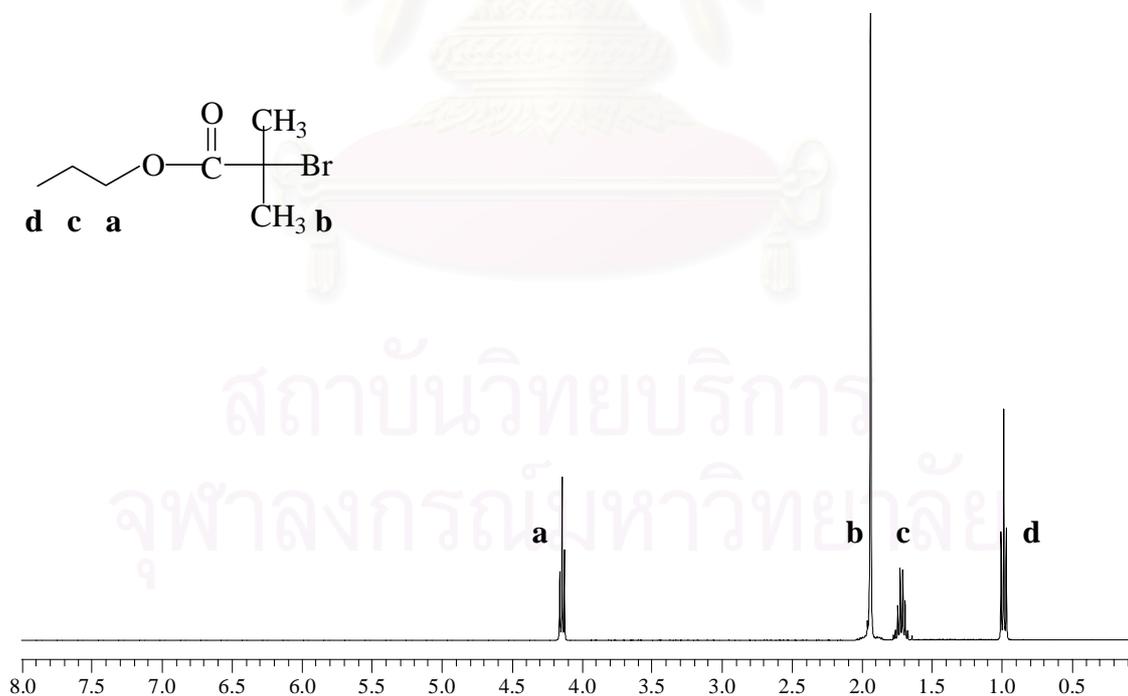
**Figure A-3** The ^{1}H-NMR (400 MHz, CDCl$_3$) of 2-bromo-2-methylpropionic acid propyl ester **(3)**.
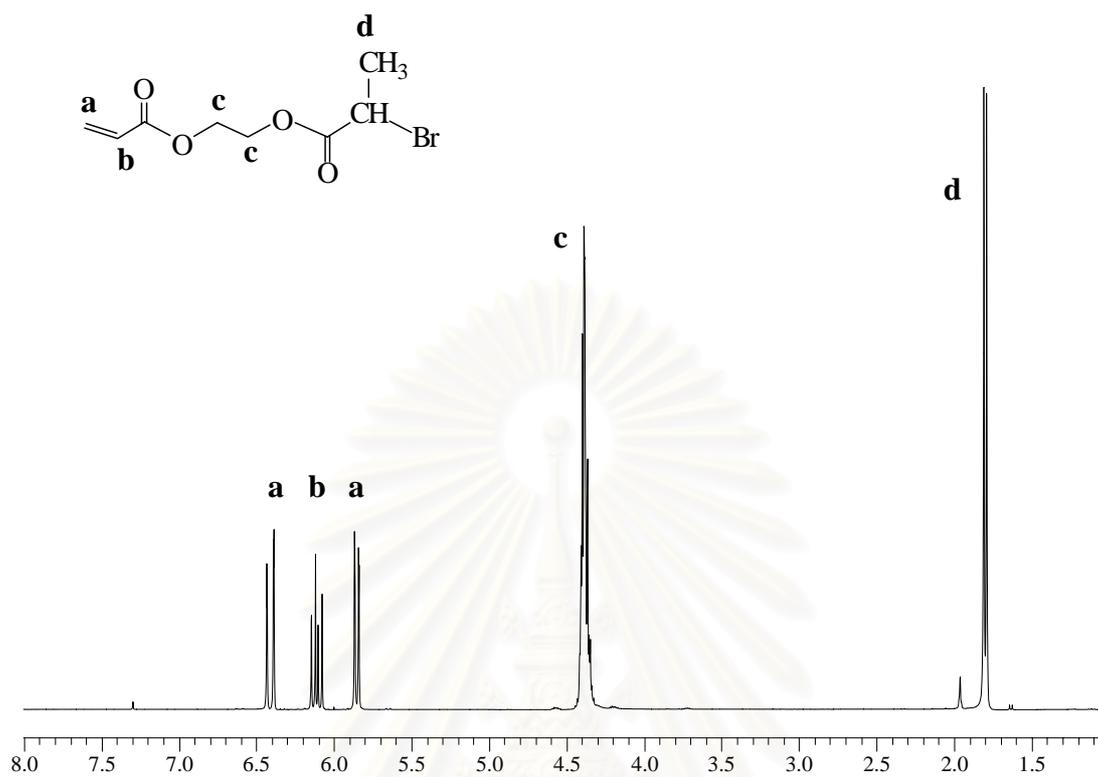
Figure A-4 The ^{1}H-NMR (400 MHz, CDCl$_3$) of BPEA.
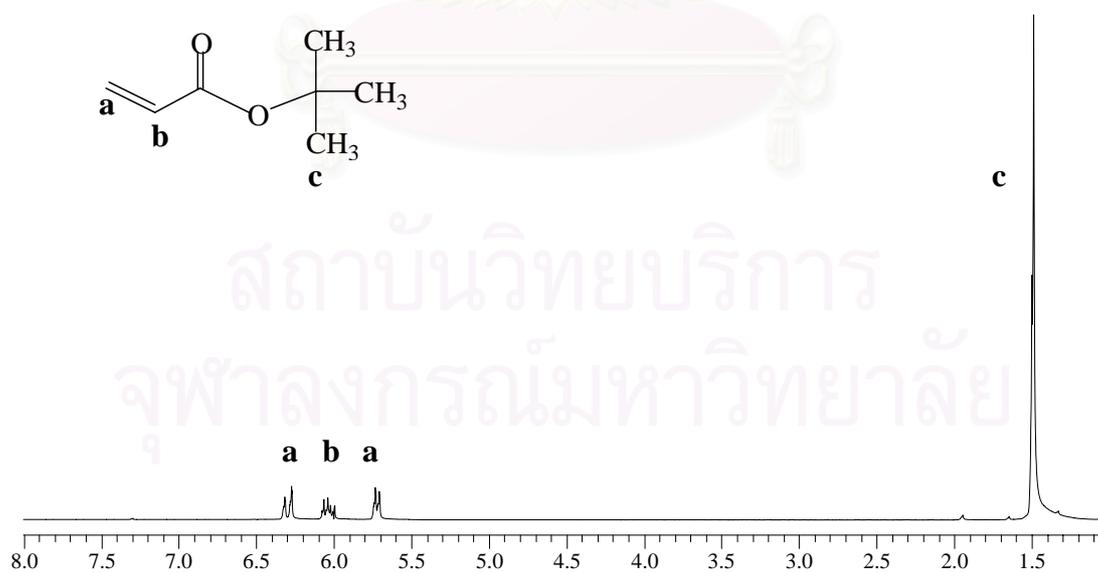
Figure A-5 The ^{1}H-NMR (400 MHz, CDCl$_3$) of *t*BuA.

103
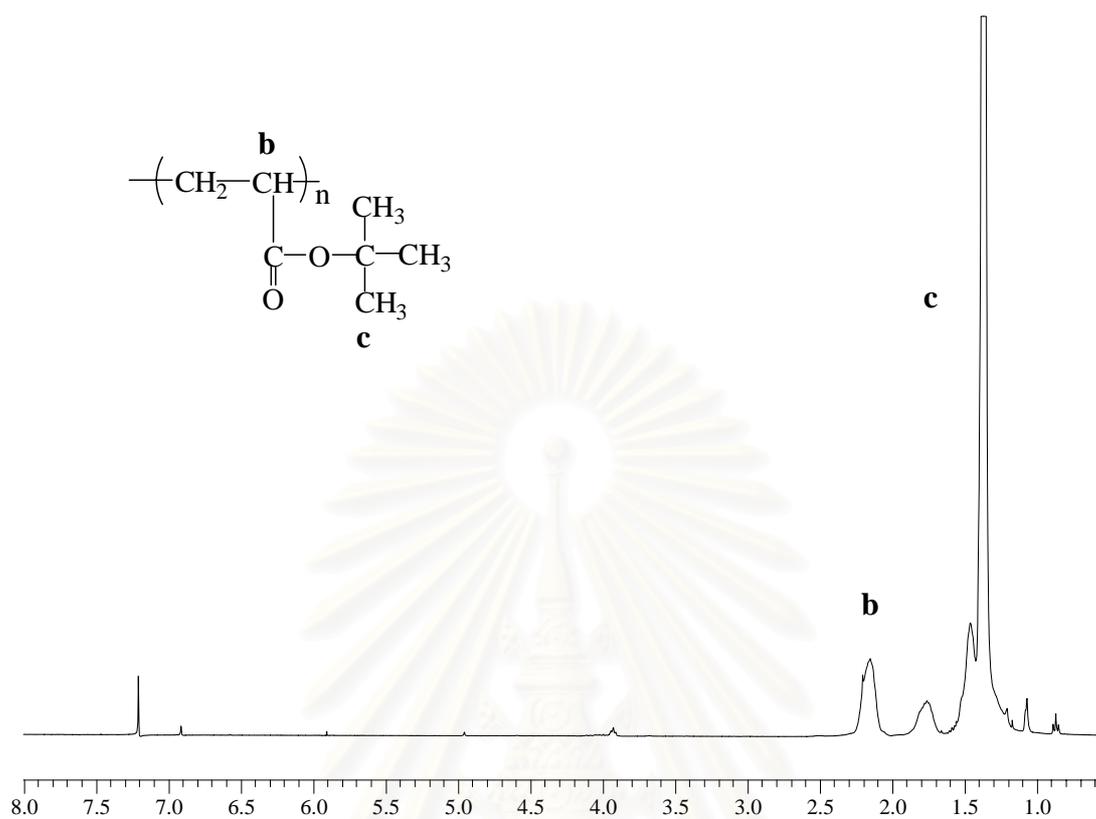
Figure A-6 The ^{1}H-NMR (400 MHz, CDCl$_3$) of P*t*BuA.
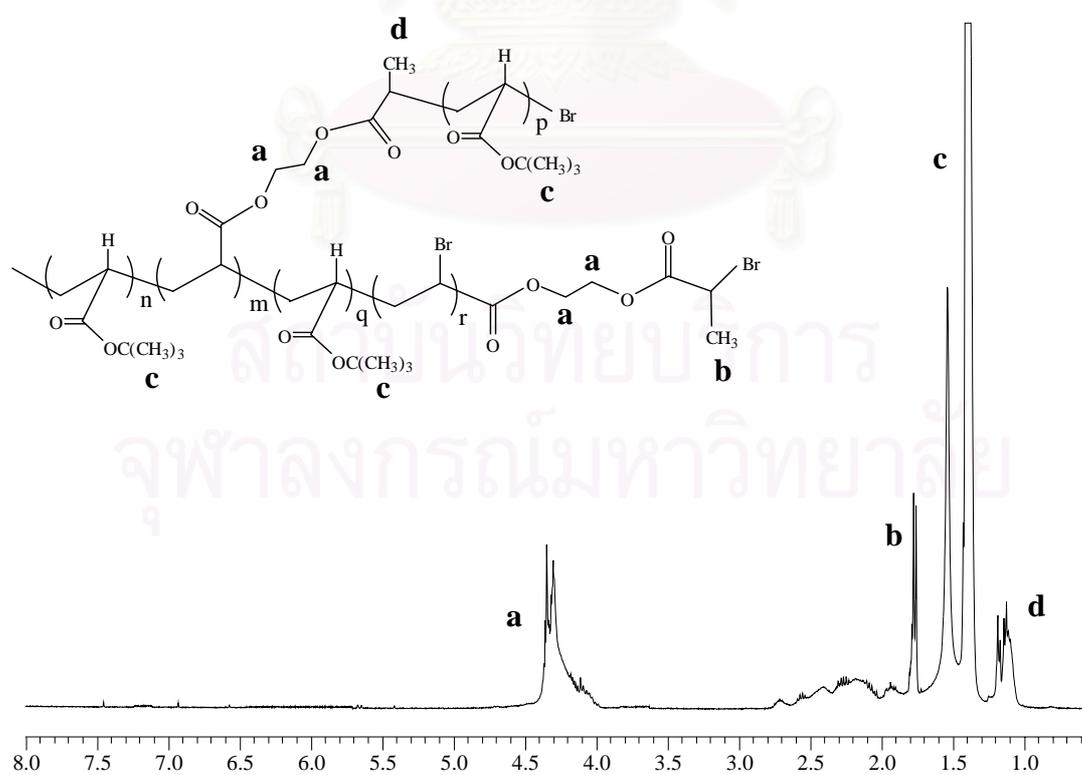
Figure A-7 The ^{1}H-NMR (400 MHz, CDCl$_3$) of branched P*t*BuA.
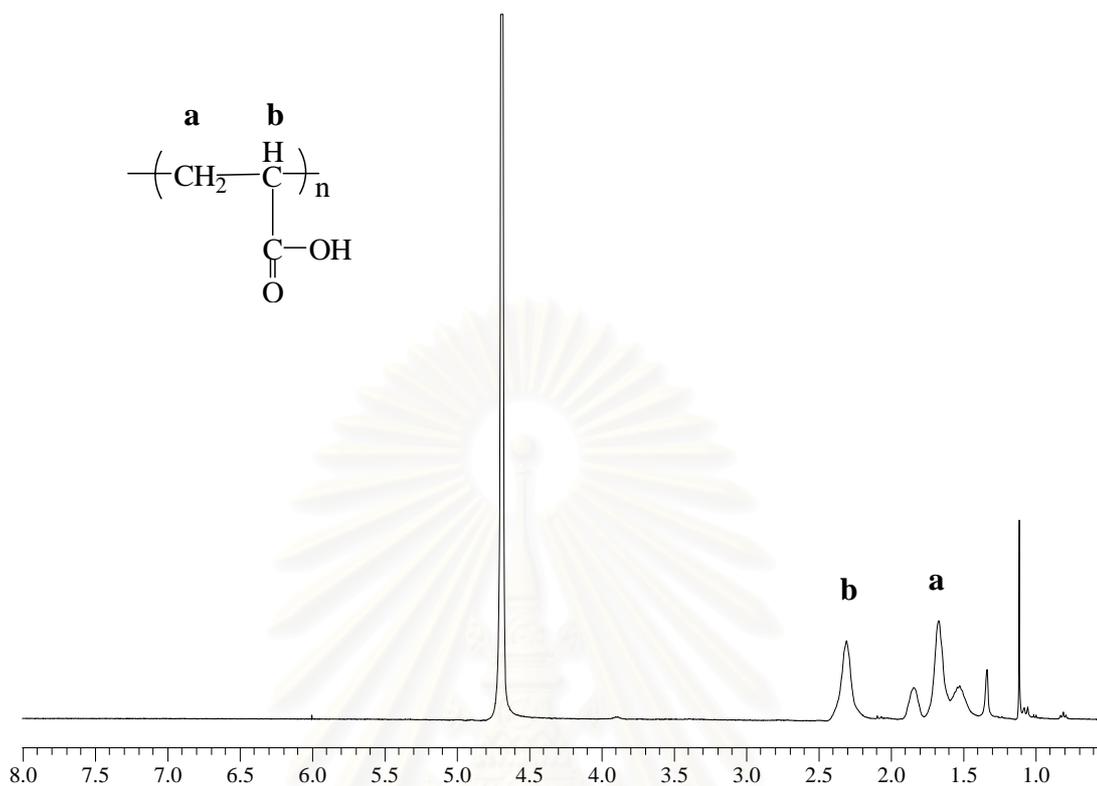
Figure A-8 The ^{1}H-NMR (400 MHz, D$_2$O) of PAA.

APPENDIX B

B. Data corresponding to the plots in Chapter IV

Table B-1 Average molecular weight and molecular weight distribution of linear PtBuA brushes analyzed by GPC and the thickness of linear PtBuA brushes calculated from ellipsometric data as a function of time (DP =100)

Time (h)	thickness (nm)	GPC data		
		$\overline{M}_n$	$\overline{M}_w$	$\overline{M}_w/\overline{M}_n$
1	NA	1001	1101	1.1
3	NA	1812	2012	1.08
6	1.1	3832	4094	1.07
15	2.2	6303	6614	1.05
24	4.0	10129	10510	1.04

Table B-2 Average molecular weight and molecular weight distribution of linear PtBuA brushes analyzed by GPC and the thickness of linear PtBuA brushes calculated from ellipsometric data as a function of time (DP =200)

Time (h)	thickness (nm)	GPC data		
		$\overline{M}_n$	$\overline{M}_w$	$\overline{M}_w/\overline{M}_n$
1	NA	1273	1302	1.1
3	NA	2597	2985	1.1
6	2.4	4368	4753	1.09
15	4.6	9248	9770	1.06
24	8.5	18207	18752	1.03

Table B-3 Advancing (θ_A) and receding (θ_R) water contact angles of linear P*t*BuA as a function of time

Time (h)	DP =100		DP = 200	
	θ_A (°)	θ_R (°)	θ_A (°)	θ_R (°)
6	87 ± 2.4	69 ± 0.6	88 ± 1.7	72 ± 1.2
15	89 ± 0.5	69± 2.1	90 ± 0.5	73 ± 1.5
24	92 ± 2.4	71± 1.5	95 ± 1.2	76 ± 1.2

Table B-4 Advancing (θ_A) and receding (θ_R) water contact angles of linear P*t*BuA after hydrolysis by trifluoroacetic acid.

Time (h)	DP =100		DP = 200	
	θ_A (°)	θ_R (°)	θ_A (°)	θ_R (°)
6	71 ± 2.2	52 ± 1.2	67 ± 0.8	50 ± 1.2
15	67 ± 1.2	49 ± 1.4	63 ± 0.5	45 ± 0.9
24	62 ± 0.8	46 ± 1.7	60 ± 1.7	43 ± 0.8

Table B-5 Average molecular weight and molecular weight distribution of branched P*t*BuA brushes analyzed by GPC and the thickness of branched P*t*BuA brushes calculated from ellipsometric data as a function of comonomer ratio (γ)

comonomer ratio (γ)	thickness (nm)	GPC data		
		$\overline{M}_n$	$\overline{M}_w$	$\overline{M}_w/\overline{M}_n$
2.5	1.95 ± 0.5	1323	2359	1.78
5	2.00 ± 0.2	1454	2249	1.55
10	2.25 ± 0.1	1558	2128	1.37
25	3.12 ± 0.5	3606	4864	1.35
100	5.00 ± 0.3	10807	12999	1.20

Table B-6 Composition of copolymer and degree of branching (DB) as a function of comonomer ratio (γ)

comonomer ratio (γ)	% BPEA in polymer	% tBuA in polymer	DB_{NMR}	DB_{theo}
2.5	23.3	76.7	0.27	0.38
5	13.6	86.4	0.21	0.30
10	6.4	93.6	0.11	0.14
25	2.2	97.8	0.05	0.08
100	-	100	-	0.02

Table B-7 Advancing (θ_A) and receding (θ_R) water contact angles of branched PtBuA before and after hydrolysis by trifluoroacetic acid

comonomer ratio (γ)	before hydrolysis		after hydrolysis	
	θ_A (°)	θ_R (°)	θ_A (°)	θ_R (°)
2.5	103.2 ± 2.0	73.4 ± 8.4	75.8 ± 1.3	60.4 ± 4.9
5	103.2 ± 3.0	74.0 ± 8.0	75.4 ± 1.7	53.6 ± 4.7
10	106.2 ± 1.1	79.0 ± 2.7	74.6 ± 1.2	68.0 ± 1.3
25	99.4 ± 0.9	65.8 ± 6.0	68.0 ± 0.8	47.4 ± 4.7
100	100.2 ± 3.3	77.8 ± 2.1	66.8 ± 0.7	55.2 ± 1.9

Table B-8 Amount of COOH group on linear PAA brushes as a function of molecular weight

DP	$\overline{M}_n$	Amount of COOH x 10^{-9} (mol/cm^2)
100	3832	2.21 ± 0.30
	6303	4.79 ± 0.28
	10129	6.13 ± 0.50
200	5235	2.88 ± 0.60
	7972	5.36 ± 0.32
	14029	7.04 ± 0.70

Table B-9 Amount of COOH group on branched PAA brushes as a function of comonomer ratio (γ) and degree of branching (DB)

comonomer ratio (γ)	DB	Amount of COOH x 10^{-9} (mol/cm^2)
2.5	0.27	5.20 ± 0.10
5	0.21	5.43 ± 0.18
10	0.11	5.83 ± 0.09
25	0.05	6.30 ± 0.19
100	-	6.44 ± 0.20

Table B-10 Advancing (θ_A) and receding (θ_R) water contact angles of functionalized polymer brushes

Sample	Linear polymer (DP =200, 24h)		Branched polymer ($\gamma = 25$)	
	θ_A (°)	θ_R (°)	θ_A (°)	θ_R (°)
PtBuA	95 ± 1.2	76 ± 1.2	99 ± 0.9	66 ± 6.0
PAA	60 ± 1.7	43 ± 0.8	68 ± 0.8	47 ± 4.7
PAA + NHS/EDC	80 ± 0.8	47 ± 1.4	78 ± 0.6	52 ± 2.0
PtBuA + NHS/EDC	79 ± 0.8	78 ± 2.0	80 ± 0.8	53 ± 1.7

APPENDIX C

C. Toluidine blue O assay

Toluidine blue O assay is a method used for determination of the amount of carboxyl groups. The carboxyl groups of PAA brushes can form a complex with toluidine blue o. The absorbance of the solution containing the desorbed complex was measured at 633 nm. The COOH content was obtained from a calibration plot of the optical density versus dye concentration which is displayed in Figure C-2.
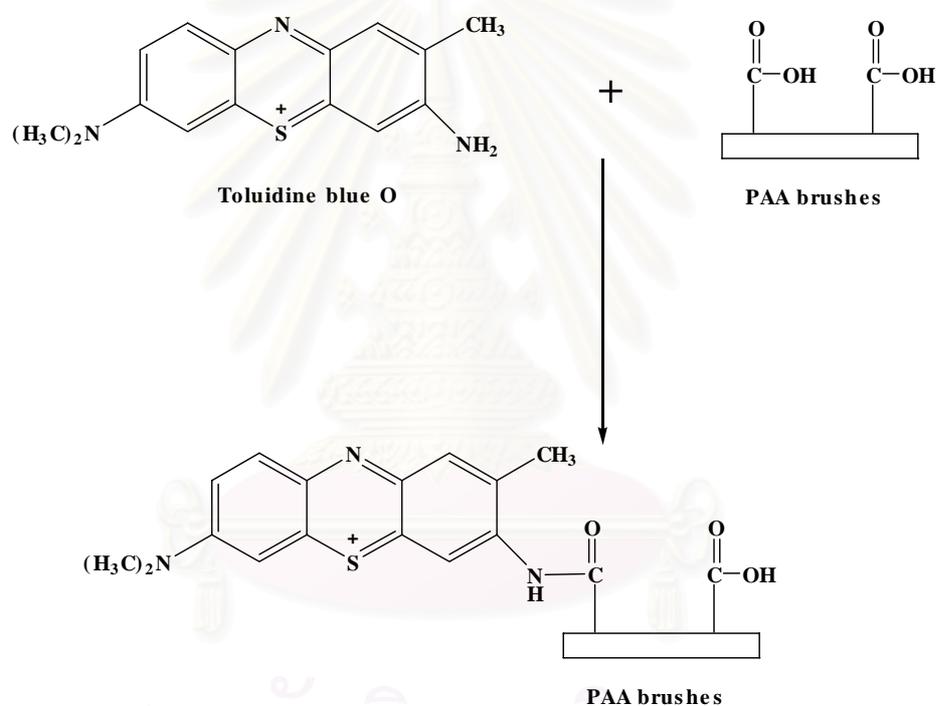

**Figure C-1** Formation of toluidine blue O complex with carboxyl group.

The plot shows: Abs. (y-axis, 0 to 1.6) versus Concentration of toluidine blue o ($\times 10^{-3}$ M) (x-axis, 0 to 0.05).

$$y = 29.83x$$
$$R^2 = 0.9935$$
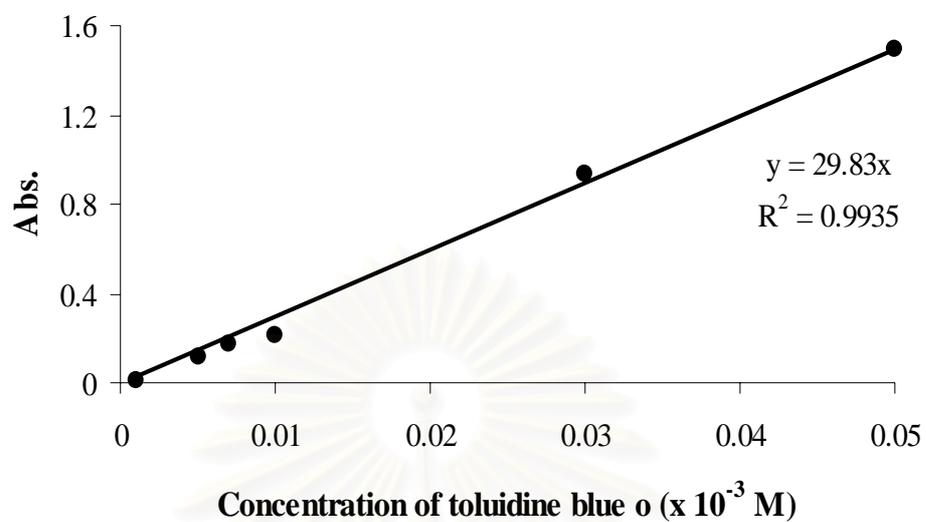
Figure C-2 Calibration curve of UV absorbance as a function of toluidine blue o concentration.

VITAE

Miss Piyaporn Akkahat was born on February 22, 1980 in Sakonnakorn, Thailand. She received a bachelor degree of science from Department of Chemistry, Faculty of Science, Burapha University, Bangsean, Chonburi, Thailand in 2003. In the same year she was admitted to a Master's Degree in Program of Petrochemistry and Polymer Science, Faculty of Science, Chulalongkorn University and completed program in 2006. Her address is Moo 1 Bantai, Sawangdandin, Sakonnakorn 47110.